NEW APPROACHES IN NUMERICAL ANALYSIS IN CIVIL ENGINEERING

Rodian Scînteie, Constantin Ionescu
– editors –

Editura Societatii Academice “Matei - Teiu Botez”
Iasi 2011

Proceedings of the 9th International Symposium "Computational Civil Engineering 2011", Iasi, Romania, May 13, 2011

Descrierea CIP a Bibliotecii Nationale a României
New approaches in numerical analysis in civil engineering / ed.: Rodian Scînteie, Constantin Ionescu. - Iasi : Editura Societatii Academice "Matei - Teiu Botez", 2011
Bibliogr.
ISBN 978-606-582-006-7
I. Scînteie, Rodian (ed.)
II. Ionescu, Constantin (ed.)
624

Editura Societatii Academice "Matei - Teiu Botez"
B-dul Dumitru Mangeron nr. 43
Director: Prof.univ.dr.ing. Constantin Ionescu,
e-mail:cionescu@ce.tuiasi.ro

Table of Contents

ORGANIZERS

Asociación Española de Ingeniería Sísmica, Barcelona
Academic Society "Matei Teiu Botez" Iasi
Faculty of Civil Engineering and Building Services Iasi

Coordination Committee

prof. dr. ing. Constantin Ionescu - Chair
prof. dr. ing. Nicolae Taranu
prof. dr. ing. Alexandru Horia Barbat
prof. dr. ing. Mihai Budescu
arh. Tudor Gradinaru

Scientific Commission

dr.ing. Rodian Scînteie - coordinator
prof. dr. ing. Mihai Budescu
secretary - drd. Ing. Costel Plescan

Organizing Commission

dr. ing. Ionica Modoi - coordinator
drd. ing. Cristian Ciobanu
drd. ing. Cristian Blejeru
drd. ing. Gheorghita Boaca
drd. ing. Andrei Jantea
secretary - ing. Nicoleta Pasehonov

"Computational Civil Engineering 2011", International Symposium
Iasi, Romania, May 13, 2011

High-Strength Concrete Modulus of Elasticity Evaluation

David Procházka[1], Jirí Brožovský[2] and Klára Krížová[3]
[1] *Institute of building Materials and Components, Faculty of Civil Engineering , Brno University of Technology, Brno, 662 00, Czech Republic*
[2] *Institute of building Materials and Components, Faculty of Civil Engineering , Brno University of Technology, Brno, 662 00, Czech Republic*
[3] *Institute of building Materials and Components, Faculty of Civil Engineering , Brno University of Technology, Brno, 662 00, Czech Republic*

Summary

Modulus of elasticity is one of the fundamental attributes characterizing each material. Besides the strength it is perhaps the most important parameter for a structural engineer designing constructions. It indicates the deformation degree of material exposed to loads. For given material the modulus of elasticity is never the same. Its size depends e.g. on: composition of such material, deformation, temperature, direction or determination method. The concrete takes a wide range of values. The lowest is lightweight concrete, the highest usually high-strength concrete. Modulus of elasticity determination is currently the most commonly performed by loading in pressing machines or by ultrasonic impulse method. Both methods have their specifics. Evaluation of elastic modulus on the loaded test specimen or structure is generally considered more accurate. Disadvantages compared to ultrasound measurements are higher costs and time consumption.

Best explored is this problematics on the field of ordinary concrete. It is understandable. Ordinary concrete is the most common type of concrete. For high-strength concrete, the situation is different. Although this type of concrete has been known for several decades, it was accomplished very little work with the modulus of elasticity. However, with its use for static calculations it is necessary to solve problems of its size determination for various types and classes of concrete. Only then can a structural engineer, who usually uses a table values, fully exploit the potential of the HSC he proposes. In addition, the investor can also save considerable money.

KEYWORDS: High-strength concrete, modulus of elasticity

1. INTRODUCTION

Modulus of elasticity is known as the basic material property describing materials stiffness or structures stiffness respectively. This parameter is important namely from the viewpoint of structural design and their behavior modeling. In order for a structural engineer to create a quality structure model with sufficient predictive value, he needs to know the most accurate value of modulus of elasticity. When modeling static and dynamic loads or designing effects of fire this variable is among the key. Its unfamiliarity or bad determination may have fatal consequences for finished construction in the future. Modulus of elasticity is important strength-deformation characteristics e.g. in verifications of ultimate limit state in calculation of deviation and deformation, in calculations of vibration caused by wind or seismicity, in linear elastic analysis calculations or in nonlinear analysis (e.g. models of mechanical behavior of load-bearing elements at elevated temperatures).

Modulus of elasticity is essentially determined as physically test on material or construction, then by deduction from the tables or rarely from theoretical computational relations. Widely acclaimed and most recommended is its destination directly in real conditions, either on the construction work or on test specimens. In such determination simultaneous measurement of loading and deformation is supposed, which this loading causes. Synchronous and accurate recording of these two variables is not easy, so there are efforts for finding easier ways to predict modulus of elasticity either from theoretical or empirical considerations. Here is the modulus of elasticity usually expressed as a function of compressive strength, Poisson's ratio or dynamic modulus of elasticity.

A very attractive way for determining the modulus of elasticity of concrete is a (re)computational relationship between dynamic and static modules, determined from measurements on specimens in laboratory conditions. Creating of accurate calibration relationships would greatly simplify the process of ascertaining this elastic-deformation characteristic. In principle it would be enough to measure structure or component respectively by e.g. ultrasonic device and from created calibration curves simply to make static modulus that is so necessary for structural analysis.

Creation of recomputational relations is not so clear and simple. It should be noted that concrete is a composite multi-phase system and its final properties and behavior are a function of many interacting parameters. New modern types of concrete (SCC, HSC, RPC and others) also enhance this variability and thus make difficult, if not impossible, finding of preferably versatile recomputational relations.

The presented article shows in short form outputs from measurements of statical and dynamical modules of HSC.

2. MODULUS OF ELASTICITY

Modulus of elasticity or Young's modulus can be defined as ratio of stress and through it caused relative deformation. This can be expressed as:

$$E = \frac{s}{e} \tag{1}$$

where E . . . modulus of elasticity [MPa]

s . . . stress [MPa]

e . . . strain, relative deformation [-]

Modulus of elasticty determined from the strain dependence on the deformation is called the static modulus of elasticity. The formula shows that higher modulus of elasticity of concrete means lower strain at the same stress. Or also to achieve the same strain it is necessary to develop higher stress. Concrete with a higher modulus of elasticity will thus less deform. [2]

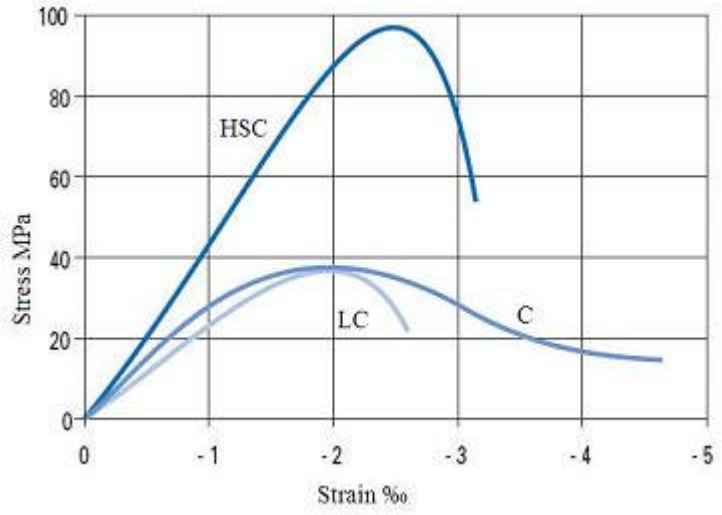

Figure 1. Stress-strain diagram of high-strength concrete, ordinary concrete and lightweight concrete [5]

As shown in Figure 1 the ratio of s-e is not constant, but changes with increasing stress. Also the modulus of elasticity is not constant too. In fact, its value depends on the size of the stress the modulus is determined. According to this, there are differentiated tangent and secant modulus (Fig. 2).

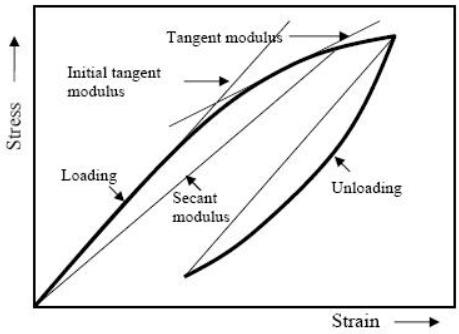

Figure 2. Illustration of different modules of elasticity [2]

As seen from the figure, the highest is the initial tangent modulus. It coincides with the linear part of the load curve. Deformation is elastic according to Hooke's law. The secant modulus is lower and is used in structural analysis. The stres at which the secant modulus is determined is given by convention. According to CSN ISO 6784 it is determined on samples at stress equal to one third of the samples strength according to formula 2. [3, 6]

$$E_c = \frac{\Delta s}{\Delta e} = \frac{s_a - s_b}{e_a - e_b} \tag{2}$$

where E_c . . . static modulus of elasticity [MPa]
s_a . . . upper loading stress [MPa]
s_b . . . lower loading stress [MPa]

As already mentioned the modulus of elasticity is not linear. The strength increase may therefore not correspond an adequate increase in modulus of elasticity. This is due to the fact that concrete is a composite made from components with various modules of elasticicity (Fig. 3).

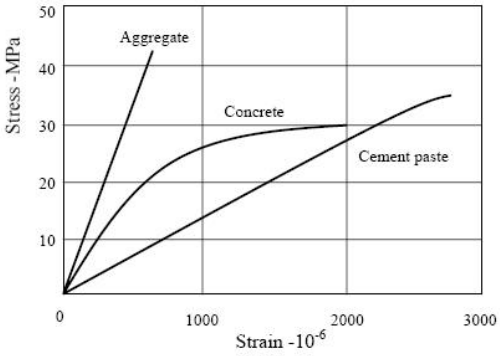

Figure 3. Stress-strain for aggregate, concrete and cement paste [2]

The resulting modulus of elasticity depends on the modules of elasticity of particular concrete components (present air including), then the concrete processing and the production technology. Its size also depends on test specimens and the test procedure. To the resulting modulus value size contributes most aggregate and cement paste, which occupies largest volume of concrete. In addition, high-strength concrete may occur to the seemingly paradoxical situation. A higher binder amount, which is at the expense of aggregate amount, may even reduce the value of concretes modulus of elasticity. But generally it can be said that the modulus increases with the strength. For ordinary concrete, its value usually ranges between 20-40 GPa, for most HSC it is 35-50 GPa.

In addition to static modulus of elasticity there can be found dynamic modulus of elasticity too. This is usually determined by an ultrasonic pulse or resonant method. The measurement is performed by sending of mechanical stimulus to the test sample, which is then registered by the given device. In the case of an ultrasonic pulse method it is measured the transit time through the sample and then according to the formula 3 the dynamic modulus of elasticity is calculated.

$$E_{bu} = r \cdot v_L^2 \cdot \frac{1}{k^2} \cdot 10^{-6} \tag{3}$$

where E_{bu} . . . dynamic modulus of elasticity in compression, tension [MPa]

? . . . density or volume weight of the material [kg·m^{-3}]

v_L . . . longitudal wave impuls velocity [m·s^{-1}]

k . . . medium dimensionality coefficient

Dynamic modulus of elasticity is measured on an unloaded specimen, so its value is higher than the static modulus. It is considered that it corresponds to the initial tangent modulus.

3. STATIC AND DYNAMIC MODULUS OF ELASTICITY MEASUREMENT

For the actual measurement it has been proposed high-strength concrete that reached strength of 90 MPa after 28 days. As the aggregate was used quartz sand and crushed granodiorite. The superplasticizer was polycarboxylate and admixture silica fume. Concrete composition is shown in Table 1.

Table 1. Concrete mixture composition of 1 m^3

Component	Amount [$kg \cdot m^{-3}$]
Cement CEM I 42,5 R	470
Sand 0-4 Žabcice	800
Coarse aggregate 4-8 Olbramovice	335
Coarse aggregate 8-16 Olbramovice	590
Water	146
Microsilica	47
Superplasticizer	8

Before testing the test specimens were stored in damp room (? = 20 ± 2 ºC, f = 95 %). Static modules were tested on prisms 100 x 100 x 400 mm according to the CSN ISO 6784 standard. Dnamic modules based upon the standard CSN 73 1371. The development of modules over time as well as some other dependencies are shown in Figures 4-13.

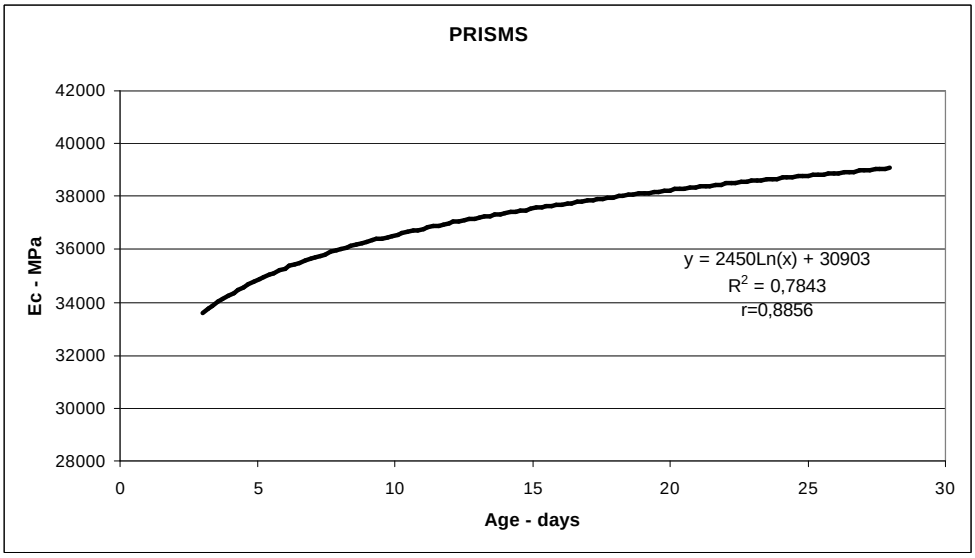

Figure 4. Static modulus of elasticity development in time

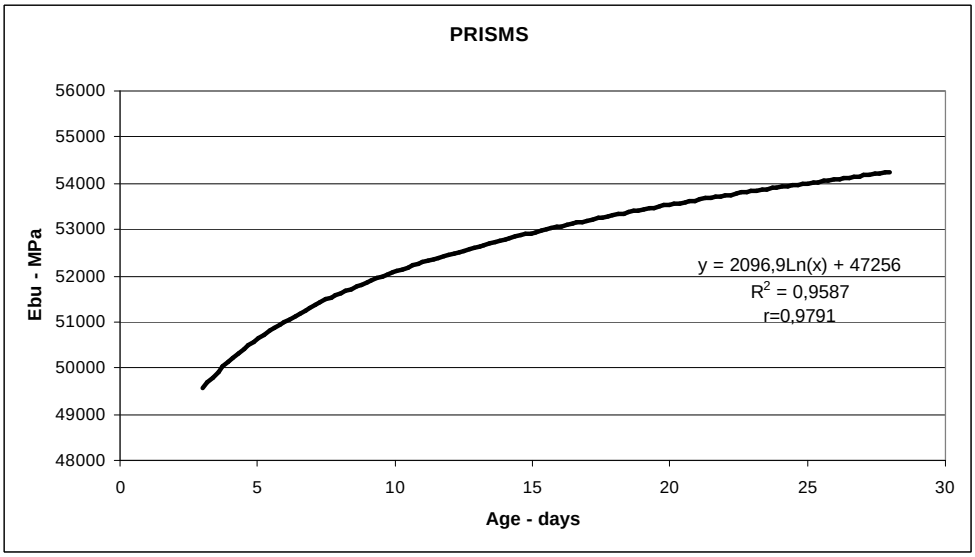

Figure 5. Dynamic modulus of elasticity development in time

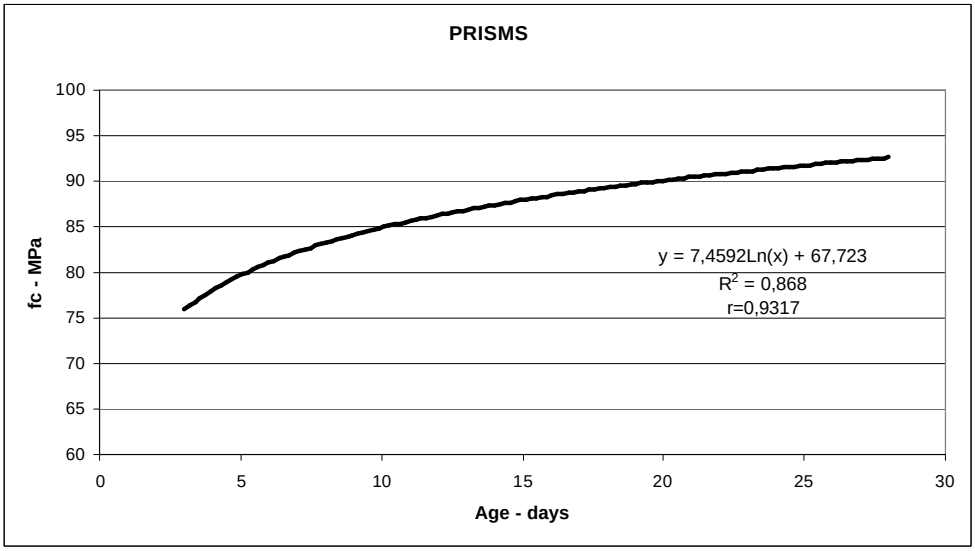

Figure 6. Prisms fragments compressive strength development in time

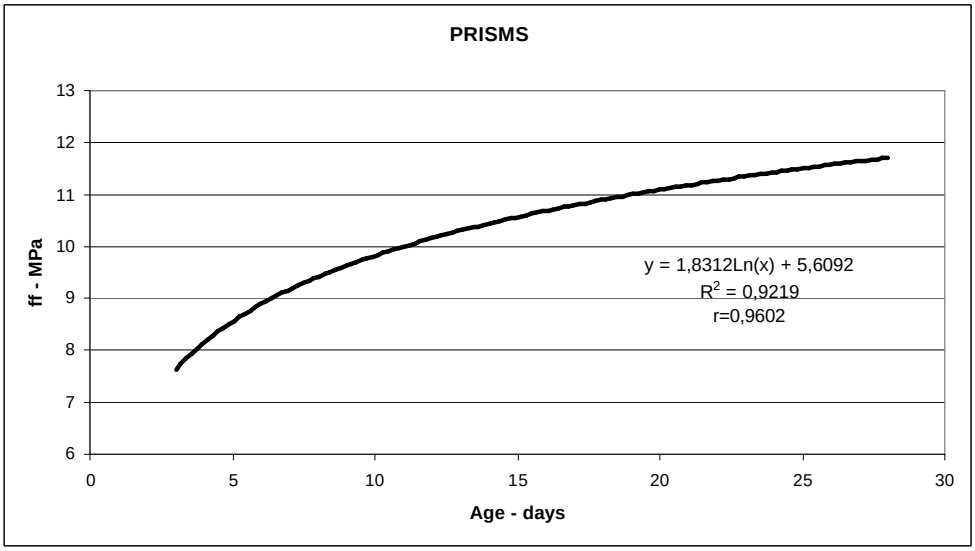

Figure 7. Bending strength development in time

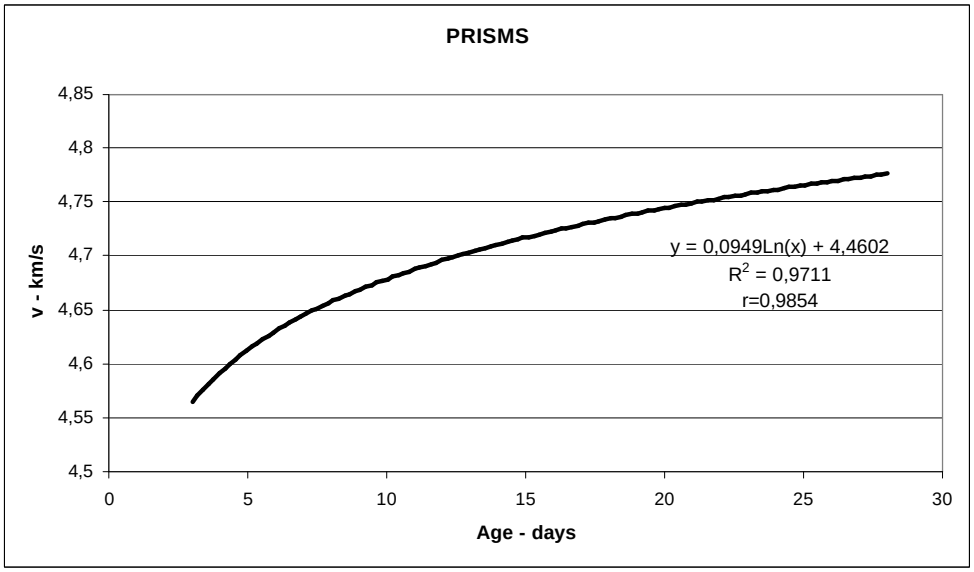

Figure 8. Ultrasonic pulse velocity development in time

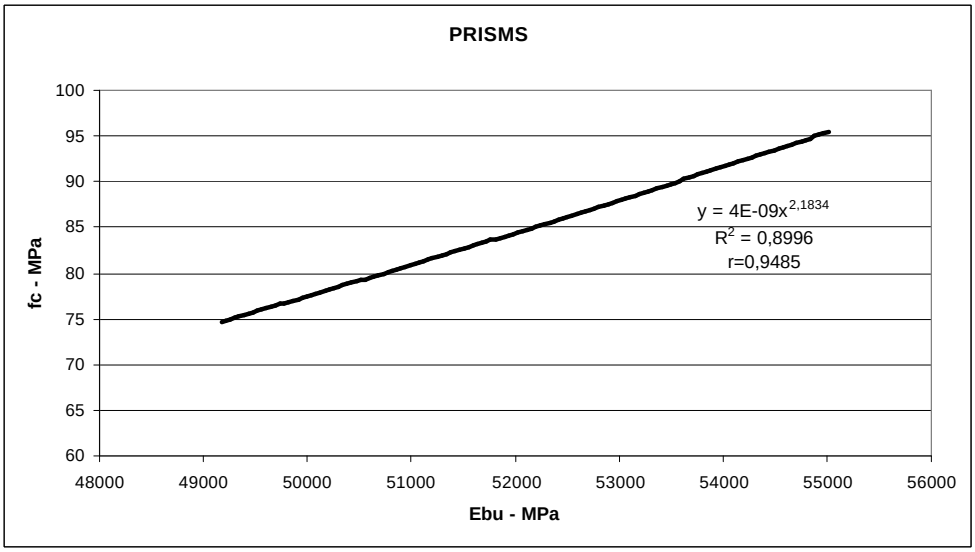

Figure 9. Fragments compressive strength dependence on dynamic modulus of elasticity

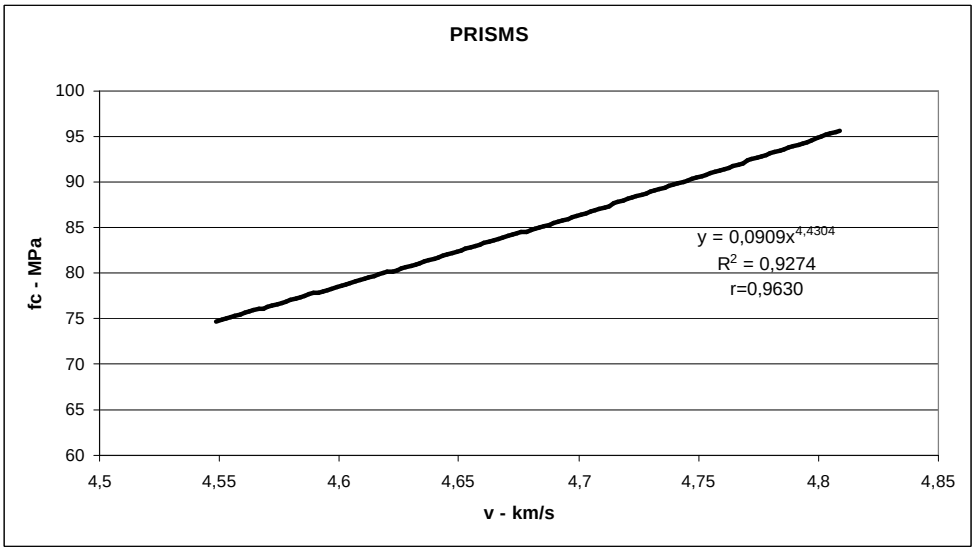

Figure 10. Fragments compressive strength dependence on ultrasonic pulse velocity

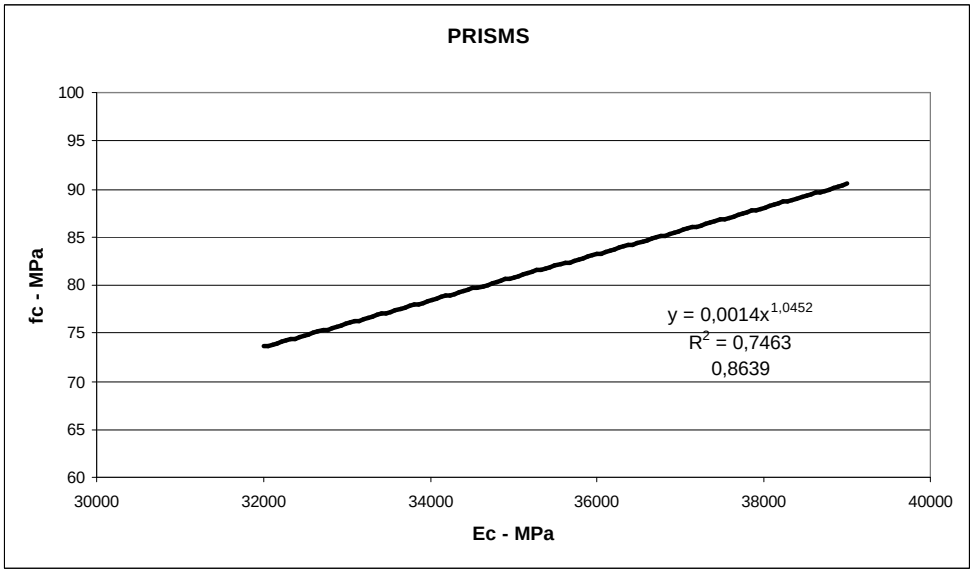

Figure 11. Fragments compressive strength dependence on static modulus of elasticity

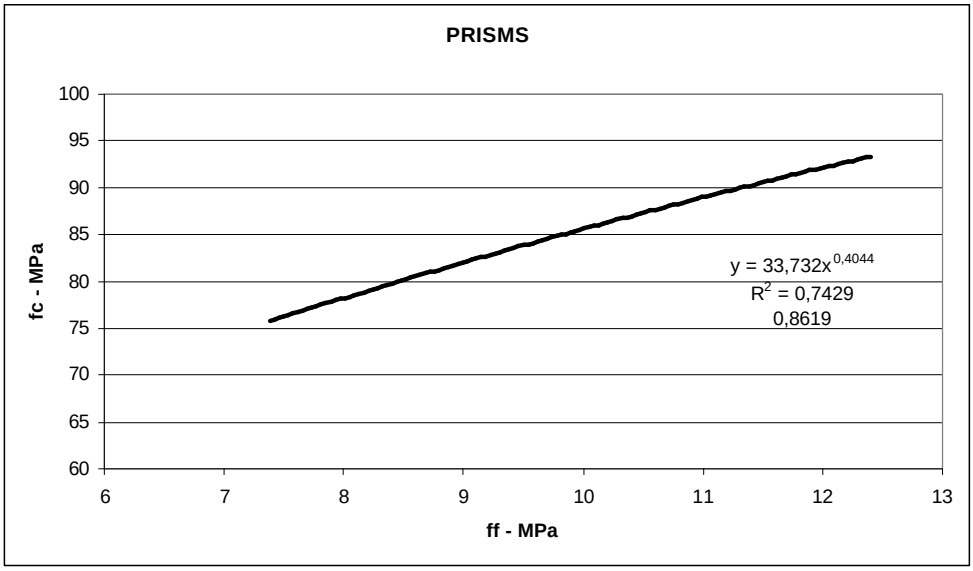

Figure 12. Fragments compressive strength dependence on bending strength

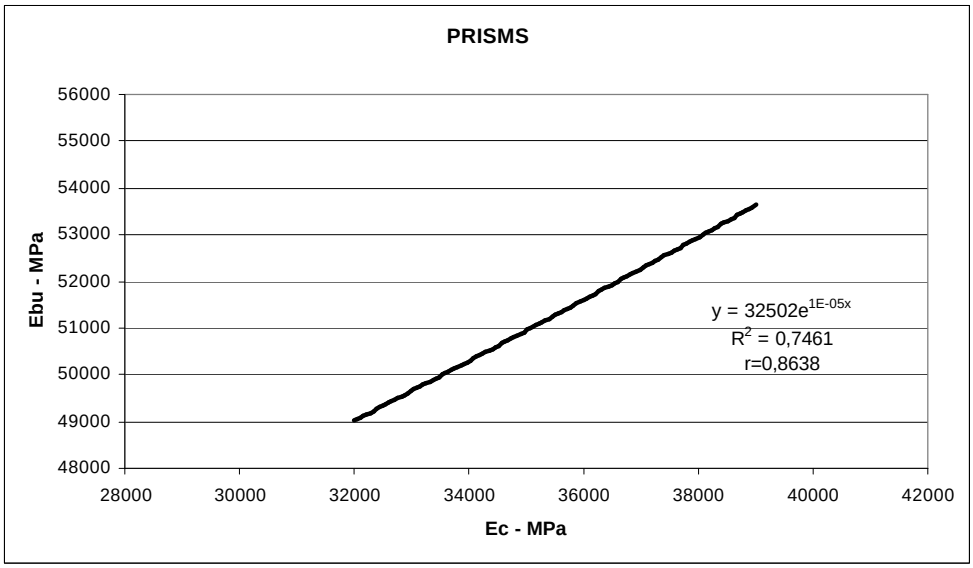

Figure 13. Dynamic modulus of elasticity dependence on static modulus of elasticity

As is evident from the graphs the development of studied HSC parameters over time is as with ordinary concrete approximately logarithmic. Relationships that have a correlation coefficient greater than 0.85 are generally technically usable. However, from a practical point of view it is better to take more account for dependence with correlation coefficient of 0.90 and above. Derived dependencies are, however, only valid for given type of concrete. They can not be generalized in any way.

4. CONCLUSIONS

Study of modules of elasticity of HSC is in comparison with ordinary concrete in beginning. Previous researches shows that this problematics is quite complex, if not more complicated than that of ordinary concrete. Despite the obvious difficulties, that in connection with this theme arise, it is necessary to solve this field because the structural designing of high-strength concrete is today without knowledge of the elastic modulus indispensable. The article demonstrated that deriving dependencies of physical and mechanical characteristics of high-strength concrete is actually possible. In curent only dependencies for given type of concrete can be created. However only the future will show to which degree it will be real to create general calibration relationship(s) for as much as possible types of concrete.

Acknowledgements

The work was supported by the projects: *FAST-S-11-44: Efficiency of high volume of fine admixtures in current concrete mix design in the Czech Republic* and project *MSM 0021630511 plan: Progressive Building Materials with Utilization of Secondary Raw Materials*.

References

1. Tia, M., Liu, Y., Brown, D. *Modulus of Elasticity, Creep and Shrinkage of Concrete. Final report.* 2005.
2. Neville, A. M. *Properties of Concrete (Fourth and Final Edition)*. London: Pearson Education Limited, 1996. 844 pp. ISBN 0-582-23070-5.
3. Uncík, S., Ševcík, P. *Modul pružnosti betónu.* Trnava: Edícia betón racio, 2008. 15 pp. 978-80-969182-3-2. (in slovak)
4. Procházka, D. Křížová, K., Hela, R. Problematika modulu pružnosti u vysokopevnostních betonu. *17. Betonárské dny*. Hradec Králové: CBS Servis, s.r.o., 2010. ISBN 978-80-87158-28-9. (in czech)
5. *Zement-Taschenbuch 2002*. Verlag Bau und Technik. 864 pp. ISBN 978-3764004279. (in german)
6. *CSN ISO 6784 Beton. Stanovení statického modulu pružnosti v tlaku*. Praha: Federální úrad pro normalizaci a merení, 1992. 8 str. (in czech)
7. *CSN 73 1371 Ultrazvuková impulzová metóda skúšania betónu*. Praha: Úrad pro normalizaci a merení, 1983. 19 str. (in czech)
8. *CSN EN 12390-3 Zkoušení ztvrdlého betonu – Cást 3: Pevnost v tlaku zkušebních teles*. Praha: Ceský normalizacní institut, 2002. 20 str. (in czech)
9. *CSN EN 12390-5 Zkoušení ztvrdlého betonu – Cást 5: Pevnost v tahu ohybem zkušebních teles*. Praha: Úrad pro technickou normalizaci, metrologii a státní zkušebnictví, 2009. 12 str. (in czech)

The application of Computer Aided Facilities Management (CAFM) in civil engineering

Dragos Georgescu[1], Ion Serbanoiu[1]
[1]Civil Engineering, the "Gheorghe Asachi" Technical University of Iasi, Faculty of Civil Engineering and Building Services, Iasi, 700050, Romania

Summary

The International Facility Management Association defined Facility Management (FM) as being "an integrative management process that considers people, processes and place in organizational context". It involves individuals engaged in the process of managing buildings, constructions and people.

The Facilities Management supports managers not to manage facilities directly, but information, a process that so far has been done with heavy, inadequate time and cost consuming tools.

The CAFM tools have the ability to remedy this situation by realizing performance and financial gains and increasing productivity. They are software packages designed to help managing locations, finances and employees. A CAFM system basically represents any combination of CAD and data base software designed for facility management functions. It is successfully used at commercial level, organizational and research activities. The areas in which CAFM finds its application differ from maintenance and operation, constructions and project management to finance and budgeting or property management, only to name a few.

The necessity for civil engineers to manage large scopes of information as well as the different data bases that CAFM helps linking and connecting makes the use of Computer Aided Facilities Management an advantage for civil engineering, especially in what concerns budgeting, project management, building specifications, tracking milestones and critical information vital for the successful completion of every project.

KEY WORDS: CAFM, management, engineering, efficiency, tools.

1. INTRODUCTION

Facility management can be defined as being the process of administrating the working space together with the related personnel and equipment. The large quantity of information related to this type of management is the cause for implementing programs and measures in order to aid managers in obtaining a more efficient space management.

The advantages of using this type of management system are represented mostly by the correct records of the existent facilities (i.e. buildings, parking spaces, garages etc.) with the purpose of efficient management, the possibility of generating exact reports within a very short period of time, such as the total surfaces for painting, the exact components of the installations, pipe length etc., with the record of the material and equipment to be used, budget planning and contracts' tracking; the precise record of the surfaces/volumes and installations with the purpose of correct programming and evaluation of building/repair costs, necessary material and manual labor. The facility management also benefits the managers by offering the possibility for time programming, without overlapping, maintaining/repair as well as time and budget allocation of the necessary funds. The access to this type of information is easier when using a facility management program and the record keeping becomes more efficient. The facility management comprises different types of information about each location: architectural planning, installation design, the 3D design of the buildings, copies of all documents related to a specific estate (contracts, notifications, permits, property documents etc.).

Completed with the facilities offered by intelligent buildings, the system becomes an active element that can control the status of the buildings within a patrimony.

The Facility management incorporates the following fields: architecture, engineering, business management, financial business etc. The activities that can be performed using the facility management are the coordination of construction activities and building renovation, engineering works within buildings, financial planning and budget planning, preventive and corrective maintenance, design and modification of architecture and engineering, space allocation and movement supervision, building security and protection, Computer Aided Facility Management that involves the use of computer science in facility management.

CAFM is related to a collection of software programs which are used more and more by facilities managers. CAFM has six major components, related to the popularity and usefulness in the applying computer aided facilities management, namely the computer aided design, computer aided engineering, decision support systems, management information, project management systems and word processing.

Together with the appearance of CAD technology and other facilities related to facility administration a new business emerged: the Computer Aided Facility

Management which interconnects the CAD systems with other IT systems, such as data bases, EDM, GIS. Eliminating the unnecessary information and avoiding losing data when transferring the information from one department to another, the central management of buildings allows an administrator to immediately access all the information needed at a certain point.

CAFM can be applied anywhere, in architecture, engineering, financial institutions, insurance companies, hotels, cities, plants, television stations etc. In industry and administration, the development of CAFM is a new topic in the context in which every organization faces significant competition and is therefore forced to develop efficient and effective structures in management.

2. CAFM STRUCTURE AND APPLICATION

Computer Aided Facilities Management can be understood best when analyzing its components, namely the six major software applications most frequently used. These are Computer Aided Design (CAD), Computer Aided Engineering (CAE), Decision Support Systems (DSS), Management Information Systems (MIS), Project Management Systems (PMS) and Word Processing (WP).

When using the term CAFM, the general understanding is of an “electronic tool box” available to the manager to use, each of the applications having a specific and correct application. The correct and precise use of these tools results in information and data bases with great accuracy and the successful use of this software package is based in the first place on understanding their general nature and application in analysis, planning, construction and other tasks of the managers.

CAFM hands out the possibility to combine every type of information regarding buildings and facilities. The information on buildings is collected using different methods and different sorts of data collection.

Regarding the construction of buildings, what the civil engineer is interested in, in the first place, is the structural analysis of the building, such as the static component not only at the beginning of the construction but also during its entire “lifetime”. An efficient facility management is run using information such as architectural plans, workflows or climate control system and combining this information with the front design view of the architect.

These component elements and information on the same object require accurate and precise building information. CAFM presents the tools to manage all the different data that need to be stored, analyzed, managed, data such as graphic, attribute, management and routine maintenance.

Each of the six software applications CAFM components also offer planning advantages besides economic benefits. The components of CAFM software package will be briefly presented in the following pages. The Computer Aided Engineering component will be dedicated a different and more detailed chapter.

Computer Aided Design, better known as **CAD** software package uses interactive graphics on computer terminals to develop facilities plans and designs in two and three dimensional formats. CAD is technology concerned with using computer systems to assist in the creation, modification, analysis, and optimization of a design. Any computer program that embodies computer graphics and an application program facilitating engineering functions in design process can be classified as CAD software.

The most basic role of CAD is to define the geometry of design – a mechanical part, a product assembly, an architectural structure, an electronic circuit, a building layout, etc. The greatest benefits of CAD systems are that they can save considerable time and reduce errors caused by otherwise having to redefine the geometry of the design from scratch every time it is needed.

Computer-aided design (or CAD) software has become the main tool of architects and engineers when designing anything from new homes to elaborate circuit boards. While AutoCAD is the most popular CAD software on the market, there are a number of other programs available that allow the user to create highly technical designs. Employing mostly architectural symbols and drafting standards, the plans can automatically produce design drawings and bills of materials.

CAD software has been extremely useful in civil engineering even from its introduction in the late 60's and early 70's in architectural and engineering work but required the allocation of immense amounts of money in order to acquire a minicomputer- based CAD working station. Together with the powerful computers that are currently available, CAD and its capabilities were brought into the reach of even the smallest professional offices, being also extremely suitable for home working, in its less complex formats.

CAD is a very well developed technology that has been employed by a wide variety of specialists, from facility managers, architects to engineers. With a large variety of sizes, price ranges, levels of sophistication and capabilities, CAD requires a significant period of time, commitment and energy for the necessary training in order to implement this software in an efficient and effective tool.

Decision Support Systems (DSS) has a mathematical approach consisting from mathematical algorithms and statistics and assists the user in deriving solutions or sets of alternative solutions, basically explaining the alternatives. This component is mostly used in interactive financial planning models. For the managers of facilities, DSS finds its application in building or leasing, building or renovation and provides assistance in determining how much space will be used for different purposes.

The usefulness of DSS is that it comprises also algorithms in order to determine the best use and arrangement of space, equipments and organization of that space. These functions are best known as layout and process plans for equipment and materials and block layout for spaces. While these decisions can be reached with analytical approach, DSS may not provide the best optimal solution but can assist with estimations and proposals that would lead the manager to the right answer.

The user has a wide variety of DSS programs which he has to tailor in order to fit best to his necessities. In many cases the simulation models must be built according to the specific circumstances and not just purchased off the shelf. This an essential condition for all software that are to be used in specific conditions, in order to provide the best internal decision making support. DSS can be run of mainframes, minicomputers or microcomputers and the correct selection of the hardware depends always on the purpose of the application and user.

Management Information Systems (MIS) was developed as a response to the necessity for better developed computers that would provide computational capabilities at high speed and accuracy. The subsequent use of these devices was data storage. Together with the technological developments, functions such as design of files, data input, update, security and reporting information from these files got to be labeled as MIS. This technology incorporates calculation routines supporting the statistical analysis of the stored information.

The main reason why facility managers use this software is the basis level of management of the assets. The most common uses of MIS are for lists of assets, buildings, equipment, personnel etc. After establishing these primary functions, the manager is concerned with focusing on the use of these assets and the answer to the query of how well are the assets used is provided with the support of MIS. Utilization studies, ratio analysis allow managers to be aware of the effectiveness of their investments and use of facilities, equipment, personnel.

MIS can be used on all sorts of hardware and the key factor is of course the size of the database, the amount of data that will be stored and also the storage capacity required to accommodate the collection of data becoming available once the MIS software is put in place.

Project Management Systems (PMS) is shortly used for charting the progress. Having its origin in military programs, it was developed in the late 50’s and early 60’s by the US Navy and was known as Program Evaluating Review Techniques. It provides the capability to model activities and events that depend one upon the other to predict expected completion dates of events and expected costs implicated.

The construction industry quickly took over these techniques, slightly modifying the algorithms and terminology, applying them to construction projects and renaming it PMS. The use of this software in large and small construction projects attests the effectiveness and value of PMS and makes it useful also for non construction projects.

These project management systems are usable on mainframes, minicomputers and microcomputers and selection of proper tools to be used depends upon the criteria of the activity network to be stored and manipulated by the system and the speed with which the algorithms for the schedule process have to be calculated.

Last but not least, **Word Processing (WP)** tool is probably the most commonly used tool in the CAFM package. The proliferation of the WP packages was made possible after the Management Information Systems and the advent of the microcomputers. These packages comprise a multitude of capabilities at a

reasonably low cost. WP represents an invaluable support to the facilities management teams for documentation, specifications, reports and also other areas in which writing is necessary.

The WP includes features such as electronic spelling checking, electronic publishing providing the user with the ability to prepare camera ready documents that looks as if they were done by a graphic designer. The WP is extremely easy to use and any reader familiar with word processing should have no difficulties in using its capabilities and applications.

3. COMPUTER AIDED ENGINEERING (CAE)

The behavior of new designs can be predicted and evaluated by engineering analyses, as well as to evaluate the performance of existing designs. Computers are being used by the engineers for a number of tasks, including conceptual design, engineering analysis, detailed design, drafting and documentation, and manufacturing design. In the past, engineers analyzed designs by building and testing physical prototypes or by performing calculations by hand.

Some analyses were so time-consuming that, when done at all, they could be completed only for one simplified example. This frequently led to under- and over-designed systems. Physical prototypes were and still are very costly and time-consuming to build and test – and they often have to be recreated as designs are changed.

Computer Aided Engineering – CAE- technology uses a computer system to analyze the functions of a CAD-created product, allowing designers to simulate and study how the product will behave so that the design can be refined and optimized. CAE tools are available for a number of different types of analyses. For example, kinematic analysis programs can be used to determine motion paths and linkage velocities in mechanisms. Dynamic analysis programs can be used to determine loads and displacements in complex assemblies such as automobiles. One of the most popular methods of analyses is using a Finite Element Method (FEM). This approach can be used to determine stress, deformation, heat transfer, magnetic field distribution, fluid flow, and other continuous field problems that are often too tough to solve with any other approach.

CAE became the computer solution of engineering problems with the assistance and support of interactive computer graphics together with the improvement of graphics displays, engineering workstations, and graphics standards.

This software can be used on various types of computers, such as mainframes and super-minis, engineering workstations, and even personal computers. The choice of a computer system is frequently dictated by the computing power required for the CAE application or the level and speed of graphics interaction desired. The CAE tools are used as a solution for engineering problems. The communication of information between the software tools represents a challenge

for the majority of applicants and the procedure is usually passing the data through proprietary neutral file formats, data interchange standards, or a system database.

A typical CAE program is made up of a number of mathematical models encoded by algorithms written in a programming language. The natural phenomena being analyzed are represented by an engineering model. The physical configuration is described by a geometric model. The results, together with the geometry, are made visible via a user interface on the display device and a rendering model namely graphics image.

The CAE software technology uses extensive calculation mechanisms to design and also analyze the intended structures. The two essential purposes for modeling a structure are to compare the performance with alternative designs and assure the compliance with professional standards and costs.

CAE is used also as a simulation method to show the possible response of a design to physical situations such as earthquakes, strong wind and other potentially physical forces that might damage the construction.

After the design has been accepted and approved, CAE facilitates the engineer the possibility to calculate precise sizes and quantities of structural members, components and materials. Materials calculation comprises the items to be installed in all building trades such as heating, ventilating, conditioning, plumbing, piping, lighting and electrical installations, providing thus significant decrease in hours of manual labor, a higher accuracy and broader perspective.

The main goals for which CAE is one of the most important tools at hand in computer supported engineering are improving product quality, improving safety, reducing engineering time achieved through hard and time consuming design labor, improving product functionality and usability, reducing the number of prototypes and in many cases leading to their elimination and last but not least, reducing product costs.

The use of CAE has a series of advantages as well as disadvantages.

The main advantage of using the CAE software is the ability to test, simulate and possibly validate a product 3D without having to build it physically. For this process, the product is designed in CAD, is then endorsed in CAE. This process may be necessary to draw the piece several times until it meets the necessary requirements. At the end is machined through CAM. The reduced costs and time consuming work as well as the reduction of the probability of errors and a better preparation of the project are also advantages that support the engineer in his projects.

The disadvantages of the CAE are represented firstly by the computational requirements that are still very high for applications based on PC platforms as it implies a high cost of hardware. The software also has considerable costs, as well as the training that is needed in order to be able to work with this type of application.

Among the software programs that form the CAE package the **Catia-Cadam** tools of analysis and simulation has the objective to combine the processes of

design and simulation in order to reduce the cycle time of product development. This solution provides tools for analysis and simulation, which can be used both in development, expert analysis, generate images of very real digital quality, simulation of automatic movements and fitting the parts for assembly and maintenance.

The **Daystar Software-Steel Designer** was founded in 1984. This company offers an application called Steel Designer, with special focus to work with the area of Civil Engineering and structures. The **Algor** includes tools for design, analysis and simulation that offer engineers the ability to predict behavior of their products and offers them the possibility to improve them in the production stage by testing and simulations.

Elcad is a CAE Professional software whose purpose is to help the development of electric project, particularly in the construction of electrical schemes, automatic generation of documentation (lists and diagrams) and integration with other software tools.

4. CONCLUSIONS

Facility management can be defined as being the process of administrating the working space together with the related personnel and equipment. The large quantity of information related to this type of management is the cause for implementing programs and measures in order to aid managers in obtaining a more efficient space management.

The behavior of new designs can be predicted and evaluated by engineering analyses, as well as to evaluate the performance of existing designs. Computers are being used by the engineers for a number of tasks, including conceptual design, engineering analysis, detailed design, drafting and documentation, and manufacturing design. In the past, engineers analyzed designs by building and testing physical prototypes or by performing calculations.

A CAFM system basically represents any combination of CAD and data base software designed for facility management functions. It is successfully used at commercial level, organizational and research activities. The areas in which CAFM finds its application differ from maintenance and operation, constructions and project management to finance and budgeting or property management, only to name a few.

CAFM hands out the possibility to combine every type of information regarding buildings and facilities. The information on buildings is collected using different methods and different sorts of data collection. Computer Aided Facilities Management can be understood best when analyzing its components, namely the six major applications software most frequently used. These are Computer Aided Design (CAD), Computer Aided Engineering (CAE), Decision Support Systems

(DSS), Management Information Systems (MIS), Project Management Systems (PMS) and Word Processing (WP).

CAD primary purposes are improving product quality, improving safety, reducing engineering time achieved through hard and time consuming design labor, improving product functionality and usability, reducing the number of prototypes and in many cases leading to their elimination and last but not least, reducing product costs. CAE became the computer solution of engineering problems with the assistance and support of interactive computer graphics together with the improvement of graphics displays, engineering workstations, and graphics standards with the main advantages to test, simulate and possibly validate a 3D product without having to build physically.

These software packages have a great influence in facilities management and a positive effect on those who have discovered their potential but a possibly negative one for those who are not able to take advantage of their capabilities.

Bibliography

Pulko, S.H., D. de Cogan, Computer-Aided Engineering Journal, July 1991
Walsh, John, *Secrets of CAFM Success***,** July 2002,
http://www.facilitiesnet.com/facilitiesmanagement/article/Secrets-of-CAFM-Success--1419
Cyros, Kreon L., *Computer aided facilities management* (CAFM) - http://www.eric.ed.gov
Hamer, J., *Facility Management Systems* New York: Van Nostrand Reinhold, 1988.
http://www.caddprimer.com
http://software.cae.wisc.edu/
http://www.cadhelpcenter.com/2010/02/04/definition-of-cadcamcae//

"Computational Civil Engineering 2011", International Symposium
Iasi, Romania, May 13, 2011

Production of thermal insulations using waste cullet

Tomáš Melichar[1], Jirí Bydžovský[2], David Procházka[3]
[1]*Faculty of civil engineering, Institute of Technology of Building Materials and Components, Brno University of Technology, Brno, 602 00, Czech Republic, melichar.t@fce.vutbr.cz*
[2]*Faculty of civil engineering, Institute of Technology of Building Materials and Components, Brno University of Technology, Brno, 602 00, Czech Republic, bydzovsky.j@fce.vutbr.cz*
[3]*Faculty of civil engineering, Institute of Technology of Building Materials and Components, Brno University of Technology, Brno, 602 00, Czech Republic, prochazka.d@fce.vutbr.cz*

Summary

Currently there are several types of recycled glass which do not find any further use and which mean a certain problem for the environment. Regarding the view of consumption of primary raw materials and energy sources, it is also evident that the recycled glass offers enormous potential when choosing appropriate production technology and its optimization. However, there are still no further processing and using in the form of secondary material. In the form of background research, the article discusses potential possibilities of using waste glass which is currently land filled. The intention primarily consists in approaching and defining the difficulties of this issue in relation to current knowledge taken from practice and scientific fields.

The paper discusses several types of thermal insulation. At first, it is about materials based on glass which contain a high percentage of gas phase in the form of closed pores. Then it is also about insulating materials based on drawn glass fibers. All these materials, respectively the products, can even be made of recycled glass too. But not all the types of cullet are used right here.

The conducted research in theoretical field show that production of insulating materials based on waste glass seems to be possible and advantageous while regarding several aspects. However, it is necessary to distinguish between different types of waste cullet. This is mainly due to their chemical composition, specifically the presence of elements which may adversely affect either the production process, final parameters of the produced materials or the environment (toxicity). In the case of TV monitor glass, it is, however, necessary to properly choose the type of expansion additive and suitable temperature mode so that there is no leach of some undesirable elements. As more suitable one, we can see another research with other types of these expansion additives, such as those of secondary energy products.

KEYWORDS: cullet, thermal insulating materials, recycling.

1. INTRODUCTION

Currently, there are many types of recycled glass which find further use in re-manufacturing of glass. It is worth noting that there is, for example, glass from dismantled TV-monitors, light sources and also the cullet from dismantled glued windshield glasses of cars. We can say that these difficult groups of recycled cullet are considered as a problem all over Europe.

For many types of cullet, which also include the TV-monitor glass, fluorescent light tubes as well as the glued glass of cars, there are specialized recycling lines existing. Because of the fact that there are specific types of products, these lines are equipped with new and sophisticated technological devices which allow obtaining a relatively good glass metal. The following figure shows selected elements of the recycling line for processing the TV-monitors.

Figure 1. Line intended for separating various parts of the TV-monitor glass (on the left), technological equipment intended for removing luminophor from the CRT monitor (on the right) [2]

For the recycling of fluorescent lamps and gas tubes, there is only one company adapted for this purpose in the Czech Republic. It is the company that deals with complete processing of fluorescent lamps and gas tube lights. Fluorescent lamp glass is obtained from the recycling line in relation with the equipment intended for processing of linear fluorescent lamps, whereas the fluorescent lamp is to be dismantled to original components by using the controlled mechanical procedure. At first, you have to remove aluminium bases and iron screening slides. Glass body of the fluorescent lamp is then crushed by a crusher and the glass cullets are deprived of the luminophor layer by using vibration techniques. This luminophor consists of calcium halo-phosphate mixed with additive of metals of rare moulds and very low amount of mercury which is essential for creation of discharge. Crushed glass, free of the luminophor and additives, is then later stored in bags of 1 m3. Residual content of the above-mentioned mercury is then less than 5 ppm. A similar method is used also for processing the energy saving lamps. Glass of these

compacts is characterized by the same parameters as in the case of fluorescent lamps.

In the case of car glass recycling, there is some problem with the security foil which is located throughout the area. There is also a problem with content of various resins and toning coating. Car glasses are recycled here mostly by crushing. Of course, the glasses are divided into those with and without the foil. The requirement for strict separation of different types of car glasses has its technological and also financial reasons. The cost of processing windshields containing the foils is almost two and half times more expensive than the cost for processing the windshields which are not connected with this foil. After crushing, the remains of the foil, resins and other impurities shall be removed by using various ways.

Figure 2. The front windshields (with the safety foil) taken from land filled cars (before recycling) [3]

2. THERMAL INSULATION BASED ON GLASS

So-called foam glass is probably the most famous thermal insulation based on glass. This is the material in which the gas phase predominates, i.e. the phase in the form of a closed lightweight system. The skeleton is formed by glass. With regard to the technology used and the final parameters of the components which are produced, it is possible to meet several types of foam glass.

At first, it is the conventional foam glass which is made of a special alumino-silicate glass. This glass shall be ground to particles of very small dimensions to which a frothing agent shall be added - carbon dust in this case. The resulting mixture is spread to steel moulds in a thin layer. These moulds are then subjected to a temperature mode in the tunnel furnace to reach the temperature of about 1000 °C. At this temperature, there is the process of oxidation of carbon particles to the form of CO2 and simultaneously the process of melting glass powder. Leaking gas creates little bubbles which increase the original volume of melted glass up to the

twenty times larger volume, which fills in the entire mould. After this stage of manufacturing process, the generated block of foam glass shall be slowly cooled to the temperature of 200 °C. After the final cooling of the foam glass, there is still CO2 remaining in its individual cells in the vacuum of about one-third of the atmospheric pressure which originates due to reducing the volume of the cooled gas. The blocks which suit all controls are then later cut to the boards of the format of 600×450 mm with a constant thickness (from 30 to 160 mm) or to gradient boards or other shapes.

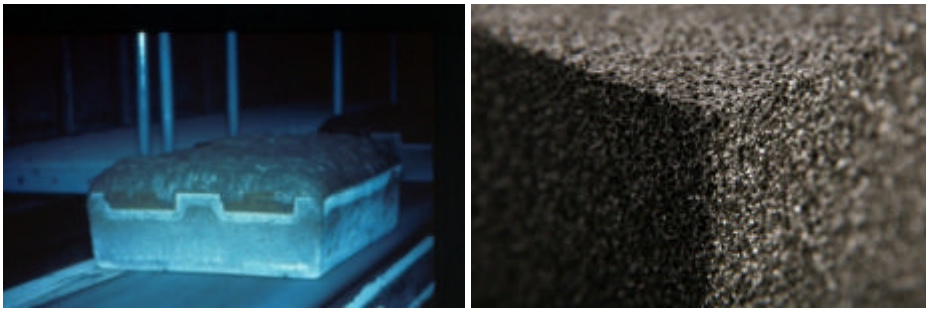

Figure 3. A form with foamed glass outgoing from the furnace (on the left), detail of structure of the processed block of foam glass (on the right) [1]

Furthermore, in recent years, as a response to the current conditions of waste management and the environment, there appeared production technologies which use, for example, waste wrapping glass for production of foam glass which is then used as a lightweight aggregate. Production process is similar to the previous method, however with some variations - temperature mode, input raw materials, strengthening additives etc. It is apparent already from the nature of the input raw materials and method of application of final products that this is not the material of such quality as in the case of classical foam glass which is made of primary raw materials.

Figure 4. Lightweight aggregate based on foam glass and its application in practice as a backfill material [4], [5]

When using the recycled glass, you can also produce the insulating materials on a different basis. These are, for example, blown mineral insulations of glass or mineral-fibre insulation material based on glass. For these purposes, there is the glass of vehicles, specifically the glued windshield glass, now widely used. In the Czech Republic, there are already some production lines intended for recycling of this secondary raw material. There are also some processors who use these cullets. There is an undeniable contribution in this field; this is the fact that it is about processing the raw material which is not suitable for glass production plants. It means that there is a complete processing of waste material in the form of secondary raw material.

Figure 5. Mineral-fibre insulation of glass fibres (on the left) and blown mineral insulation based on glass [6], [7]

3. RESEARCH IN THE AREA OF FOAM GLASS BASED ON RECYCLED CULLETS

Since the recycling of glass and various types of waste recycled glasses have already been known for several decades, the research in this field has been conducted and is still conducted. Even the thermal insulations based on waste glass are not an exception. As stated in the introduction, the current problem, taken from an environmental point of view, consists in the cullet of specific glasses, such as TV-monitors, fluorescent lamps etc, which contain undesirable elements about which the subsequent potential producers and processors are worried. These undesirable elements may result in deterioration of eco-toxicological properties of materials produced and they may also adversely affect the manufacturing process and final parameters of the products.

In [6], glass foams were produced using sheet glass cullet and fly ashes from thermal power plant with added carbonates (commercial dolomite- and calcite-based sludges) as foaming agents. The influence of type and amount of carbonates as well as of the sintering temperature on the apparent density, compressive strength, microstructure and crystalline phases was evaluated. The experimental results showed that homogenous microstructures of large pores could be obtained by adding just 1–2 wt.% carbonates and using low sintering temperature (850 °C), leading to foams presenting apparent density and compressive strength values of about 0.36–0.41 g/cm^3 and 2.40–2.80 MPa, respectively. Good correlations between compressive strength, apparent density and microstructure (pore size, struts' thickness and internal porosity) were observed. [6]

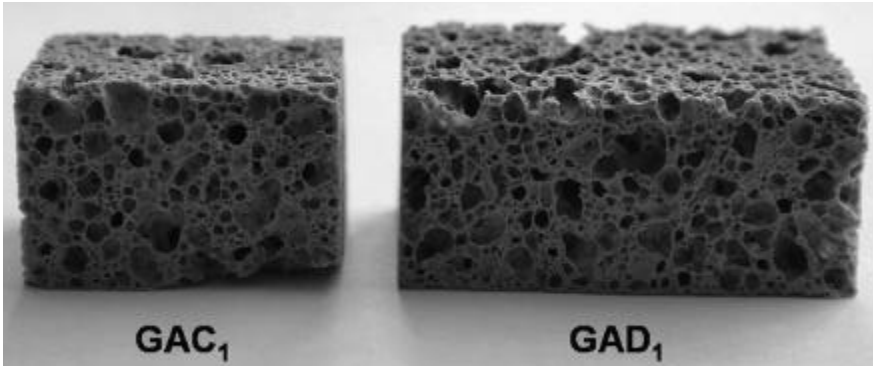

Figure 6. The typical aspect of the glass foams after rectifying – calcium carbonate foaming agent (CAC_1), dolomite foaming agent (CAD_1). [6]

The results presented and discussed along with work [6] enable to draw the following conclusions:

- Glass-based foams with low apparent density (0.36–0.41 g/cm^3) and relatively high compressive strength values (2.40–2.80 MPa) can be produced from a mixture containing 80% of sheet glass and 20% of fly ash with low added amounts of carbonates (1–2%) as foaming agents.
- Increasing the amount of foaming agents tends to enhance crystallization, which in turn is expected to increase the overall viscosity of the system, limiting the expansion and leading to higher values of apparent density and compressive strength.
- For each formulation, the minimum values of apparent density observed at 850 °C depend on a balance between the decrease of viscosity with temperature increase, which favors the expansion of the melt under the internal gas pressure, and the gas release accompanied by the gradual collapse of the foam.

- Besides the apparent density values and the extent of crystallization, the compressive strength of the foams also depends on the internal porosity and thickness of the struts.
- The production of glass foams is a good way to recycle glass wastes and fly ashes, allowing high incorporation percentages of 95–99 wt.%. [6]

In [7], glass foams were produced using glass industrial waste and aluminium nitride as foaming agent. Steelmaking dusts were also used to prepare these expanded materials. Time and temperature process parameters were tuned to adjust physico-chemical properties such as density and porosity. Structural characterisation by X-ray diffraction reveals the amorphous or crystalline nature depending on process parameters. Apparent density varies from 0.2 to 1.2 g cm^{-3} and pycnometric density from 1 to 2.2 g cm^{-3}. The pore nature (close or open) is correlated to the preparation process and the initial batch composition. When doped or coated by titanium dioxide, expanded glasses present a photocatalytic activity in the UV region and were tested for toluene decomposition in gas phase. It was shown that TiO_2- coated foam glasses are efficient, as a support for total toluene photodegradation, in comparison with cellulose/TiO_2 based commercial support. [7]

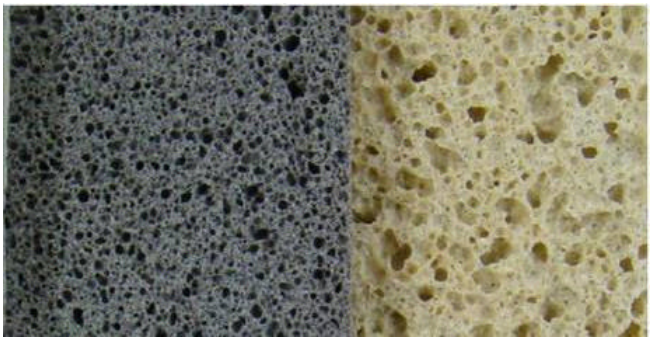

Figure 7. Photography of foam glasses prepared at 850 °C for 4 h – with steel waste (on left) and TiO_2 (on right) [7]

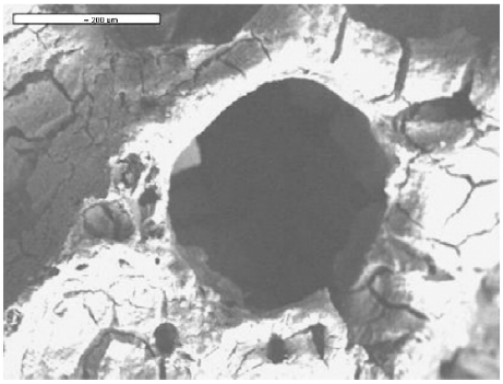

Figure 8. SEM picture of a TiO_2 coated glass foam. [7]

The incorporation of blast furnace smoke or titanium dioxide in the initial batch improves the foaming process. Prepared expanded glasses presented open porosity higher than 70%. Temperature and time influences on foam characteristics were checked and explained. Medium temperature such as 850 °C is sufficient to prepare cellular glasses which were then coated by TiO_2 using a water/alcohol slurry. These coated foams were compared to a commercial catalyst media for the toluene degradation under UV illumination. By analyzing these different materials, the scientists determined that the coated foam glasses are photoactive. The coated foams, that which were analyzed, present a similar effectiveness than commercial photocatalyst paper, but for higher catalyst concentration. However, these first results are very encouraging, and it can be underlined that the glass support presents a strong advantage on cellulose media: after a number of efficient uses, heat treatment or other cleaning treatment are possible on foam glass to potentially restore their photocatalysis power,which ismore delicate to realise with the cellulose support. Therefore, this work [7] shows the real possibility to use industrial waste glass to transform them into photocatalyst support for environmental applications. [7]

Using the AFNOR X 31-210 leaching assessment procedure, the degree of element inertization in foam glasses synthesized from waste CRT glasses (funnel and panel glasses, containing lead and barium/strontium respectively) were determined in [8]. The amount of leached lead from foam glasses prepared from funnel glass depends on the nature and concentration of the reducing agent. The effects of the reducing agents on the generation of cellular structure in the fabrication of foam glass were studied. The fraction of lead released from foam glass was less than those extracted from funnel glass and was lower than the statutory limit. Leached concentrations of barium and strontium were found to be approximately constant in various tests and were also below regulatory limits.

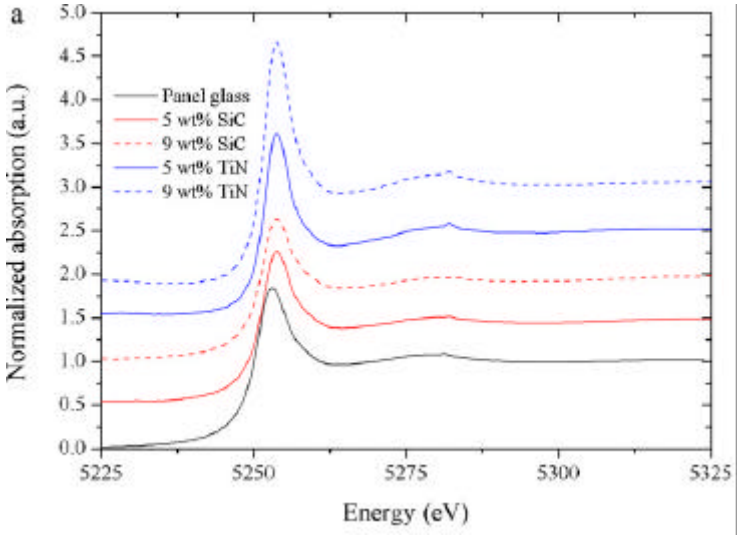

Figure 9. Normalized Ba–L_{III} XANES spectra for funnel glass and foam glasses elaborated with SiC and TiN (C) compared to initial panel glass (for a clear presentation each profile was shifted by 0.5 from its lower-lying profile). [8]

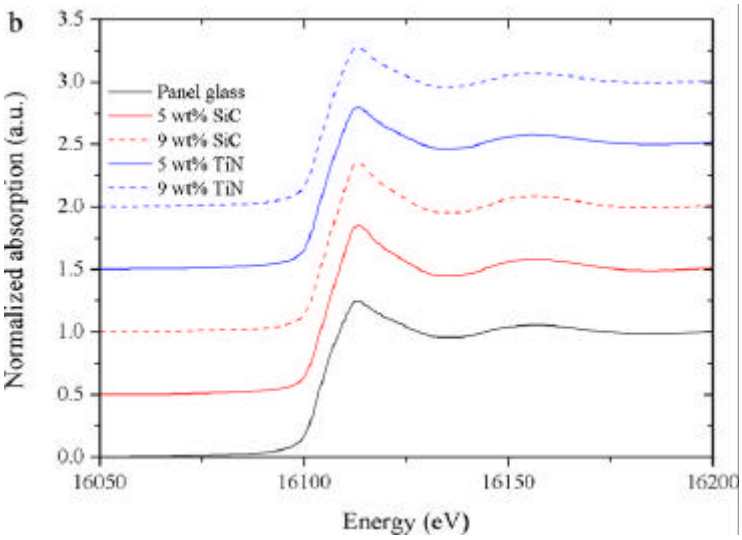

Figure 10. Normalized Sr–K XANES spectra for funnel glass and foam glasses elaborated with SiC and TiN (C) compared to initial panel glass (for a clear presentation each profile was shifted by 0.5 from its lower-lying profile). [8]

The results of leaching tests have shown variations in the behaviour of tested materials depending on the nature of the reducing agent employed and the type of

CRT glass used to obtain the cellular material. The influence of the reducing agent was evidenced by a rise in leached Pb concentration, increasing in line with the accessible surface area of the sample. The scientists showed that the amounts of Pb released from samples prepared with low concentrations of reducing agent, particularly those synthesized employing SiC, were under the regulatory limits. In contrast, when TiN was employed, the highest amounts of Pb released exceeded the legislative limits. The use of TiN for foam glass synthesis was appropriate when a mixture of the two types of glass–funnel and panel was employed. A porous material with lower lead leachability was obtained. The amounts of released Ba were under the regulatory concentration whatever the reducing agent content. Finally, the levels of released Sr depended on the accessible porosity of the material, and this was in turn influenced by the proportion of funnel glass and the concentration of the reducing agent. [8]

4. CONCLUSIONS

The article was focused on production of heat insulation materials made of waste glass which for now do not find a broader ways of use (TV-monitors, fluorescent lamps, etc.). These cullet are problematic particularly due to the content of certain elements which cause negative chemical effects during the production, or also during incorporating the particular product to the structure frame (e.g. leaching of harmful chemical elements).

Regarding the above-mentioned findings and facts, which are supported by the results of the research works of scientific experts, we can clearly state the following:

- Production of insulating materials based on waste glass is possible and advantageous from several aspects. However, it is necessary to distinguish between different types of waste cullets. This is mainly due to their chemical composition, specifically the presence of elements which may adversely affect either the production process, final parameters of the produced materials or the environment (toxicity).
- In the case of foam glass, especially the following factors play the crucial role:
    - chemical composition of input raw materials,
    - size of charge particles,
    - type of expansion additive,
    - temperature mode curve.
- The following fact means quite a significant finding [8] in the case of the TV-monitor glass. This is the fact that leaching of lead, strontium and barium is strongly influenced by the type, it means the chemical composition, of frothing additive. Therefore, when exceeding the limits which are specified by

the particular legislation or normative documents, it could be possible avoid the adverse effects by using appropriate additives in combination with suitably chosen temperature mode.

- Possibility of using expansion additives on a different basis seems to be the best solution, ideally on the basis of one of the secondary energy products with a suitably modified temperature mode and specified size of the charge fraction.

Acknowledgements

The text has been drawn up within the MSM 0021630511 research project – "Progressive Building Materials with Utilization of Secondary Raw Materials and their Impact on Structures Durability".

References

1. URL:< http://www.foamglas.cz/infor_produkt.htm>.
2. Zpetný odber, magazín ASEKOL, C. 1/2007 URL:< http://www.asekol.cz/cs/download/spotrebitele/casopis-zpetny-odber/zpetny_odber_1_07.pdf>.
3. URL:<www.splrecycling.com>.
4. URL:<http://www.pasivnidomy.cz/akce/pozvanka-na-prezentaci-penoveho-skla-refaglass.html>.
5. URL:< http://zateplovani.name/author/admin>.
6. Fernandes, H., R.; Tulyaganov, D., U.; Ferreira, J., M., F. *Preparation and characterization of foams from sheet glass and fly ash using carbonates as foaming agents*, Ceramics International 35, ELSEVIER, 2009, p. 229 - 235. URL: <www.sciencedirect.com>
7. Lebullenger, R.; Chenu, S.; Rocherullé, J.; Merdrignac-Conanec, O.; Cheviré, F.; Tessier, F.; Bouzaza, A.; Brosillon, S. *Glass foams for environmental applications*, Journal of Non-Crystalline Solids 356, ELSEVIER, 2010, p. 2562 – 2568. URL: <www.sciencedirect.com>
8. Yot, G., P.; Méar, O., F. *Characterization of lead, barium and stroncium leachability from foam glasses elaborated using waste cathode ray-tube glasses*, Journal of Hazadous Materials 185, ELSEVIER, 2011, p. 236 – 241. URL: <www.sciencedirect.com>

Dynamic nonlinear analysis of structural reinforced concrete walls energy dissipators with shear connections

Sergiu Andrei Baetu[1], Ioan Petru Ciongradi[1], Andrei-Ionut Stefancu[1]
[1]*Department of structural mechanics,* "Gheorghe Asachi" Technical University, Jassy, *Zip code, Romania*

Summary

Structural reinforced concrete walls are a structural system that provides lateral resistance, high stiffness and strength to a building. Because the energy dissipation is made only by the base of the structural walls, they do not exhibit ductile and redundant behavior. The structural reinforced concrete wall energy dissipator named and structural slit wall with shear connections remove some of the problems encountered with ordinary structural walls. Yielding of shear connections in this wall may cause increase in energy dissipation, forming a structural damper that is based on structural passive control.

In this paper, the dynamic nonlinear analysis on energy dissipator wall with shear connectors is done and the influence of the elasto-plastic behavior of the shear connections is evaluated. This type of structural wall is compared to an ordinary solid wall. In order to obtain the optimal control effect, the stiffness and strength of the energy dissipation device should be optimized by selecting the dimensions of the shear connections.

The objective of this solution is to create an ideal structure for tall multi-storey buildings, that behaves as a rigid structure at low seismic action and turns into a flexible one in case of a high intensity earthquake action.

KEYWORDS: structural reinforced concrete walls energy dissipators, dynamic nonlinear analysis, ductile behavior, shear connections.

1. INTRODUCTION

Reinforced concrete walls are strength elements frequently used in construction in seismic areas, because they have a high lateral stiffness and resistance to external horizontal loads.

If the wall stiffness is high, the seismic loads taken by the structure become higher, resulting non-economic sections for the wall. This phenomenon occurs particularly in multi-storey tall buildings. In case of high intensity earthquakes flexible

structures are preferred because can accept large deformations, instead for low intensity earthquakes that occur frequently, or for wind action, rigid structures should be considered, because prevent large displacements. The dissipation of the accumulated energy in the structural wall systems occurs generally through concentrated degradation at the base of the wall, which is difficult to repair. Numerous investigations have been made to improve redundancy and ductility of structural walls exposed to horizontal actions and some practical solutions were proposed.

1.1 Slit walls literature review

Slit walls are a special variant of structural walls with improved ductility. The specialists intention was to reduce the degradation from the base of the wall and distribute it on the wall height.

First reinforced concrete structural wall, with good properties of seismic energy dissipation, called slit wall was patented by Professor Kiyoshi Muto in Japan in 1973 (Figure 1) [1]. These walls are the first energy dissipation system used in the structures of Japan.

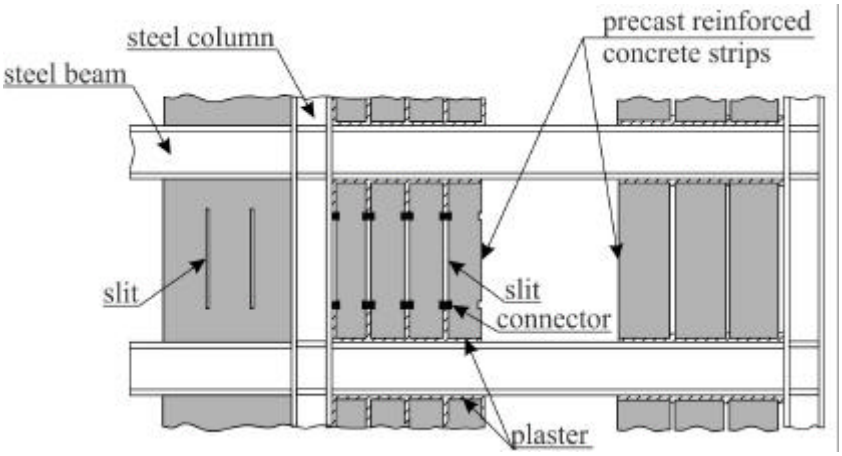

Figure 1. Slitted panels

The structural reinforced concrete energy dissipator wall with shear connections is first analyzed by researchers from Chinese University of Hong Kong (Figure 2) [2]. Reinforced concrete connections were placed on the slit height which attach the structural walls forming a dissipative zone.

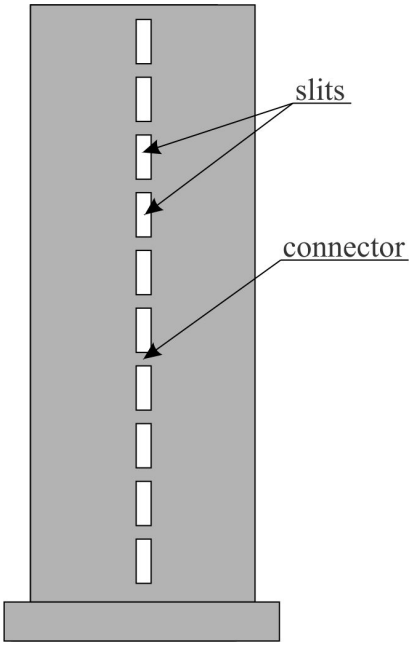

Figure 2. Structural slit wall with shear connections

It is designed in such a way that under normal wind and earthquakes, the shear connections would remain elastic so that the structural slit wall behaves like a solid wall but when overloaded due to earthquake attack, the shear connections would yield thereby decreasing the lateral stiffness and increasing the damping capacity of the structural system. Although the shear connections would be damaged after yielding, their sacrifice would help to protect the wall itself, which is very difficult to repair. Seismic performance depends on the yielding resistance of the connections. An efficient design of these systems must take into account a rational design of the connectors. The premature yielding of the connectors must be avoided and also the destruction of walls without yielding of the connectors.

1.2 Modeling techniques for RC shear walls

During the recent years, an enormous effort has been done to provide analytical models that are able to simulate the actual behavior of RC elements including shear walls. The rapid increase in the computational efficiency of computers helped the researchers to develop more sophisticated models that can account for several phenomena of RC shear walls that were used to be ignored in the analysis due to their complexity. For these models to be verified, experimental research is continuously conducted on RC shear walls tested under monotonic, cyclic, or dynamic loading. The numerical modeling of RC elements started by Clough in 1965 when he proposed the first nonlinear macro-model, and by Ngo and Scordelis

in 1967 who proposed the first application of the finite element method of analysis in RC elements. Since then several advancements were done in the area of modeling of RC elements including shear walls. Numerical models proposed by researchers for the analysis of RC shear walls are:

- macro-models such as one- and two-component elements, multi-axial spring models, truss models, softened-strut-and-tie models, three vertical line element (TVLE) models and multiple vertical line element (MVLE) models [3][4],
- micro-models such as the finite element models, layer models and fiber models [5].

Micro-modeling is based on representing the behavior of different materials that compose the RC element and the interaction between them. The member is meshed into small elements and principles of equilibrium are applied. This approach is complex and needs high numerical processing efforts, and hence it might not be practical for large structures and it is limited to model individual structural components with small dimensions such as a column, a beam or a wall. On the other hand, macro-modeling is based on representing the overall behavior of the RC element, such as the wall deformations, strength, and energy dissipation capacity. The global behavior of the RC element using a macro-model should be calibrated using an experimental verification to adjust the parameters needed for the model. This approach is simple and does not require high numerical efforts, which makes it suitable to simulate the response of large structures. The cyclic behavior of RC shear walls should be defined using a hysteretic model that is able to simulate different inelastic phenomena of reinforced concrete materials. The modeling of the hysteretic behavior of the RC element can affect the element response significantly. These models can be used to represent the axial, flexure and shear behavior of the element. The hysteretic model consists of a primary curve (backbone curve) that control the monotonic loading and some hysteresis rules that control the loading and unloading element behavior under cyclic loading. The control parameters of the hysteresis rules are adjusted to simulate the actual cyclic behavior of the tested wall. In case of wall modeling using concrete and steel springs, the behavior of the element is controlled by the constitutive laws predefined for the model springs. Appropriate definition of the hysteretic behavior of the RC wall is an important issue, and a special attention should be directed to the interaction of the hysteresis models used for different element springs (e.g. flexure and shear springs). Several improvements in the hysteretic models were accompanied by the advancements in the wall modeling, and that will be discussed in the following sections [3][6].

1.3 IDARC 2D 7.0 Software

The first version of IDARC (Inelastic Damage Analysis of Reinforced Concrete building structures) was developed in 1987 by the National Center for Earthquake Engineering Research (NCEER) at the State University of New York at Buffalo [7]. IDARC2D is developed for modelling of inelastic structures for analysis, design and support of experimental studies and to link experimental research and analytical developments. It is an open source software built in FORTRAN and capable of taking care of material and geometric nonlinearities. Properties of members are calculated by fiber models or by mechanics based formulations and solutions are obtained using step-by-step integration of equations of motions using ß-Newmark method. The software uses distributed flexibility model that has replaced the commonly used hinge model developed for steel frames as the hinge model is not suitable for reinforced concrete elements since the inelastic deformation is distributed along the member rather than being concentrated at critical sections [8]. Structural walls are modelled using a combination of shear, axial and flexure springs connected in series (Figure 3) and using a three parameter Park model (Figure 4) (Figure 5). Beam elements are modelled as flexural-shear elements, using three parameter Park model as hysteretic model. The beam elements include a rigid length zone to simulate the increase in stiffness at the joint or wall zone.

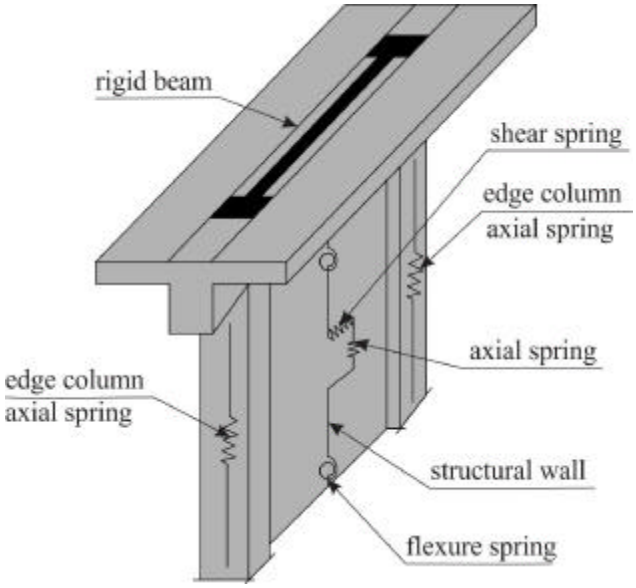

Figure 3. Structural wall model

The three parameter “Park hysteretic model” was first proposed by Park et al. (1987) as part of the original release of IDARC. The hysteretic model incorporates stiffness degradation, strength deterioration and pinching (slip lock caused by crack-closing). The model traces the hysteretic behavior of an element as it changes from one linear stage to another, depending on the history of deformations [9].

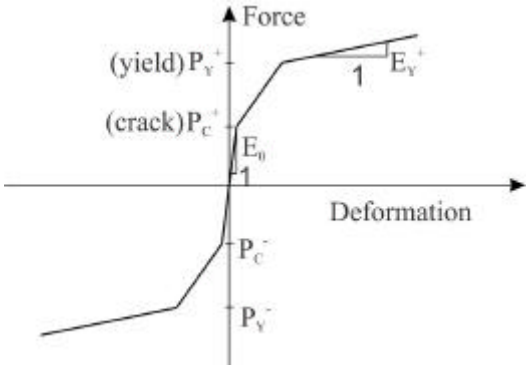

Figure 4. Tri-linear envelope

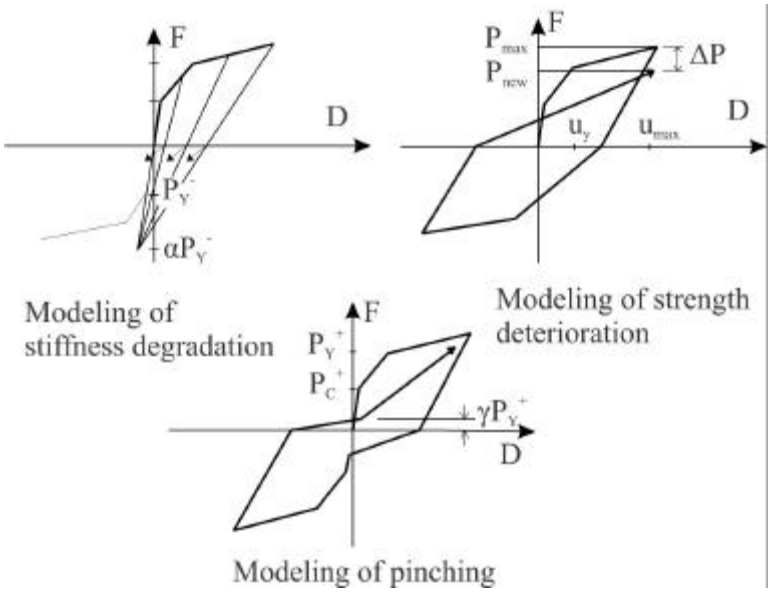

Figure 5. Hysteretic model and control parameters

Stiffness degradation is controlled by the parameter, a, and is defined by the rotation of unloading branches round the target point on the elastic branch rotating in a distance. Stiffness degradation is one of the main properties in hysteretic

behavior. From the experimental results, the stiffness degradation model is determined based on various stiffness characteristics at different stages of cracking, yielding, unloading and reloading in the cyclic loading. Stiffness degradation increases drift capacity in structures. Stiffness degradation changes the energy absorption and the period of the system.

Strength deterioration controlled by the parameter, ß, is introduced as a function of dissipated hysteretic energy. Parameter, ß, shows the rate of strength reduction. It is assumed that the strength of the hinge will be reduced after each yielding state. The amount of stress loss in each cycle is the function of section property and the maximum rotation during previous cycle.

Pinching is another principle property of hysteresis behavior and is incorporated by lowering the target point of the force-deformation curve upon crossing the force-axis through the control parameter, ?. Pinching is due to the opening and closing of the cracks under cyclic loads. When the shear accompanying the moment is high sliding along the through – depth crack can occur. This sliding shear displacement which is resisted mainly by dual action of longitudinal reinforcement is reflected in a pinching of the associated load deflection near the origin, since the area under load deflection curve is a measure of the energy dissipation capacity of the member, the pinching in this curve due to sliding shear, represent degradation which is the effect of strength and the energy dissipation capacity of the hinging region. When the longitudinal steel is not adequately retrained by lateral reinforcement inelastic buckling of the compressive reinforcement immediately follows by rapid loss of flexural strength. Pinching behavior has a very small effect on drift capacity [10].

Table 1. Values for hysteretic parameters

Element	Parameter	Meaning	Value	Effect
Structural wall	HC (a)	Stiffness degrading parameter	12	Moderate degrading
	HBD (ß1)	Strength degrading parameter (ductility-based)	0.01	No degrading
	HBE (ß2)	Strength degrading parameter (energy-controlled)	0.1	Moderate deteriorating
	HS (?)	Slip or Crack-closing parameter	1	No pinching
Shear connections	HC (a)	Stiffness degrading parameter	2	Severe degrading
	HBD (ß1)	Strength degrading parameter (ductility-based)	0.4	Moderate degrading
	HBE (ß2)	Strength degrading parameter (energy-controlled)	0.4	Severe deteriorating
	HS (?)	Slip or Crack-closing parameter	0.2	Moderate pinching

2. STRUCTURE DESCRIPTION

This building was used as a case study in a paper written at International Symposium CCE2010 [11], and is located in Jassy with site characteristics: design ground acceleration a_g =0.2g, control period T_c=1.6s, ductility class H, importance factor ?$_I$=1 [12]. It was considered a dual reinforced concrete structure, with regular form in plan and elevation. Seismic lateral loads are taken by the concrete core and by the border walls of the building disposed on short direction. The building has 20 levels resulting a height of 60 m, each level has a height of 3m (Figure 6). The concrete from critic zone is C32/40 (Table 2) and the reinforcement is S355 (Table 3) (Figure 7). Fundamental period of the structure is T_1=1.077s. The investigation focused on the research of a lateral wall with length of 10m. The design analysis was achieved in Etabs Nonlinear, resulting that the thickness wall is 40 cm and is reinforced with vertical bars F 14/15 and horizontal bars F 10/15 [13].

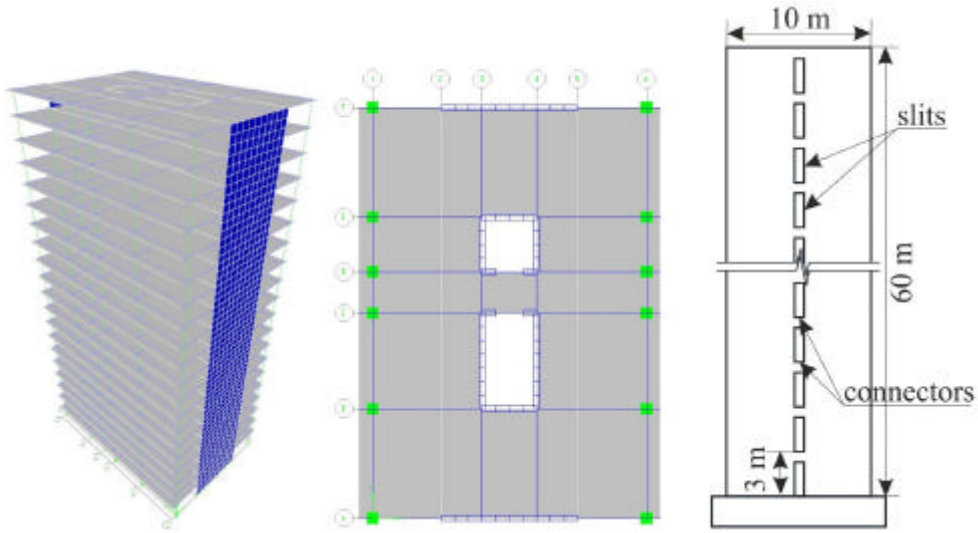

Figure 6. 3d view, building plan and wall dimensions

Table 2. Properties for concrete C32/40

Unconfined compressive strength (FC)	0.0316 (GPa)
Initial Young's modulus of concrete (EC)	36 (GPa)
Strain at max. strength of concrete (%) (EPSO)	0.2
Stress at tension cracking (FT=0.12*FC)	0.003792(GPa)
Ultimate strain in compression (%)(EPSU)	0.4
Parameter defining slope of falling branch (ZF)	0 (default)

Table 3. Properties for reinforcing bars S355

Yield strength (FS)	0.355 (GPa)
Ultimate strength (FSU=1.4*FS)	0.497 (GPa)
Modululs of elasticity (ES)	210.0 (GPa)
Modulul of strain hardening (ESH)	2.1 (GPa)
Strain at start of hardening (%)(EPSH)	3.0

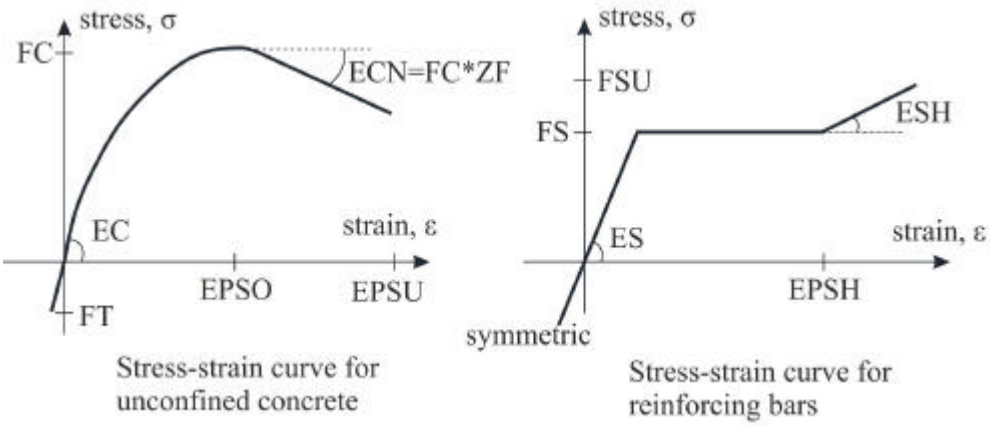

Figure 7. Material stress-strain relationships

3. DYNAMIC NONLINEAR ANALYSIS

3.1 Structural modeling

Connections are modeled as flexible beams in slit region and as infinite rigid beams in the wall region (Figure 8). In the analysis with IDARC 2D software the nonlinear inelastic behavior of the connections and of the two walls connected is considered. The gravity loads include slit wall weight and loads from floor connected to the wall and results a total force of 11180 kN. The mass of each storey is taken as 559 kN. A structural solid wall having the same dimensions and mass as the slit wall models studied is also analyzed to provide a basis for evaluating effectiveness of the proposed structural system.

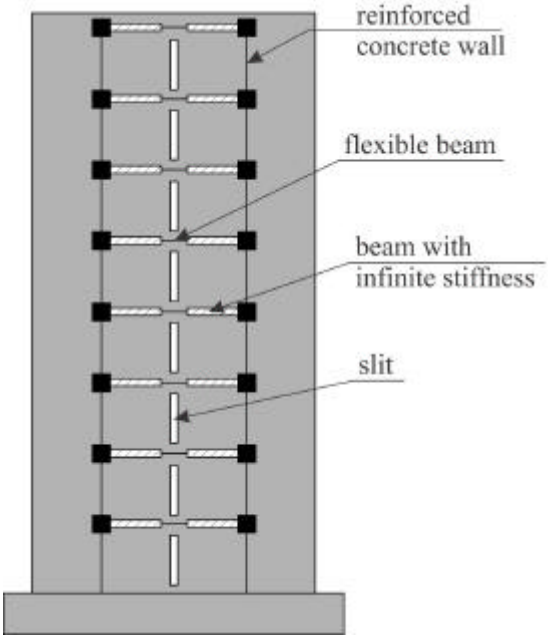

Figure 8. Structural modeling of the slit wall

3.2 Numerical solution

Step integration method ß-Newmark is used for nonlinear dynamic analysis to obtain the dynamic equation of motion solutions. To obtain a dynamic response of the structure accurately, the time step for response analysis is 0.001s. The dynamic equation of motion at any time *t* is written incrementally in the following form [9]:

$$[M]\{\Delta\ddot{u}\} + [C]\{\Delta\dot{u}\} + [K_t]\{\Delta u\} = -[M](\{L_h\}\Delta\ddot{u}_{gh} + \{L_v\}\Delta\ddot{u}_{gv}) - \{\Delta P_V\} - \{\Delta P_{FR}\} - \{\Delta P_{HY}\} - \{\Delta P_{IW}\} + c_{corr}\{\Delta F_{err}\} \quad (1)$$

[M] – is the lumped mass matrix of the structure;

[C] – is the damping matrix of the structure;

$[K_t]$ – is the tangent stiffness matrix of the structure;

$\{\Delta\ddot{u}\}, \{\Delta\dot{u}\}$ *and* $\{\Delta u\}$ – are the incremental vectors of nodal acceleration, velocity and displacement in the structure;

$\{L_h\}$ and $\{L_v\}$ – are the allocation vectors for the horizontal and vertical ground acceleration;

$\{\Delta\ddot{u}_{gh}\}$ *and* $\{\Delta\ddot{u}_{gv}\}$ – are the increment in the horizontal and vertical ground accelerations;

$\{\Delta P_V\}, \{\Delta P_{FR}\}, \{\Delta P_{HY}\}$ *and* $\{\Delta P_{IW}\}$ – are the restoring forces from viscous dampers, friction dampers, hysteretic dampers, and infill panels;

c_{corr} – is a correction coefficient (usually taken as one);

$\{\Delta F_{err}\}$ – is the vector with the unbalanced forces in the structure.

The dumping matrix is calculated in the program with the following form:

$$[C] = a_M [M] + a_K [K_t] \tag{2}$$

Coefficients a_M *and* a_K are calculated depending on the type of damping matrix selected: mass proportional damping, stiffness proportional damping or Rayleigh damping. Rayleigh damping is assumed:

$$a_M = \frac{2x_i w_i w_j^2 - 2x_j w_j w_i^2}{w_j^2 - w_i^2} \tag{3}$$

$$a_K = \frac{2x_j w_j - 2x_i w_i}{w_j^2 - w_i^2} \tag{4}$$

w_i *and* w_j – are the natural frequencies of the structure corresponding to modes i and j;

x_i *and* x_j – are the damping ratios of the structure corresponding to modes i and j. In the analysis, the damping ratios are taken as 5%.

3.3 Seismic response of the structural slit wall system

The nonlinear response of the structural slit wall system under Vrancea 1977 N-S earthquake (Figure 9) was studied.

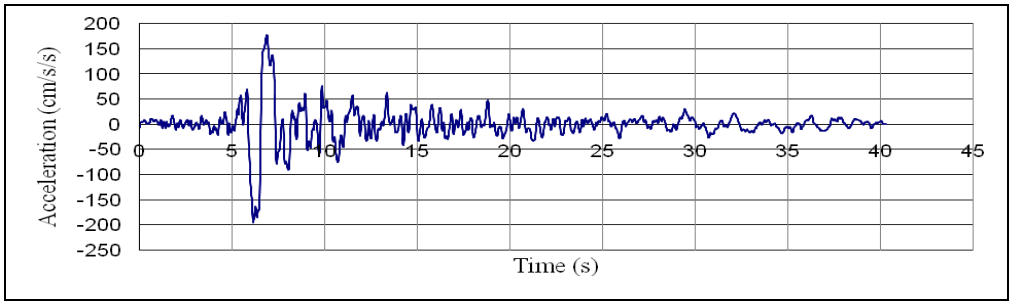

Figure 9. Acceleration record of Vrancea 1977 N-S

Two cases were studied:

- in first case was varied the peak ground acceleration and were kept constant the height of shear connectors, the thickness of the slit and the quantity of longitudinal reinforcement from connector;
- in second case was varied the height of shear connectors and were kept constant the peak ground acceleration, the thickness of the slit and the quantity of longitudinal reinforcement;

The peak ground acceleration (PGA) was increased from 0.08g to 0.70g which excited the model from elastic state to failure state. The height of shear connectors is 400 mm, the thickness of the slit is 40 mm and the longitudinal reinforcement is 3F 10 up and 3F 10 down. This structural slit wall is compared to an ordinary solid wall with the same dimensions.

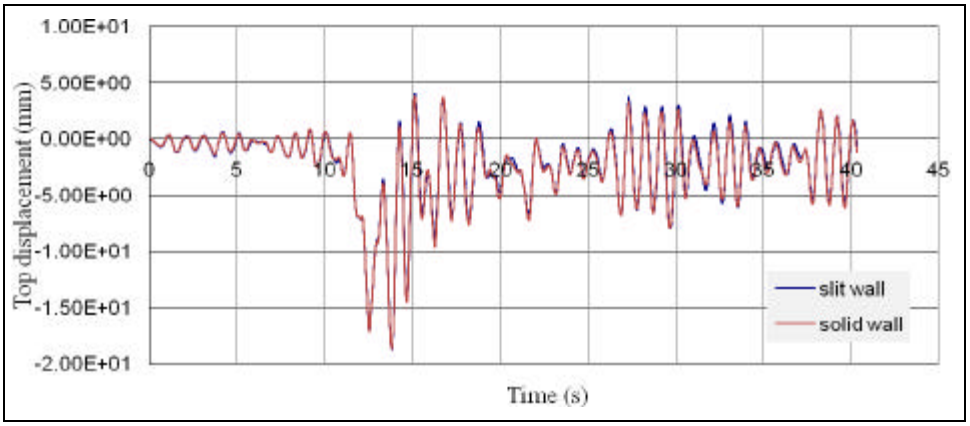

Figure 10. Comparisons between time-histories of top displacement (PGA=0.08g)

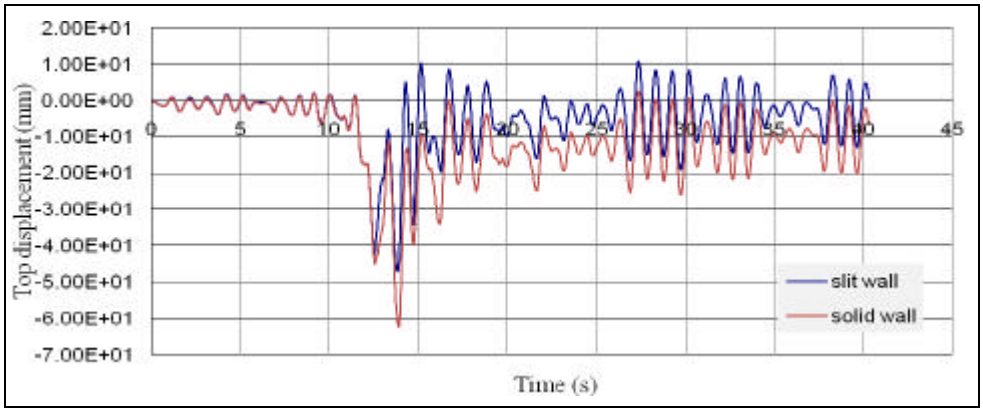

Figure 11. Comparisons between time-histories of top displacement (PGA=0.2g)

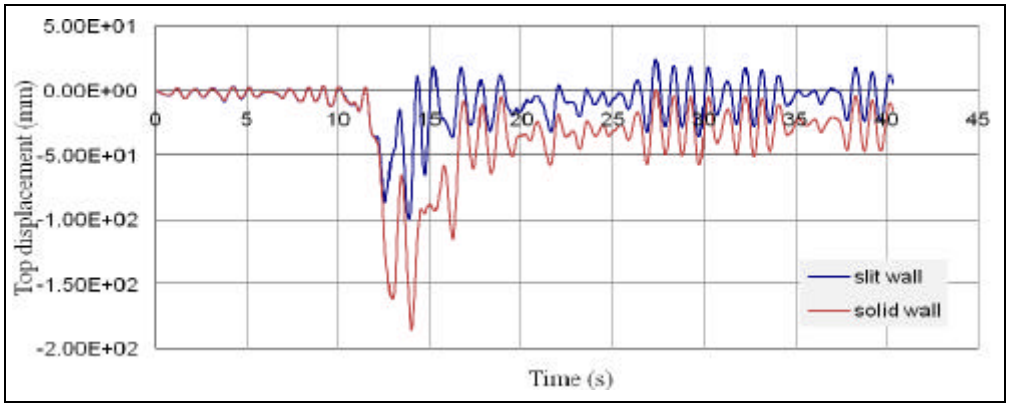

Figure 12. Comparisons between time-histories of top displacement (PGA=0.4g)

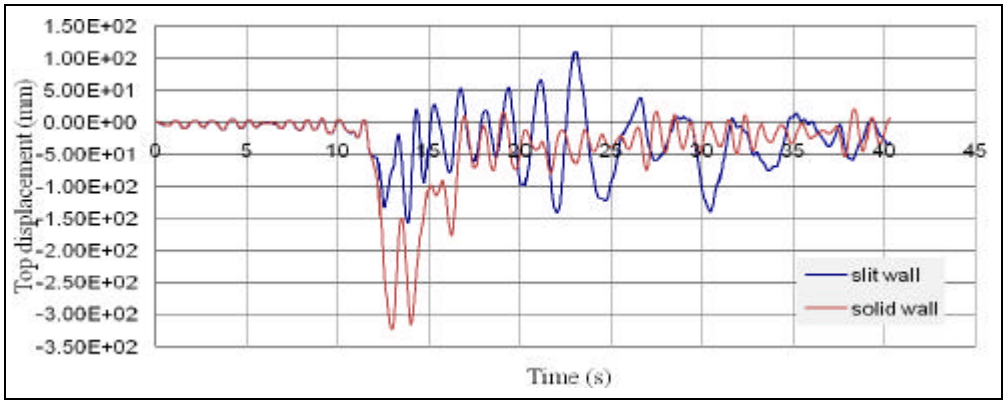

Figure 13. Comparisons between time-histories of top displacement (PGA=0.6g)

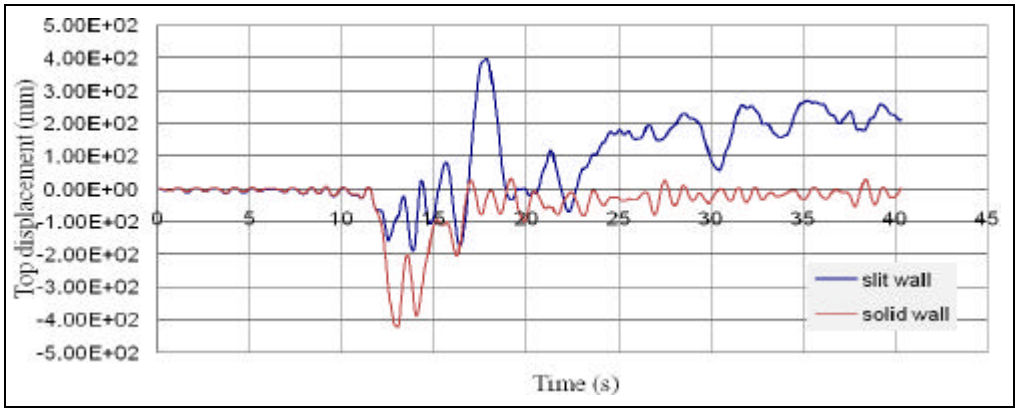

Figure 14. Comparisons between time-histories of top displacement (PGA=0.7g)

The seismic responses of the slit wall and solid wall are found to have similar patterns for PGA equal to 0.08g (Figure 10), indicating that the slit wall behave like a solid wall while the models are excited in elastic state. When PGA reaches to 0.2g, cracks appear at the base of the proposed walls, and the response of the slit wall is almost identical to that of the solid wall (Figure 11). At PGA=0.4g, the seismic response of the slit wall become smaller than response of solid wall (Figure 12), because the cracks are distributed in half of the shear connectors and at the base of the wall (energy is dissipated by connectors and by wall) compared to the solid wall were all the cracks are being concentrated at the base (energy is dissipated only by wall). At PGA=0.6g, it can be seen clearly that yielding of all shear connectors can reduce the deflection response of the structure (Figure 13). Another effect is the gradual increase in the period of vibration of the slitted wall. The increase of the PGA to 0.7g, produces crushing and expulsion of the concrete from the short connectors and results a total separation of the slit wall in two independent solid walls (Figure 14). The top displacement increased and the response of the slit wall gets worse compared to the response of the solid wall. An increase above this value is not recommended because after all connectors fail, the rigidity of the slit wall becomes very small and the displacements exceed the ultimate limit state. If we want to apply a bigger PGA, the height of the shear connection must be increased.

In second case of study was varied the height of shear connectors from 200 mm to 500 mm. The peak ground acceleration (PGA) is 0.32g, the thickness of the slit is 40 mm and the longitudinal reinforcement is 3F 10 up and 3F 10 down. These structural slit walls are compared to an ordinary solid wall with the same dimensions.

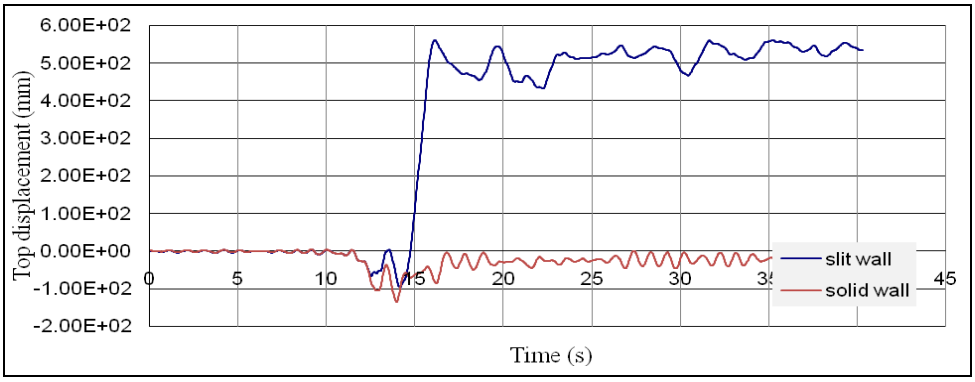

Figure 15. Comparisons between time-histories of top displacement ($H_{connector}$=200 mm)

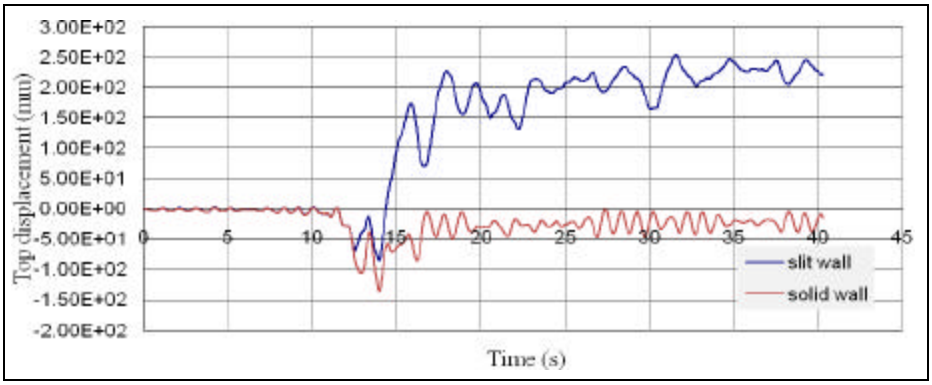

Figure 16. Comparisons between time-histories of top displacement ($H_{connector}$=250 mm)

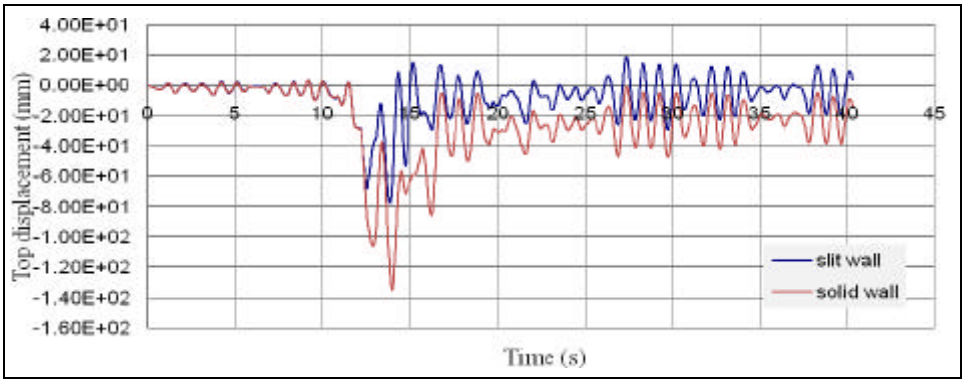

Figure 17. Comparisons between time-histories of top displacement ($H_{connector}$=300 mm)

It is evident that the performance of a slit wall depends on the yield strength of the short connectors. In this case, as the height of the short connectors increases result that the response of the slit wall become almost identical to that of the solid wall (Figure 17). For peak ground acceleration (PGA) equal with 0.32g, the height of shear connectors must be higher than 200 mm. If it is lower than this value, the connectors fail to early and a small quantity of energy will be dissipated (Figure 15). When height is 300mm or higher, the shear connectors doesn't fail, only a few connectors from the base of the wall develop cracks.

5. CONCLUSIONS

An economical design of buildings based on performance takes into account the dissipation of seismic energy accumulated in the structure. Reinforced concrete walls are frequently used as strength elements for structures designed in areas with high seismic risk. The fact is, in a tall shear wall, plastic hinge formation happens only at the base of the wall and ductility resources of the rest of the wall remains untapped. If ductility is a major concern, shear walls are not considered an efficient structural component. The main problems of these structural elements - low ductility and redundancy - are removed through the solutions presented in this article. The shear connections prevent collapse of the structure under extreme seismic excitations by dissipating energy through shear yielding. For best performance, the shear connections should maintain their load carrying and energy dissipation capacities until the whole structure fails. By introducing vertical slits into a structural wall and designing the shear connections formed between consecutive slits to yield before the wall, the deflection response of the structural wall and the seismic loading induced can be reduced.

References

1. Muto, K., Ohmori, N., Itoh, T., *Composite building structure and walls therefor*, United States Patent 3736712, 1973.
2. Kwan, A.K.H., Dai, H., Cheung, Y.K., *Non-linear seismic responce of reinforced concrete slit shear walls*, Journal of Sound and Vibration, vol. 226, 1999.
3. Galal K., El-Sokkary H., *Advancement in modeling of RC shear walls*, The 14th World Conference on Earthquake Engineering, Beijing, China, October 12-17, 2008.
4. Orakcal K., Massone L.M., Wallace J.W., *Analytical modelling of reinforced concrete walls predicting flexural and coupled-shear-flexural responses*, PEER Report, University of California, Berkeley, 2006.
5. Taucer F.F., Spacone E., Filippou F.C., *A fiber beam-column element for seismic response analysis of reinforced concrete structures*, PEER Report, University of California, Berkeley, 1991.
6. Labdaoui K., *Cercetari asupra comportarii si calculul structurilor cu pereti din beton armat supuse la actiuni seismice*, Ph.D. Thesis, University of Constructions Bucharest, 2010.
7. Yonghui R., *Nonlinear time history and push-over analyses for seismic design and evaluation*, Ph.D. Thesis, The University of Texas at Austin, 1996.
8. Ali M.S., *Study of energy dissipation capacity of RC bridge columns under seismic demand*, Ph.D. Thesis, University of Engineering and Technology Peshawar, Pakistan, 2009.
9. Valles R.E., Reinhorn A.M., Kunnath S.K., Madan A., *IDARC 2D Version 4.0: A program for inelastic damage analysis of buildings*, Tehnical Report NCEER-96-0010, State University of New York at Buffalo, 1996.
10. Motaghed S., Khooshehcharkh A., *Damage-based optimal longitudinal reinforcement for RC frames*, European Journal of Scientific Research, vol. 50, no. 2 (2011), pp. 191-201.
11. Sergiu Andrei Baetu, Ioan Petru Ciongradi, Georgeta Vasies, *Static nonlinear analysis of structural reinforced concrete walls energy dissipators with shear connections*, "Computational Civil Engineering 2010", International Symposium, Iasi, Romania, May 28, 2010.
12. *Cod de proiectare seismica* P100-1/2006. (in Romanian)
13. *Cod de proiectare a constructiilor cu pereti structurali CR 2-1-1.1-2006.* (in Romanian)

"Computational Civil Engineering 2011", International Symposium
Iasi, Romania, May 13, 2011

A New Prediction Model for Soil Deformation Modulus Based on PLT Results

Ali Mollahasani[1], Amir Hossein Alavi[2], Amir Hossein Gandomi[2,3], Jafar Boluori Bazaz[1]

[1]*Department of Civil Engineering, Ferdowsi University of Mashad, Mashad, Iran*
[2]*College of Civil Engineering, Iran University of Science and Technology, Tehran, Iran*
[3]*College of Civil Engineering, Tafresh University, Tafresh, Iran*

Summary

In this study, a new empirical model was developed to predict the secant soil deformation modulus (E_s) using linear genetic programming (LGP). The best LGP model was selected after developing and controlling several models with different combinations of the influencing parameters. The experimental database used for developing the model was established upon a series of plate load tests (PLT) conducted on different soil types. A sensitivity analysis was carried out to determine the contributions of the parameters affecting E_s. The proposed model gives precise estimations of the soil deformation modulus.

KEYWORDS: Soil deformation moduli; Soil physical properties; Linear genetic programming; Nonlinear modeling.

1. INTRODUCTION

The modulus of soil deformation is an important parameter for the behavior analysis of substructures. The soil modulus can be obtained from a stress-strain curve. According to the theory of elasticity, the strains experienced by the soil are linearly related to the stresses applied. This is not in practice true for soils since both elastic and plastic deformations occur during the loading. Because of the elasto-plastic behavior of soils, different moduli can be derived from the stress-strain (load-settlement) curves of laboratory or field test results [1, 2]. The soil deformation moduli are usually evaluated by laboratory or field methods. The field test results have been found to be more reliable than those of the laboratory methods [3]. Among different field tests, plate load tests (PLT) has been a traditional in-situ method for estimating the soil moduli. Using the results obtained from this test allows minimization of the effects of the scale factor and soil sample

disturbance [4]. Several researches have shown that the plate load test provides reliable predictions of the soil modulus [5]. Despite reliability of this testing method, little attention is devoted to developing empirical solutions relating the deformation moduli obtained from the plate load test results to the physical properties of soils. In this context, Reznik [3] proposed analytical expressions describing dependence of the plate load deformation moduli of collapsible soils on void ratio and moisture content. Nearly all of the developed empirical correlations for the soil moduli prediction have been established based on regression analysis [6]. The significant limitations the traditional statistical techniques strongly affect the prediction capabilities of the derived equations.

The main purpose of this paper is to obtain a new empirical relationship for determining soil secant modulus (E_s) utilizing linear genetic programming (LGP) method. Various predictor variables included in the analysis were coarse and fine-grained contents, grains size characteristics, liquid limit, moisture content, and soil density. The proposed model was developed based on several plate load tests performed in this study.

2. LINEAR GENETIC PROGRAMMING

Genetic programming (GP) [7] is a symbolic optimization technique that creates computer programs to solve a problem using the principle of Darwinian natural selection. The breakthrough in GP came in the late 1980s with the experiments on symbolic regression [7]. GP is an extension of genetic algorithms (GAs). This classical GP technique is also referred to as tree-based GP [7]. The main difference between the GA and GP approaches is that in GP the evolving programs (individuals) are parse trees rather than fixed-length binary strings.

Linear genetic programming (LGP) [8] is a subset of GP with a linear representation of individuals. In contrast with traditional GP, application of LGP in the field of civil engineering is totally new and original [9].The main characteristic of LGP in comparison with traditional tree-based GP is that expressions of a functional programming language (like LISP) are substituted by programs of an imperative language (like C/C++) [8, 10]. Figure 1 presents a comparison of the program structures in LGP and tree-based GP. A linear genetic program can be seen as a data flow graph generated by multiple usage of register content. That is, on the functional level the evolved imperative structure denotes a special directed graph. In tree-based GP, the data flow is more rigidly determined by the tree structure of the program [10, 11].

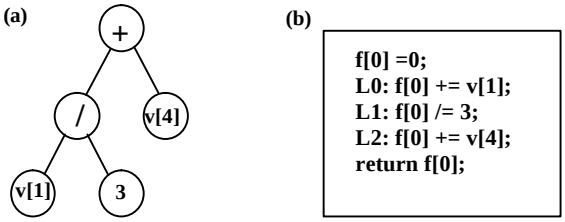

Figure 1. Comparison of the GP program structures. (a) Tree-based GP (b) LGP (after Alavi et al. [11]).

Almost all computer architectures represent computer programs in a linear fashion. In other words, computers do not naturally run tree-shaped programs. Hence, slow interpreters have to be used as part of tree-based GP. Conversely, by evolving the binary bit patterns in LGP, the use of an expensive interpreter (or compiler) is avoided. Consequently, LGP can run several orders of magnitude faster than comparable interpreting systems. The enhanced speed of LGP permits conducting many runs in realistic timeframes. This leads to deriving consistent, high-precision models with little customization [12, 13]. In the LGP system described here, an individual program is interpreted as a variable-length sequence of simple C instructions. The instruction set or function set of LGP consists of arithmetic operations, conditional branches, and function calls. The terminal set of the system is composed of variables and constants. The instructions are restricted to operations that accept a minimum number of constants or memory variables, called registers (r), and assign the result to a destination register, e.g., $r_0 := r_1 + 1$.

Here are the steps the LGP system follows for a single run [8]:

I. Initializing a population of randomly generated programs and calculating their fitness values.

II. Running a Tournament. In this step four programs are selected from the population randomly. They are compared and based on their fitness, two programs are picked as the winners and two as the losers.

III. Transforming the winner programs. After that, two winner programs are copied and transformed probabilistically into two new programs via crossover and mutation operators.

IV. Replacing the loser programs in the tournament with the transformed winner programs. The winners of the tournament remain without change.

V. Repeating steps two through four until termination or convergence conditions are satisfied.

Crossover occurs between instruction blocks. During this operation, a segment of random position and arbitrary length is selected in each of the two parents and exchanged. If one of the two children would exceed the maximum length, crossover is aborted and restarted with exchanging equally sized segments [10]. The mutation operation occurs on a single instruction set. Inside instructions, mutation randomly replaces the instruction identifier (a variable or a constant) by equivalents from valid ranges. Comprehensive descriptions of the basic parameters used to direct a search for a linear genetic program can be found in [8].

3. MODELING OF SOIL DEFORMATION MODULUS

In order to provide accurate assessment of the soil modulus, the effect of several influencing factors should be incorporated into the model development. It is well-known that the soil deformation moduli are affected by the basic soil properties (fabric characteristics), the state of the soil, and its consolidation history [1]. The main purpose of this study is to derive new relationships for the soil secant (E_s) modulus using LGP. The most important factors representing the soil deformation moduli behaviors were detected based on the literature review [1-4] and after a trial study. Consequently, E_s (kg/cm^2) was considered to be a function of several parameters as follows:

$$E_s = f\left(\frac{CC}{FC}, D_{10}, D_{30}, D_{60}, C_u, C_c, LL, W, g, g_d\right) \quad (1)$$

where,

CC (%): Coarse-grained content

FC (%): Fine-grained content

D_{10} (mm): Grain size for which 10 percentage of the sample is finer

D_{30} (mm): Grain size for which 30 percentage of the sample is finer

D_{60} (mm): Grain size for which 60 percentage of the sample is finer

C_u: Coefficient of uniformity (D_{60} / D_{10})

C_c: Coefficient of curvature ((D_{30})^2 / (D_{60} × D_{10}))

LL (%): Liquid limit

W (%): Moisture content

? (gr/cm^3): Soil bulk density

?$_d$ (gr/cm^3): Soil dry density

(Note: 1.0 kg/cm^2 = 0.1 MPa, 1.0 g/cm^3 = 0.1 KN/m^3)

CC/FC, D_{10}, D_{30}, D_{60}, C_u, C_c, and LL represent the intrinsic soil properties. W, $?_d$, and ? carry information on the state of the soil and its compressibility and previous history. Over-consolidation ratio (OCR) could have been included in the analysis. OCR was not used herein as it should be obtained from time-consuming laboratory tests. On the other hand, ? and $?_d$ can easily be calculated for a soil.

3.1. Experimental study

The experimental program consisted of laboratory and field tests. The field portion of this study included a test pit exploration and plate-load tests (PLT). For laboratory testing purposes, several disturbed and undisturbed soil samples were taken from the sites. Extensive geotechnical laboratory test programs were carried out for the basic characterization of soils. These comprised determining moisture content, unit weight of the soil, Atterberg limits, specific gravity, and grain size distribution. Different soil types tested were gravelly silt with sand (ML), silty clay with sand (CL-ML), gravelly lean clay with sand (CL), well-graded sand with silt (SW-SM), and silty gravel with sand (GM).

Within the scope of this study, 43 plate-load tests were performed to investigate the load-settlement characteristics of soils at some locations in Khorasan Province, Iran. The procedure considered for conducting the plate load tests was in accordance with the standard ASTM D1194-94. The tests were conducted using 300 mm diameter, 25.4 mm thick, rigid circular steel plates on leveled surfaces, in shallow pits or excavations within a small tunnel or adit. The load was applied through a system comprising a hydraulic jack, a 30 tone ground investigation truck and measured using a calibrated load cell. After placing a high-capacity jack on the top of the loading plate, the test loads were applied to the bearing plates utilizing this hydraulic jack. In the case of performing the test within a small tunnel, bearing plates loaded against the opposite side of the tunnel. The results of the plate load tests are presented as applied contact pressure versus settlement curves. The interpretation of the results (deformation properties) is usually made using isotropic elastic theory because of its convenience [4].

3.2. Model Development Using LGP

The available database was used for establishing the LGP prediction model relating E_s to CC/FC, D_{10}, D_{30}, D_{60}, C_u, C_c, LL, W, ?, and $?_d$. For the analysis, the available data sets were randomly divided into learning, validation and testing subsets. The learning data were used for training (genetic evolution). The validation data were used to specify the generalization capability of the evolved programs on data they did not train on (model selection). In other words, the learning and validation data sets were used to select the best evolved programs and included in the training process. Thus, they were categorized into one group referred to as training data.

The testing data were finally used to measure the performance of the models obtained by LGP on data that played no role in building the models. Of the 43 data, 22 data vectors were used for the learning process and 10 data were taken as the validation data. The remaining 11 sets were used for the testing of the derived models. The optimal models were selected after developing and controlling several models with different combinations of the input parameters. Correlation coefficient (R), root mean squared error (RMSE) and mean absolute error (MAE) were used to evaluate the performance of the proposed models.

Several runs were conducted to come up with a parameterization of LGP that provided enough robustness and generalization to solve the problem. Three levels were set for the population size (500, 1500, 3000) and two levels were considered for the crossover rate (50%, 95%) and mutation rate (50%, 90%). The initial and maximum program sizes were respectively set to optimal values of 80 and 256 bytes as tradeoffs between the running time and the complexity of the evolved solutions. In this study, four basic arithmetic operators (+, -, ×, /) and basic mathematical functions (v, sin, cos) were utilized to get the optimum LGP models. A fairly large number of tournaments (900000) were tested on each run to find models with minimum error. To evaluate the fitness of the evolved program, the average of the squared raw errors was used. For the LGP-based analysis, the Discipulus software was used. The LGP-based formulation of E_s is as follows:

$$E_S\left(\frac{\text{Kg}}{\text{cm}^2}\right)=W+\frac{\left(6g_d{}^2-LL-W\right)/C_c{}^2+C_u}{C_c}+g_d{}^2\left(6+3LL-3g_d+\frac{3\left(CC/_{FC}\right)-6D_{60}}{D_{60}}-3\frac{2+C_c}{C_u}+\frac{12+\left(-12-6C_c\right)/C_u}{\left(\left(-\left(CC/_{FC}\right)+2D_{60}\right)/D_{60}+\left(2+C_c\right)/C_u-2\right)^2}\right) \quad (1)$$

A comparison of the experimental and predicted E_s values is shown in Figure 2.

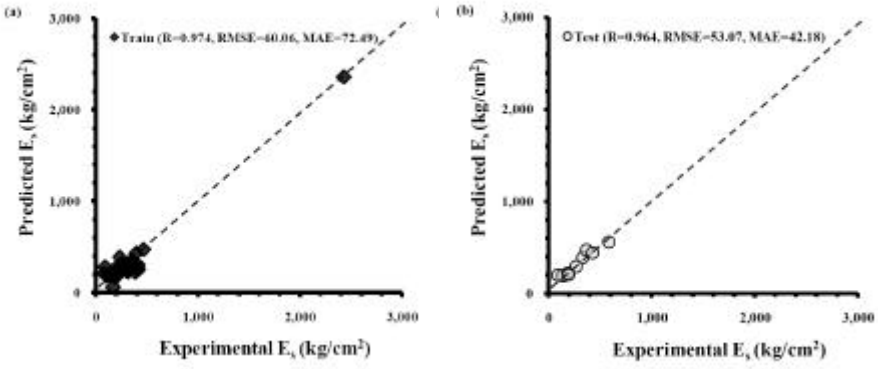

Figure 2. Predicted versus experimental E_s values using the LGP model.

(Note: 1.0 kg/cm2 = 0.1 MPa)

4. PERFORMANCE ANALYSIS

It can be observed from Figure 4 that the LGP model with high R and low RMSE and MAE values is able to predict the target values with an acceptable degree of accuracy. The performance of the models on the training and testing data suggests that they have both good predictive abilities and generalization performance. New criteria recommended by Golbraikh and Tropsha [14] were checked for external validation of the model on the validation data sets. It is suggested that at least one slope of regression lines (*k* or *k'*) through the origin should be close to 1. Also, the performance indexes of *m* and *n* should be lower than 0.1. Recently, Roy and Roy [15] introduced a confirm indicator of the external predictability of models (R_m). For $R_m > 0.5$, the condition is satisfied. Either the squared correlation coefficient (through the origin) between predicted and experimental values (Ro^2), or the coefficient between experimental and predicted values (Ro'^2) should be close to R^2_{Test}, and close to 1. The considered validation criteria and the relevant results obtained by the model are presented in Table 1. As it is seen, the derived models satisfy the required conditions. The validation phase ensures the derived LGP model for the E_s prediction is strongly valid.

Table 1. Statistical parameters of the LGP model for the external validation.

Item	Formula	Condition	E_s
1	R	0.8 < R	0.964
2	$k = \frac{\sum_{i=1}^{n}\left(h_i \times t_i\right)}{h_i^2}$	0.85 < K < 1.15	0.911
3	$k' = \frac{\sum_{i=1}^{n}\left(h_i \times t_i\right)}{t_i^2}$	0.85 < K' < 1.15	1.075
4	$m = \frac{R^2 - Ro^2}{R^2}$	m < 0.1	-0.037
5	$n = \frac{R^2 - Ro'^2}{R^2}$	n < 0.1	-0.036
6	$R_m = R^2\left(1 - \sqrt{\lvert R^2 - Ro^2 \rvert}\right)$	0.8 < R	0.758
where	$Ro^2 = 1 - \frac{\sum_{i=1}^{n}\left(t_i - h_i^o\right)^2}{\sum_{i=1}^{n}\left(t_i - \bar{t}_i\right)^2}$, $h_i^o = k \times t_i$		0.964
	$Ro'^2 = 1 - \frac{\sum_{i=1}^{n}\left(h_i - t_i^o\right)^2}{\sum_{i=1}^{n}\left(h_i - \bar{h}_i\right)^2}$, $t_i^o = k' \times h_i$		0.963

5. SENSITIVITY ANALYSIS

The contribution of each input parameter in the best LGP model was evaluated through a sensitivity analysis. For this aim, frequency values of the input parameters were obtained. A frequency value equal to 100% for an input indicates that this variable has been appeared in 100% of the best thirty programs evolved by LGP. This is a common approach in the GP-based analyses (e.g., [16]). The frequency values of the predictor variables are presented in Figure 3. In addition to frequencies, this figure presents the average impact of removing all instances of each input from the best thirty programs of the project. A value of 100% represents the largest impact value possible. The greater the value, the more impact removal had. According to Figures 3a and b, E_s is more sensitive to CC/FC, $?_d$ and W than other soil properties.

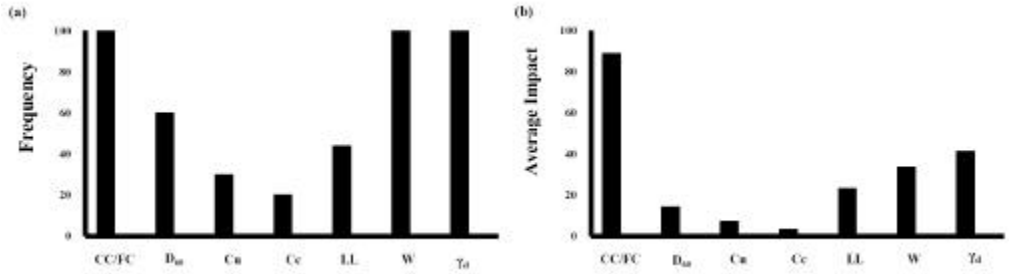

Figure 3. Contributions of the predictor variables in the LGP models.

6. CONCLUSION

A new design equation was derived for predicting the soil deformation modulus (E_s) using the LGP paradigm. The developed model gives reliable estimates of the E_s values. The validation phases confirm the efficiency of the models for their general application to the soil moduli estimation. The developed model is mostly suitable for fine-grained soils with physical properties similar to the soil samples used in this study. The results indicate that W and $?_d$ efficiently represent the initial state and consolidation history of the soil for determining the soil moduli. The predictive capability of the derived model is limited to the range of the data used in their training process. Despite this limitation, the model can easily be retrained and improved by including the data for other soil types and test conditions.

References

1. Briaud, J. L., *Introduction to soil moduli*, Geotech. News, June 2001, BiTech Publishers, Richmond, B. C., Canada, 2001.
2. Briaud, J. L., Li, Y. and Rhee, K., BCD: A soil modulus device for compaction control, *Journal of Geotechnical and Geoenvironmental Engineering (ASCE)*, 132(1), 2006.
3. Reznik, Y. M., Comparison of results of oedometer and plate load tests performed on collapsible soils, *Engineering Geology*, 39, 1995.
4. Reznik, Y. M., Plate–load tests of collapsible soils, *Journal of Geotechnical Engineering (ASCE)*, 119(3), 1993.
5. Canadian Geotechnical Society, *Canadian foundation engineering manual*, 2nd Edition, BiTech Publishers, Vancouver, Canada, 1985.
6. Reznik, Y. M., Influence of physical properties on deformation characteristics of collapsible soils, *Engineering Geology*, 92, 2007.
7. Koza, J., Genetic programming, on the programming of computers by means of natural selection, MIT Press, Cambridge (MA), 1992.
8. Brameier, M. and Banzhaf, W., *Linear genetic programming*, Springer Science + Business Media, New York, 2007.
9. Alavi A.H., Gandomi A.H., A Robust Data Mining Approach for Formulation of Geotechnical Engineering Systems, *International Journal for Computer-Aided Engineering-Engineering Computations*, 28(3), 2011.
10. Brameier, M. and Banzhaf, W., A comparison of linear genetic programming and neural networks in medical data mining, *IEEE Transactions on Evolutionary Computation*, 5(1), 2001.
11. Alavi, A. H., Gandomi, A. H. and Heshmati, A. A. R., Discussion on soft computing approach for real–time estimation of missing wave heights, *Ocean Engineering*, 37, 2010.
12. Francone, F.D. and Deschaine, L.M., Extending the boundaries of design optimization by integrating fast optimization techniques with machine-code-based, linear genetic programming, *Information Sciences*, 161, 2004.
13. Poli, R., Langdon, W.B., McPhee, N. F. and Koza, J.R., Genetic programming: An introductory tutorial and a survey of techniques and applications. Technical report [CES-475]. UK: University of Essex, 2007.
14. Golbraikh, A. and Tropsha, A., Beware of q2. *Journal of Molecular Graphics and Modelling*, 20, 2002.
15. Roy P. P. and Roy K., On some aspects of variable selection for partial least squares regression models, *QSAR & Combinatorial Science*, 27, 2008.
16. Gandomi, A.H., Alavi, A.H., Mirzahosseini, M.R., Moqhadas Nejad, F., Nonlinear genetic-based models for prediction of flow number of asphalt mixtures, *Journal of Materials in Civil Engineering (ASCE)*, 23(3), 2011.

"Computational Civil Engineering 2011", International Symposium
Iasi, Romania, May 13, 2011

Comparative aspects between linear and non-linear analysis of cable structures

Ferencz Lazar-Mand[1], Dragos Florin Lisman[2]

[1]*Dep. of Structural Mechanics, Technical Univ. of Cluj – Napoca, Cluj – Napoca, 400114, Romania*

[2]*Dep. of Structural Mechanics, Technical Univ. of Cluj – Napoca, Cluj – Napoca, 400114, Romania*

Summary

The increasing number of processors, higher frequencies and large memory resources lead to an increased computing speed using the latest hardware offered by the IT industry.

We thus entered a new era where more and more often non-linear analysis is adopted in almost all areas of structural engineering.

In this paper we try to make a comparison between the analysis of linear and non-linear cable structures.

We highlight the advantages and disadvantages of linear and non-linear analysis for these structures.

KEYWORDS: cable prestressed, dynamic, linear, nonlinear

1. INTRODUCTION

Dynamic structural analysis can be classified in two categories: linear and nonlinear structural analysis.

The differential equation of movement for a nonlinear behavioral model is [1]:

$$\mathrm{M}\cdot\ddot{\mathrm{U}}+g(\dot{\mathrm{U}})+f(\mathrm{U})=\mathrm{P(t)}, \tag{1}$$

or:

$$\mathrm{M}\cdot\ddot{\mathrm{U}}+\mathrm{g}_1(\mathrm{U})\dot{\mathrm{U}}+f(\mathrm{U})=\mathrm{P(t)} \tag{1'}$$

where: $g(\dot{U})=[g_1(\dot{u}_1,\cdots,\dot{u}_n)\ldots g_n(\dot{u}_1,\cdots,\dot{u}_n)]^T$ is the damping function;

$f(\mathrm{U}) = [\mathrm{f}_1(\mathrm{u}_1, \cdots, \mathrm{u}_n) \ldots \mathrm{f}_n(\mathrm{u}_1, \cdots, \mathrm{u}_n)]^{\mathrm{T}}$ is the stiffness function and: $P(t) = [\mathrm{p}_1(t) \ldots p_n(t)]^{\mathrm{T}}$ is the stimulus function.

The solution to equation (1) is called dynamic response in terms of displacements $\mathrm{U(t)}$, velocities $\dot{\mathrm{U}}(\mathrm{t})$ and accelerations $\ddot{\mathrm{U}}(\mathrm{t})$.

Nonlinearity can be classified into geometric nonlinearity and/ or physical non-linearity (from the composing material). In the case of cable structures, geometric nonlinearity is always present.

In the following sections different cases of nonlinearity will be discussed, especially geometric nonlinearity.

2. COMPUTATION OF THE TANGENT STIFFNESS MATRIX

For equation (2), namely:

$$\mathrm{M} \cdot \ddot{\mathrm{U}} + g(\dot{\mathrm{U}}) + f(\mathrm{U}) = \mathrm{P(t)}$$

f(U) is taken under the following form:

$$\mathrm{f(U)} = \mathrm{K}(U_0) \cdot (U - U_0) + \mathrm{R(U)} \qquad (2)$$

where:

$$U_0 = U; \quad \Delta U = U - U_0$$

K is the tangent stiffness matrix; **U** is the displacements vector in the node, $\mathbf{U_0}$ previous displacements vector and **R** is the residual terms vector which contains the non-linear terms from **U**.

The elements of the stiffness matrix are computed using a formula similar to the one presented in **[2]**.

$$
\begin{aligned}
&K_{i,j}^{xx}=\frac{1}{l_{i,j}}\left[F_i+(EA_i-F_i)\cdot(?_x^i)^2\right];\quad K_{i,j}^{yy}=\frac{1}{l_{i,j}}\left[F_i+(EA_i-F_i)\cdot(?_y^i)^2\right]\\
&K_{i,j}^{xy}=\frac{(EA_i-F_i)}{l_{i,j}}\cdot(?_x^i)\cdot(?_y^j);\quad K_{i,j}^{zz}=\frac{1}{l_{i,j}}\left[F_i+(EA_i-F_i)\cdot(?_z^i)^2\right]\\
&K_{i,j}^{xz}=\frac{(EA_i-F_i)}{l_{i,j}}\cdot(?_x^i)\cdot(?_z^j);\quad K_{i,j}^{yz}=\frac{(EA_i-F_i)}{l_{i,j}}\cdot(?_y^i)\cdot(?_z^j)\\
&l_{i,j}=l_{q,p};\quad l_{q,p}=\sqrt{(x_q-x_p)^2+(y_q-y_p)^2+(z_q-z_p)^2}
\end{aligned}
\tag{3}
$$

The directing cosines $?_d^i \quad (d=x,y,z)$ are computed through the nodes coordinates.

F – prestress force; E –modulus of elasticity; A – cross-sectional area of cable; ? – directing cosines; l – length of the elements .

$$\theta_{q,p}=\left(\frac{x_q-x_p}{l_{q,p}};\frac{y_q-y_p}{l_{q,p}};\frac{z_q-z_p}{l_{q,p}}\right)$$

The displacements vector is:

$$U=\begin{bmatrix}U_1\\U_2\\\cdots\\U_n\end{bmatrix}=\begin{bmatrix}u_{1x} & u_{1y} & \vdots & u_{2x} & u_{2y} & \vdots & \cdots & u_{nx} & u_{ny} & u_{nz}\end{bmatrix}^T=$$

$$\begin{bmatrix}u_1 & u_2 & \vdots & u_4 & u_5 & \vdots & \cdots & u_{n-2} & u_{n-1} & u_n\end{bmatrix}^T$$

The residual terms vector from (3) has the following form:

$$R=\begin{bmatrix}R_1 & R_2 & \cdots & R_n\end{bmatrix}^T=\begin{bmatrix}r_{1x} & r_{1y} & \cdots & r_{nx}\end{bmatrix}^T=\begin{bmatrix}r_1 & r_2 & \cdots & r_n\end{bmatrix}^T$$

$$r_{i,j}^{xx}=(EA_i-F_i)\cdot\left[\frac{u_{ix}-u_{jx}}{l_{i,j}}\cdot c_{i,j}^{xx}+\frac{x_i-x_j}{2\cdot l_{i,j}}\cdot d_{i,j}^{xx}\right]$$

$$r_{i,j}^{yy}=(EA_i-F_i)\cdot\left[\frac{u_{iy}-u_{jy}}{l_{i,j}}\cdot c_{i,j}^{yy}+\frac{y_i-y_j}{2\cdot l_{i,j}}\cdot d_{i,j}^{yy}\right]$$

$$a_{i,j}^{xx} = \frac{1}{l_{i,j}^2} \cdot \left[(x_i - x_j) \cdot (u_{ix} - u_{jx}) \right]; \quad a_{i,j}^{yy} = \frac{1}{l_{i,j}^2} \cdot \left[(y_i - y_j) \cdot (u_{iy} - u_{jy}) \right]$$

$$b_{i,j}^{xx} = \frac{1}{l_{i,j}^2} \cdot \left[(u_{ix} - u_{jx})^2 \right]; \quad b_{i,j}^{yy} = \frac{1}{l_{i,j}^2} \cdot \left[(u_{iy} - u_{jy})^2 \right]$$

$$c_{i,j}^{xx} = a_{i,j}^{xx} + \frac{1}{2} \cdot b_{i,j}^{xx} - \frac{3}{2} \cdot (a_{i,j}^{xx})^2; c_{i,j}^{yy} = a_{i,j}^{yy} + \frac{1}{2} \cdot b_{i,j}^{yy} - \frac{3}{2} \cdot (a_{i,j}^{yy})^2$$

$$d_{i,j}^{xx} = b_{i,j}^{xx} - 3 \cdot (a_{i,j}^{xx})^2 - 3 \cdot a_{i,j}^{xx} \cdot b_{i,j}^{xx} + 5 \cdot (a_{i,j}^{xx})^3$$
$$d_{i,j}^{yy} = b_{i,j}^{yy} - 3 \cdot (a_{i,j}^{yy})^2 - 3 \cdot a_{i,j}^{yy} \cdot b_{i,j}^{yy} + 5 \cdot (a_{i,j}^{yy})^3$$

The simplified P. Krishna's formulae are:

$$f_{Kr.}(U) = \mathbf{P}$$
$$f(U) = 0$$
$$f(U) = f_{Kr.}(U) - P = 0 \tag{4}$$
$$A(U) = K(U_0) + A_R \tag{5}$$

For evaluating the jacobian $\mathbf{A_R}$, the numerical derivation through devised differences procedure from [3] was used. At step (k) the expression of the differential coefficient is:

$$\left. \frac{\partial r_i}{\partial u_j} \right|_{u^{(k)}} = \frac{r_i(u_1, \ldots, u_j + h^{(k)}, \ldots, u_n) - r_i(u_1, \ldots, u_j, \ldots, u_n)}{h^{(k)}}$$

where $\boldsymbol{h}$ is small.

The movement equation is solved using the Newmark [4] integration operator described in [5].

For the Newmark formulae [6] in the case of geometrical nonlinearity the following algorithm is used:

1. the X_0 coordinates are read (at time t_0)
2. initialization of i = 0

3. computation of l_i, $?_i$ (the length, the directing cosines at t_i)
4. computation if the stiffness matrix according to (3) $K(U_i)$ (for each t_i)
5. by integration U_{i+1}, $\dot{U}_{i+1}$ are obtained
6. $X_{i+1} = X_i + U_{i+1}$ (in the Newmark formula $U_{i+1} = \overline{\mathbf{U}}_{i+1} + bh^2\mathbf{W}$)
7. i = i+1
8. if i < TT/h (where TT is the Total Time) go to 3, else go to 9
9. write the results

3. CASE-STUDY STRUCTURES

The analyzed structure is a saddle surface (hyperbolic paraboloid) **[7]**. The properties of the structure are presented in Figure 1 and the coordinates in the table below.

Table 1. Coordinates of the structure

Node no	X [m]	Y [m]	Z [m]
1	-15.24	-19.05	-1.2954
2	0.0	-19.05	-1.905
3	15.24	-19.05	-1.2954
4	-15.24	0.0	0.6096
5	0.0	0.0	0.0
6	15.24	0.0	0.6096
7	-15.24	19.05	-1.2954
8	0.0	19.05	-1.905
9	15.24	19.05	-1.2954
10	-15.24	-38.1	-7.0104
11	0.0	-38.1	-7.62
12	15.24	-38.1	-7.0104
13	-30.48	-19.05	0.5334
14	30.48	-19.05	0.5334
15	-30.48	0.0	2.4384
16	30.48	0.0	2.4384
17	-30.48	19.05	0.5334
18	30.48	19.05	0.5334
19	-15.24	38.1	-7.0104
20	0.0	38.1	-7.62
21	15.24	38.1	-7.0104

The following types of cables were used for obtaining the structure:

In the direction of X: ? 76.20 mm	A_x = 34.84 cm^2
In the direction of Y: ? 101.60 mm	A_y = 61.935 cm^2

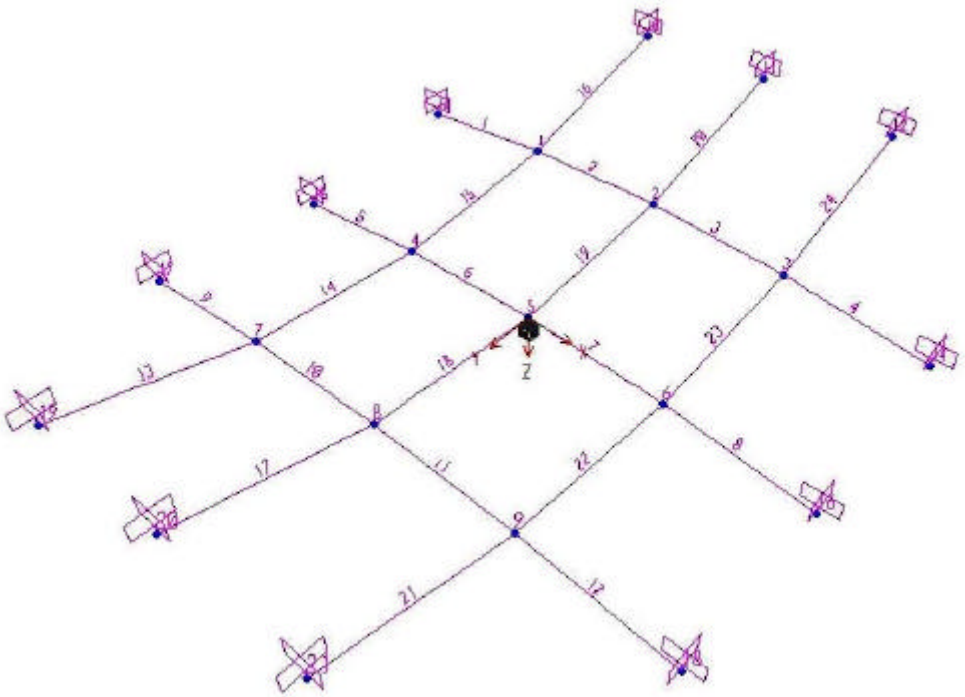

Figure 1. The analized structure

The characteristic curve was considered linear (even if the authors use a material with nonlinear behavior), where the modulus of elasticity is 15858 kN/cm^2.

The masses are considered lumped in the nodes. The equivalent node masses were computed according to the proper weight 960 N/m^2 given in Ma & Leonard example [7], thus resulting a forced of 288 kN applied to the node, which represents a mass concentration *mc* = 28.41 kNs^2/m.

$$q = 960\ \text{N/m}^2 \Rightarrow \text{P}_{\text{nod}} = 15.24 \cdot 19.05 \cdot 0.960 = 278.71\ \text{kN/node}$$

$$\text{mc} = 278.71/9.81 = 28.41\ \text{kN} \cdot \text{s}^2 / m$$

A very important phase during the design and execution of cable structures is the prestress which assures the proper behavior [8] to different types of dynamic stresses (wind, earthquake) over the structure's exploitation period.

The prestressing forces are approximately equal in all the composing elements such that the ratio between the sag/ span is reduced (the structure can be considered flat shaped). The cables in the X direction were prestressed with a force of 28 kN /cm2, thus resulting a prestressing force $T_x^0 = 975.52\,kN$,

T_y^0 = 1781.87 kN – for the intermediate elements;

T_y^0 = 1858.05 kN – for the edge elements.

The prestressing forces are synthesized in Table 2.

Table 2.

Cables on direction	Prestressing forces (kN/cm^2) Marginal elements	Intermediate elements
X	28.0	28.0
Y	30.0	28.77

It is considered that the system is in equilibrium under the action of its own weight and the prestressing forces. This structure is subject to a uniformly distributed load of 27.54 daN /m^2 which is transformed to a equivalent node load of 501 kN, applied in each node.

4. RESULTS

In the following, the authors will present graphically the displacements and velocities for node 5 on Z axis, with $t_0 = 0$, TT = 6 seconds and $h = 10^{-2}$.

The differences computed through direct numerical integration using both the linear and non-linear Newmark operators can be observed.

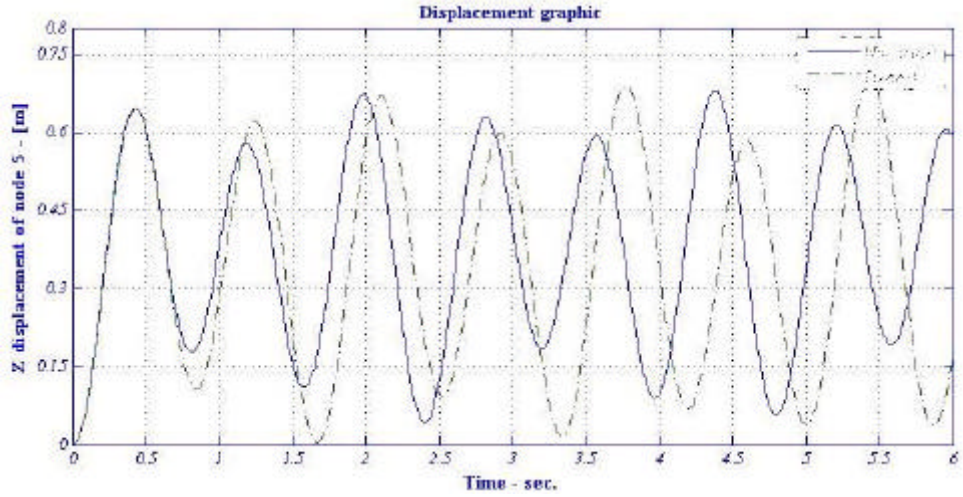

Figure 2. Displacement graphic

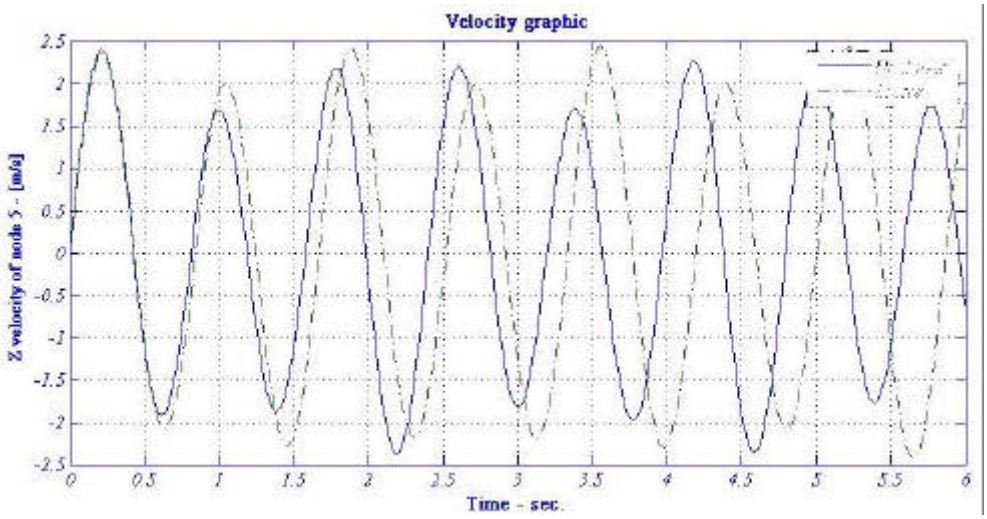

Figure 3. Velocity graphic

5. CONCLUSIONS

In the graphics above a interesting difference can be observed between the linear and non-linear computations. In both cases the Newmark method was used, with the difference that for the linear case the integration using the constant stiffness matrix was used and for the non-linear the matrix was updated step by step. The differences are not large but significant. It is clear that the processing time is higher in the case on non-linear analysis. Naturally in the case of the displacements the differences are larger than in the case of the velocities. The final conclusion is that structures built of trailing (suspended) cables must be non-linearly analyzed for obtaining accurate results or at least geometrically non-linear analyzed.

References

1. Clough, R.W., Penzien, J., *Dynamics of structures*, McGraw-Hill, New York, 1975.
2. Krishna, P., *Cable – Suspended Roofs*, McGraw-Hill Inc., 1978.
3. Chisalita, A., *Numerical Analysis*, Universitatea Tehnica din Cluj Napoca, 2002.
4. Newmark, N. M., A Method of Computation for Structural Dynamics, *ASCE Journal of the Engineering Mechanics Division*, Vol. 85 No. EM3, (1959).
5. Chisalita, A., Chisalita, F., Analyse de l'operateur de Newmark, *Studia Univ. Babes-Bolyai*, Mathemathica, XXXVIII, 4, 1993.
6. Bathe, K. J., *Finite Element Procedures*, Prentice-Hall Inc., 1996.
7. Ma, D., and Leonard, J., Slack-Elasto-Plastic Dynamics of Cable Systems, *ASCE Journal of the Engineering Mechanics Division*, Vol. 105 No. EM2, (1979).
8. Chisalita, A., *Program DINSAS – Manual de utilizare*, Universitatea Tehnica din Cluj Napoca, 2007. (romanian)

Influence of pigment addition on the macro-structure of sintered components based on recycled glass

Tomáš Melichar[1], Jirí Bydžovský[2] Vít Cerný[3]
[1]*Faculty of civil engineering, Institute of Technology of Building Materials and Components, Brno University of Technology, Brno, 602 00, Czech Republic, melichar.t@fce.vutbr.cz*
[2]*Faculty of civil engineering, Institute of Technology of Building Materials and Components, Brno University of Technology, Brno, 602 00, Czech Republic, bydzovsky.j@fce.vutbr.cz*
[3]*Faculty of civil engineering, Institute of Technology of Building Materials and Components, Brno University of Technology, Brno, 602 00, Czech Republic, cerny.v@fce.vutbr.cz*

Summary

The article deals with the sintered elements based on recycled waste glass which still has not found another use (application) in the re-manufacturing of glass or other materials. These cullets, which are currently not further utilized, represent a problem throughout Europe. This is especially about glass from recycling of TV monitors, fluorescent lamps, which means the electrical equipment in general. Sintered elements are commonly used in plate format (e.g. for wall and floor tiles) as well as in various colours, which is achieved by adding pigment to the charge before thermal finishing.

When optimizing the pigment dose, modification of the temperature regime and other parameters of production regime, one of the first steps includes visual assessment of macro-structure of the produced materials. In the experimental part of the paper, there is description of the influence of adding such pigment on the final macro-structure which is, next to physical-mechanical and chemical parameters, one of key aspects in terms of competitiveness of these materials on the market. The resulting macro-structure is also connected with the physical and mechanical properties.

The influence of quantity and type of colouring pigment on the final macro-structure of sintered elements based on recycled glass has clearly been proven, whereas the ability of colouring the structure of these elements also depends on the nature of used charge entering into production. Except for cullet chemistry, it is also about granulometric composition and content of impurities (residues of macro-molecular compounds and also the residues of a variety of inorganic pieces).

Outputs and findings are meant as the considerable benefit to further research that is focused on physical and mechanical parameters of the sintered elements based on recycled glass.

KEYWORDS: macro-structure, temperature, waste, pigment.

1. INTRODUCTION

Glass recycling is fairly well known activity, it has been in use for several decades. In the case of recycled glass which shall be used for re-manufacturing of glass, it is necessary to distinguish between two concepts. This is about the own cullet which have been used in glass production plants for many years. The process of melting completely without own cullet is performed just in the case of certain glass insulation fibres. And then it is also about foreign cullet, whereas the transition to utilization of foreign cullet by glass companies in the Czech Republic has been known since the fiftieth years of the last century. Theoretically, the term foreign cullet means any type of glass coming from recycling of products which have exhausted their lifetime. In the case of foreign cullet, it is necessary to assure that they are not applied into the production process together with any potential impurities that may represent a significant percentage (depending on type of glass, respectively products and also depending on methods of collection and selection of the cullet). Presence of various impurities can cause both a negative impact on the course of production process, then the impact on resulting parameters of glass (e.g. unwanted colour tone) and they can also cause deterioration of some parts of the production line (corrosion of the furnace bottom, etc.) [1].

One of the possible potentially usable variants of utilizing problematic (usually not-used) types of cullet is modification of the charge of glass sintered tiles. At the present time, there is a wide range of materials and elements currently used for surface finishing. The tiles based on sintered glass have also their unique position in this area, although they are not used as much as traditional ceramic tiles. This is mainly due to their higher price and also the impossibility of making very subtle plates (minimum thickness is 12 mm). However, the advantage of sintered glass tiles consists in their characteristic texture which makes them interesting in visual, resp. architectural, terms. Tiles which are based on sintered glass are also characterized by excellent physical and mechanical and chemical parameters (bending strength, frost resistance, chemical resistance, resistance to surface wear, etc.), which makes them usable in many applications both in interior and exterior. Regarding the fact that the dominant part of charge of sintered glass-based tiles is formed by granulated glass, there is a wide range of possibilities for the use of selected types of recycled glass which so far does not find any larger application, which means that the glass landfills represent problems for the environment.

2. EXPERIMENTAL RESEARCH

For the purposes of this research, there have been three types of "difficult" cullet chosen, i.e. the cullet which do not find wider application. The exception belongs to a recycled piece from glued wind-shield glasses of cars which is partially used by glass making factories and partially by manufacturers of thermal insulations based on subtle fibres. These shards are shown in the following picture (see Figure 1).

Figure 1. Recycled cullet used, from the left side - glass coming from recycling the TV monitors cones (CR), recycled piece of front car windshield (AG), glass of fluorescent lamp (FT)

To achieve desired colour-tone of the structure, there were powdered pigments used, i.e. the pigments which are commonly used in the ceramics industry for glazing. There were three colour tones in total - green, yellow and blue. In terms of chemical composition, these pigments are usually formed by one so-called colouring oxide. To achieve a homogeneous look and then to achieve distribution around the entire structure, the powders are milled to very small fractions.

2.1. Analysis of the input raw materials

In terms of the resulting parameters and macro-structure, it was first necessary to analyze the raw materials used. Then there were mesh screen analysis and chemical composition analysis of the cullet performed some later.

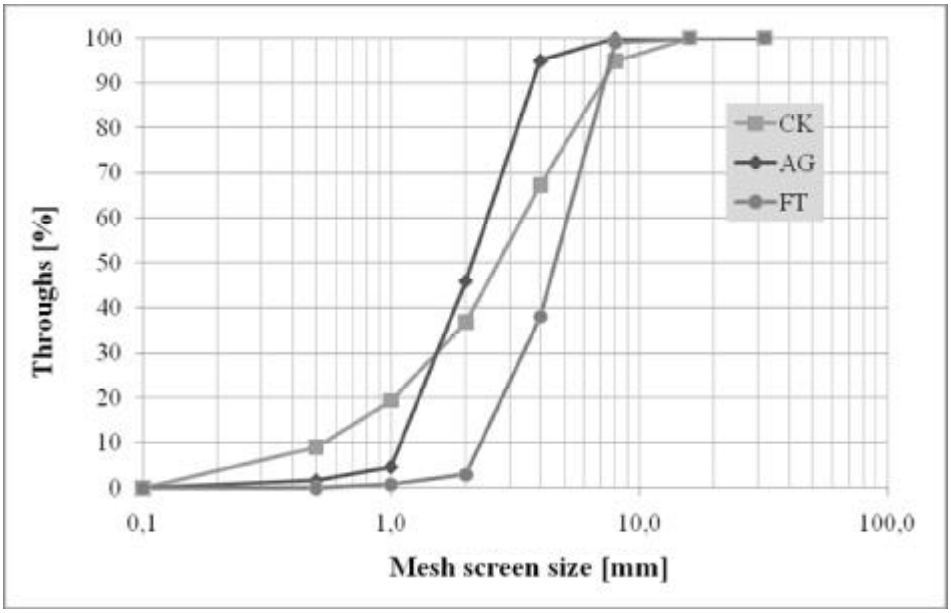

Figure 2. Mesh screen analysis of tested samples of recycled glass

The results of mesh screen analysis advert to uniformity of distribution of fractions of TV-monitor glass. On the other hand, the cullet of fluorescent lamps adverts to almost mono-fractional composition, whereas the dominant representation is formed by the fraction of 4-8 mm and 2-4 mm. In the case of fluorescent lamp glass, it can be assumed that distribution of pigment in the charge will be implementable with some more difficulties and it will show itself on the final texture of produced samples. It is also quite significant that the cullet of fluorescent lamps are very subtle, which will certainly have a significant impact on the course of temperature curve.

Table 1. Chemical composition of investigated samples

Component	Sample CK	AG	FT
SiO_2	52.39	73.21	71.7
Al_2O_3	3.11	2.35	2.15
Fe_2O_3	0.10	0.89	0.12
BaO	1.41	0.15	0.32
CaO	3.60	4.26	4.63
MgO	2.07	2.94	3.02
Na_2O	6.08	11.25	16.9
K_2O	7.72	1.87	1.02
PbO	17.90	0.02	-

Component	Sample CK	AG	FT
SrO	0.92	-	-
TiO_2	0.06	0.01	-
LiO_2	0.030	-	-
Organic compounds	-	0.15	-
Hg	-	-	< 0.000005

Results of the chemical analysis show similarity of car windshields and cullets of fluorescent tubes. However, the recycled piece which comes from the fluorescent lamps does not contain any remains of polymeric materials. On the contrary, there is a tiny amount of mercury present here. On the other hand, the cullets of TV monitors have markedly different character, i.e. the cullets in which there have been the lowest content of siliceous oxide and the high content of lead oxide identified. The lead oxide together with alkali acts as a flux material.

2.2. Impact of pigments on the final structure

With regard to the facts found in the frame of analyzing of input raw materials, there were temperature regimes designed for charge burning, i.e. the charge containing the examined alternative raw materials - recycled cullet. The following figures show representative samples characterizing the course of burning. There were three alternative raw materials in combination with three types of pigments used here. To achieve the optimal coloured structure and to some extent related physical-mechanical and chemical parameters, it was primarily necessary to modify the temperature regime in relation to several major factors:

- chemical composition of cullet;
- granulometric composition of the charge;
- type - chemical composition of pigment;
- dose of pigment.

The first case was a type of alternative, resp. secondary, raw material, more precisely its chemical composition. The more SiO_2, was contained in this raw material the higher temperature was necessary to be set up during the production process. On the other hand, in the case of lower content of siliceous oxide and increasing the percentage of alkali, or lead oxide, it was not necessary to use high temperatures in the area of maximum isothermal endurance. Granulometric composition of the charge also participated in this process as one of the decisive factors determining the conditions of manufacturing process and the final parameters of the sintered elements based on glass. With increasing amount of small particles or subtle cullet, it was not so necessary to use such higher temperatures like in the case of larger fractions.

A dose and chemical composition of powder colours also represented a crucial criterion in terms of final properties. Regarding the significant impact of these colours even in relatively small dose (in the order of percents), it is also possible to conclude that use of inorganic pigments has a key influence on final parameters of the products based on sintered glass.

In connection with the wholeness of colouring, i.e. a uniform distribution of colour tone in the entire volume of the produced samples, it was also very important to know the content of fine fraction and the extent of consecutiveness of grading curve; i.e. if there was not a larger dominance of the content of just one or two fractions. There have been several sets of testing samples produced, the amount was quite large. However, here below you can see just the representative samples with which the required parameters were achieved, i.e. the characteristic texture.

Figure 4. Capturing the structure of a sample made of TV monitor cullets at the maximum temperature of 900 °C, with the addition of 0.7% of green pigment.

Figure 5. Capturing the structure of a sample made of TV monitor cullets at the maximum temperature of 900 °C, with the addition of 1.2% of blue pigment.

Figure 6. Capturing the structure of a sample made of TV monitor cullets at the maximum temperature of 930 °C, with the addition of 1.4% of yellow pigment.

Figure 7. Capturing the structure of a sample made of car glued glass at the maximum temperature of 1050 °C, with the addition of 0.7% of green pigment.

Figure 8. Capturing the structure of a sample made of car glued glass at the maximum temperature of 980 °C, with the addition of 0.5% of blue pigment.

Figure 9. Capturing the structure of a sample made of car glued glass at the maximum temperature of 980 °C, with the addition of 1.5% of yellow pigment.

Figure 10. Capturing the structure of a sample made with using the cullets of linear fluorescent lamps at the maximum temperature of 820 °C, with the addition of 0.5% of green pigment.

Figure 11. Capturing the structure of a sample made with using the cullets of linear fluorescent lamps at the maximum temperature of 820 °C, with the addition of 0.5% of blue pigment.

Figure 12. Capturing the structure of a sample made with using the cullets of linear fluorescent lamps at the maximum temperature of 830 °C, with the addition of 1.0% of blue pigment.

3. CONCLUSIONS

The purpose of the research presented in this article consisted in clarifying the effect of pigments on the macro-structure of sintered elements based on recycled glass. There were three types of cullets subjected to the examination - TV monitor

cullets (CK), car glasses (AG) and linear fluorescent lamps (FT). To achieve coloured structure, there was the addition of green, blue and yellow pigment performed. It was found that the influence of these powder colours is very significant, even in small doses (in the units of single percents). It was also proven that several essential criteria play the decisive role here. It is necessary to take these criteria into account in the manufacturing process. These criteria or factors cannot be taken only individually, but also their synergistic effect must be taken into account, it means the effect in which the change of one parameter is passed on the others too. Specifically, these are the following factors:

- chemical composition of cullets;
- granulometric composition of the charge (size and representation of individual fractions);
- type - chemical composition of pigment;
- dose of pigment.
- homogenization of the charge.

The primary objective in the manufacture of sintered materials based on glass consists in achieving the desired structure (resp. texture) while maintaining adequate physical-mechanical and chemical parameters, which was the initial point of the experimental burnings. Based on the above mentioned points, there were modifications of the temperature mode in the area of maximum isothermal endurance and dosage of pigment performed here. The resulting macro-structure of the materials made is reflected in the figures (see Figure 4 - 12) in Chapter 2.2 Regarding the fact that each colour tone was achieved by using a different colouring oxide, this factor should have been considered when modifying the temperature mode too.

An interesting finding is that in the case of different types of cullets used here there were different influences of an addition of pigments on the required maximum temperature. For example, as for the TV monitor glass, it was necessary to get the highest temperature for the charge with a yellow colour. However, the cullets from car glasses required higher temperature together with the addition of green pigment. This could be attributed to, inter alia, the presence of a certain amount of impurities of organic origin (remains of foils) in the car glasses. Samples with blue pigments were produced at lower temperatures in comparison with the others, i.e. the green and yellow ones. With regard to granulometry and shape of the cullets, the cullets of fluorescent lights were different. Here we demonstrated the absence of small fractions where a perfect homogenization could not be performed, which also means that the colour tone could not be equally distributed in the entire volume of the samples produced.

Acknowledgements

The text has been drawn up within the MSM 0021630511 research project – "Progressive Building Materials with Utilization of Secondary Raw Materials and their Impact on Structures Durability".

References

1. Smrcek, A., Voldrich, F. *Sklárské suroviny*, INFORMATORIUM Praha, 1994.
2. Zpetný odber, magazín ASEKOL, C. 1/2007 URL:< http://www.asekol.cz/cs/download/spotrebitele/casopis-zpetny-odber/zpetny_odber_1_07.pdf>.
3. URL:<www.splrecycling.com>.
4. Fanderlik, I. *Silica glass and its application*, Elsevier Amsterdam, 1991.
5. Matoušek, J. *Anorganické nekovové materiály*, VŠCHT v Praze, 1992.

Nonlinear Finite Elements Modeling of Spherical Voided Bi-Axial Concrete Floor Slabs

Sergiu Calin[1], Sergiu Baetu[2]
[1]*Department of Concrete Structures, Building Materials, Technology and Management, "Gh. Asachi" Technical University of Iasi, Faculty of Civil Engineering and Building Services, Iasi, 700050, Romania, e-mail: sergyu_kalin@yahoo.com*
[2]*Department of Structural Mechanics, "Gh. Asachi" Technical University of Iasi, Faculty of Civil Engineering and Building Services, Iasi, 700050, Romania, e-mail: sergiubaetu@yahoo.com*

Recently, new types of reinforced concrete floors appeared, floors meant to ensure a higher economical efficiency through a more rational distribution of concrete along the section and an increase of the interior couple's arm.

In this article it is detailed the numerical analysis with the finite elements method by the computational means for an experimental reinforced concrete floor with spherical gaps made up at natural scale inside BMTO Department Laboratory at Faculty of Civil Engineering and Building Services Iasi.

The numerical values resulted are compared with the information obtained by experimental studies, presenting possible applications of the behavior particularities under the loads.

KEYWORDS: nonlinear FEM analysis, nonlinear material, voided slab, pushover analysis, correlation with experimental results.

1. INTRODUCTION

Concrete structural components require the understanding into the responses of those components to a variety of loadings. There are a number of methods for modeling the concrete structures through both analytical and numerical approaches.

Finite element analysis (FEA) is a numerical one widely applied to the concrete structures based on the use of the nonlinear behavior of material. FEA provides a tool that can simulate and predict the responses of reinforced concrete members. A number of commercial FEA codes are available in markets along with the use of FEA has increased because of progressing know ledge and capability of computer package and hardware [2].

Any attempts for engineering analyses can be done conveniently and fast using such versatile FEA packages. These result in the modernization of structural modeling by new generation practical engineers, in order to verify their structural designs. Nonlinear material models have been integrated in many of general

purpose finite element codes. These nonlinear models play a vital role in nonlinear response analyses since each material component tends to possess the complicated stress-strain behaviors.

The objective of this study was to develop a numerical model where nonlinear material properties of voided slabs can be included in detailed analyses for static investigations in the future.

Concrete section was modeled using SOLID 65 solid element where the compressive crushing of concrete is facilitated using plasticity algorithm and the concrete cracking in tension zone is accommodated by the nonlinear material model.

The use of truss element LINK8 for discrete reinforcement modeling (main and transverse reinforcements), however, it was assumed that perfect bonding between concrete and steel reinforcement occurs during loading exposes.

2. SPECIMENS DETAILS

The voided slab was cast and tested by the team of BMTO Department of Faculty of Civil Engineering and Building Services Iasi [3]. Dimensions of experimental element are 6520x6520x280 mm, are tested simply supported over 5000 mm span and loaded uniform distributed load having a distance of 750 mm between point of loading, Figure 9. For analysis several models have been made, Figures 6 and 7, but they could not run on an regular PC because of the large number of FEM. To simplify the calculation it was used a strip support, charged with the same charging scheme. Strip support has the dimensions in plan 6600x600x280 mm.

2.1. Material Models

2.1.1. Concrete

ANSYS software has the ability to model different types of material properties. Cracking of concrete and stress-strain relation in tension is modeled by a linear elastic tension stiffening relationship. Concrete is a quasi-brittle material and has different behavior in compression and tension. Development of a model for the behavior of concrete is a challenging task for researchers. The Solid 65 element was used to model the concrete. This element has eight nodes with three degrees of freedom at each node – translations in the nodal x, y and z directions. This element is capable of plastic deformation, cracking in three orthogonal directions, and crushing. The geometry and node locations for this element type are shown in Figure 1 [1],[4],[8].

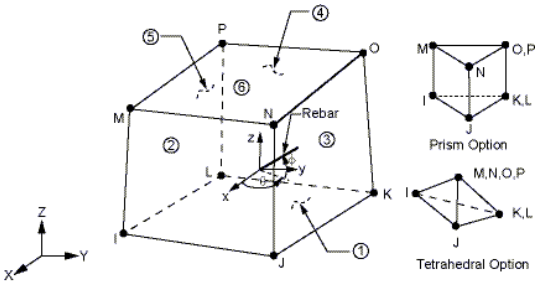

Figure 1. Solid 65 geometry

The Solid 65 element requires linear isotropic and multilinear isotropic material properties to properly model concrete as can be seen in Table 1.

Table 1. Material properties for Solid65

Linear Isotropic (C25/30)		
E_c	3E+010 Pa	
n	0,2	
Multilinear Isotropic (C25/30)		
	strain e(m/m)	stress fc(Pa)
0	0	0
1	0.0003	9.75E+006
2	0.0006	1.8173E+007
3	0.0012	3.0181E+007
4	0.0018	3.5296E+007
5	0.00222	3.6075E+007

The multilinear isotropic material uses von Mises failure criterion along with the Willam and Warnke (1974) model to define the failure of the concrete. E_c is the modulus of elasticity of the concrete, and n is the Poisson's ratio. The compressive uniaxial stress-strain values for the concrete model was obtained using the following equations with this is computed the multilinear isotropic stress-strain curve for the concrete [5],[9],[11],

$$f = \frac{E_c e}{1 + \left(\frac{e}{e_0}\right)^2}, \tag{1}$$

The multilinear isotropic stress-strain implemented curve requires that the first point of the curve to be defined by the user, this must satisfy Hooke's Law.

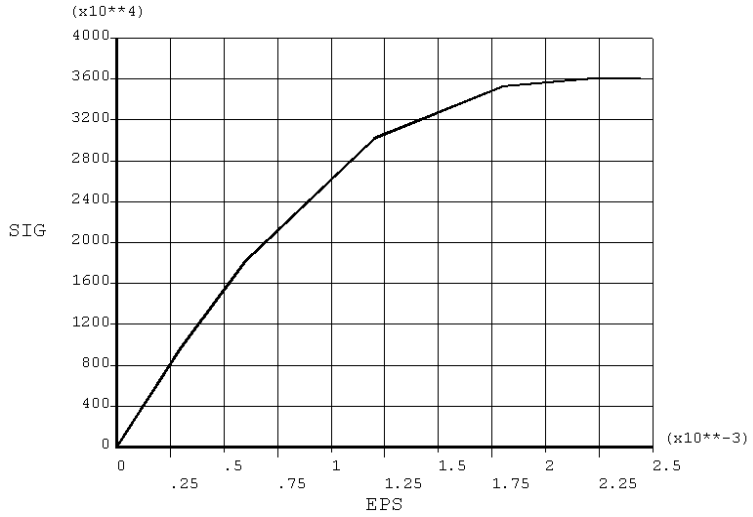

Figure 2. Stress-strain curve for concrete in ANSYS model

Implementation of the Willam and Warnke material model in ANSYS requires different constants be defined (Table 2).

Table 2. Concrete constants

1	Shear transfer coefficients for an open crack (b_t)	0,4
2	Shear transfer coefficients for an closed crack (b_c)	0,8
3	Uniaxial tensile cracking stress (f_r)	2E+006 Pa
4	Uniaxial crushing stress (f_c)	3,33E+007 Pa
5	Biaxial crushing stress	0
6	Ambient hydrostatic stress state for use with constants 7 and 8	0
7	Biaxial crushing stress under the ambient hydrostatic stress state	0
8	Uniaxial crushing stress under the ambient hydrostatic stress state	0
9	Stiffness multiplier for crack tensile condition	0

The shear transfer coefficient, b, represents conditions of the crack face. The value of b ranges from 0 to 1, with 0 representing a smooth crack (complete loos of shear transfer) and 1 representing a rough crack (no loss of shear transfer) [7],[10].

2.1.2. Reinforcement modeling

The reinforcement bars may be included in the finite element model in two ways: as a discrete model (individual bars) (figure 3), or through a smeared model (figure 1) [5],[6],[9],[11].

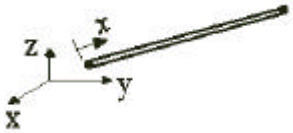

Figure 3. Link 8 geometry

In the cases analyzed in this paper reinforcement were modeled by using separate element called Link 8, a 3-D spar element. The geometry and node locations for Link 8 are show in figure 3. This element has two nodes and three degrees of freedom for each node, translations in the nodal x, y and z directions. The bond between concrete and reinforcement was assumed to be perfect. In figure 4 is shown the stress-strain curve of reinforcement used in this study. The bilinear kinematic hardening model (BKIN) was used [5],[11]. The bilinear model requires the yield stress (f_y) and the hardening modulus of the steel ($E_s^{'}$).

Constitutive law for steel behavior is:

$$\begin{cases} s_s = E_s e_s \quad , \quad e_s \le e_y \\ s_s = f_y + E_s^{'} e_s \quad , \quad e_s > e_y \end{cases} \tag{2}$$

Table 3. Material properties for Link 8

Linear Isotropic (S 355)	
Elastic modulus E_s	2,1E+011 Pa
Poisson's ratio n	0,3
Bilinear Isotropic (S 355)	
Yield stress f_y	3,55E+008 Pa
Tangent modulus $E_s^{'}$	2,1E+009 Pa

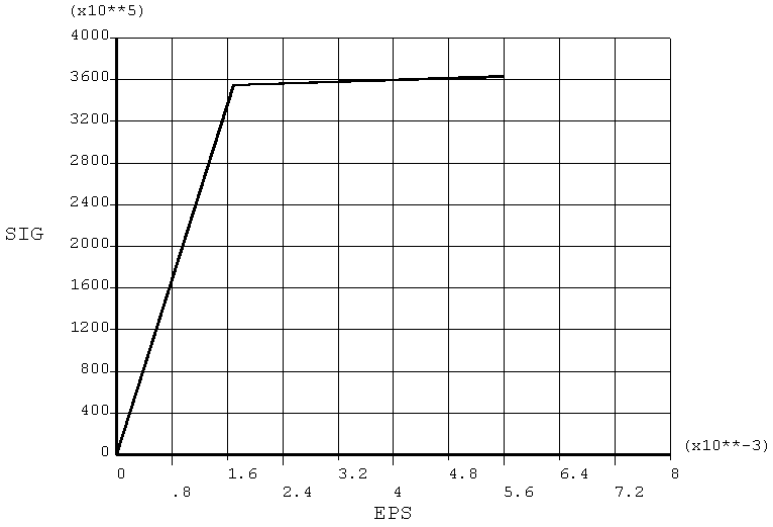

Figure 4. Stress-strain curve for reinforcement in ANSYS model

2.1.3. Steel plate modeling

The Solid 45 element is being used for the steel plates at loading points on the voided slab figure 5. This element has as a linear isotropic behavior with modulus of elasticity and Poisson's ratio as steel [5],[11].

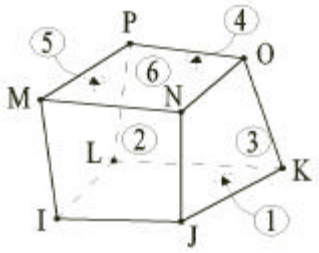

Figure 5. Solid 45 geometry

2.1.4. Finite element mesh

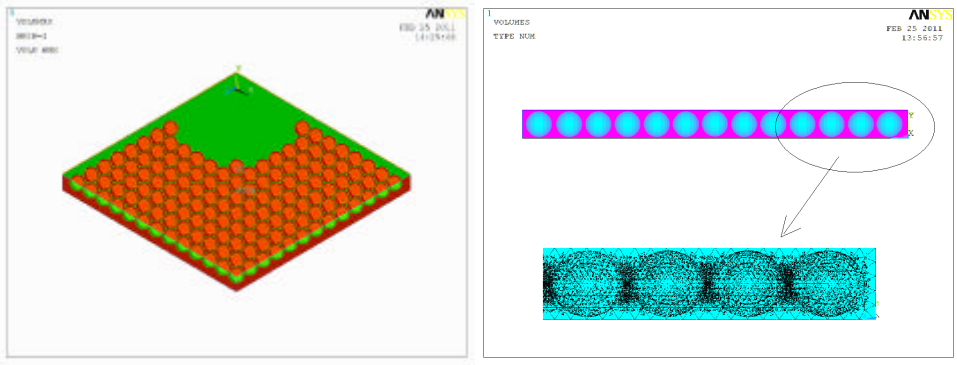

Figure 6. Attempt Finite Element Analysis of spherical gaps -Variant I

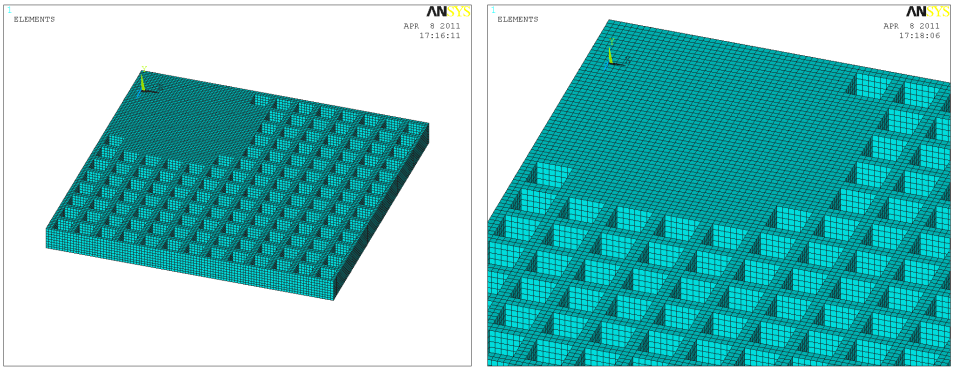

Figure 7. Attempt Finite Element Analysis of cubes -Variant II

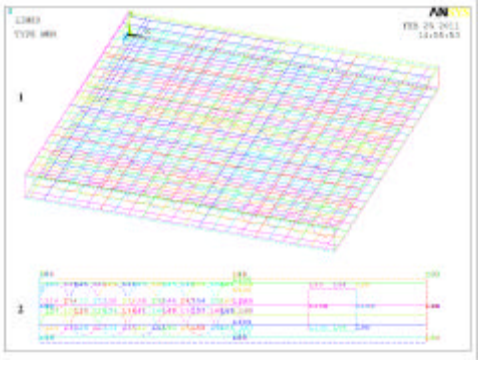

Figure 8. Model elements distribution of reinforcement

To obtain good results from Solid 65 element, the use of a rectangular mesh is recommended Figures 7 and 8. Concrete of the voided slab was meshed with Tetrahedral Option element of dimension 50 mm and all the reinforcement were meshed with 50 mm long link element [9].

2.1.5. Loading and boundary conditions

The voided slab is fully restrained at the base. It is symmetrical about XZ plane, in this way we reduce in half the number of finite elements and computation time, and symmetry boundary conditions will be set so that all nodes at Y=0 plane of symmetry were given the constraint UY=0.

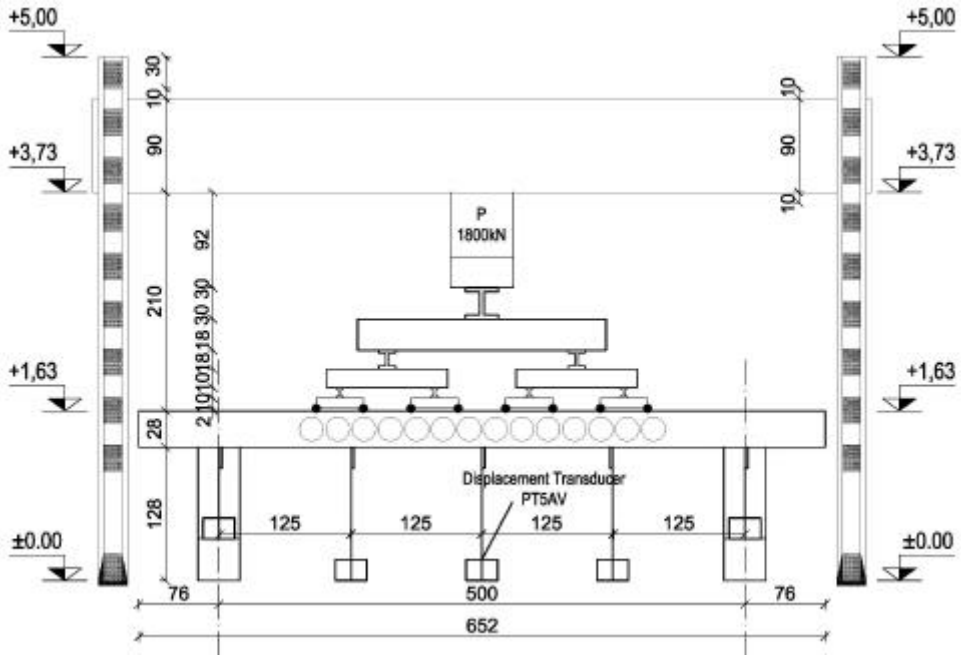

Figure 9. Loading and Section Experimental Model Details

Loads are disposed linearly along the surface of voided slab. Concentrated forces are applied at each point through steel plates to avoid the stress concentrations, Figures 9 and 10. The gravity loads include voided slab weight which is taken by the program.

2.2. Finite Element Analysis

One strip support is analyzed by nonlinear finite element. It has ϕ6, ϕ8, ϕ14 and ϕ18 in the main flexural reinforcements. Modeling of reinforced concrete specimens using Soild65 and Link8 elements for concrete and steel reinforcements respectively, the elements are arranged as shown in Figures 8 and 10.

The experimental and FEA load-deflection curves obtained for the element are illustrated in Figures 11, 12 and 13. The curves show good agreement in finite element analysis with experimental results throughout the entire range good behavior and failure mode. With observation, the results from the finite element model are small than experiment because of simplifying of calculation, it was used a strip support, concluding certain equivalent coefficients (the results can be multiplied by five). Experiment was done in two stages, to the SLS and SLU.

Figures 14, 15, 16 and 17 have explained the crack patterns of Axes A-B and 2-1 and compared with photo from the experiment [3]. Where is have very closed direction and types of the cracks. ANSYS has capability to display the cracks at locations of cracking or crushing in concrete elements. Cracking is shown with a circle outline in the plane of the crack, and crushing is shown with an octahedron outline. The first crack at an integration point is shown with a red circle outline, the second crack with a green outline, and the third crack with a blue outline.

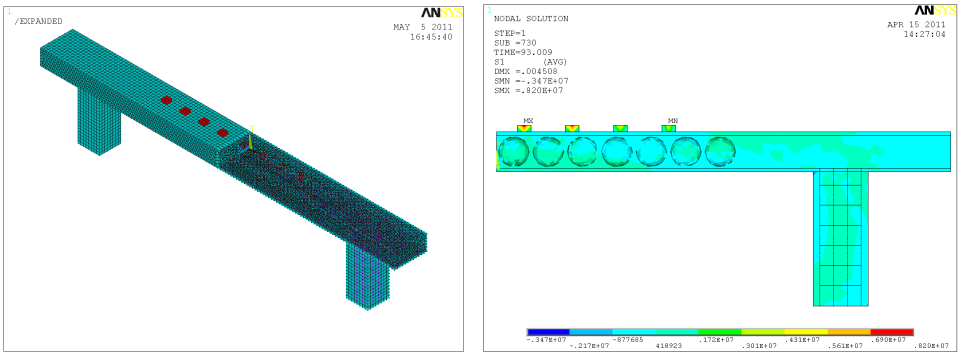

Figure 10. FEM of Strip Support and Tension Map to SLS

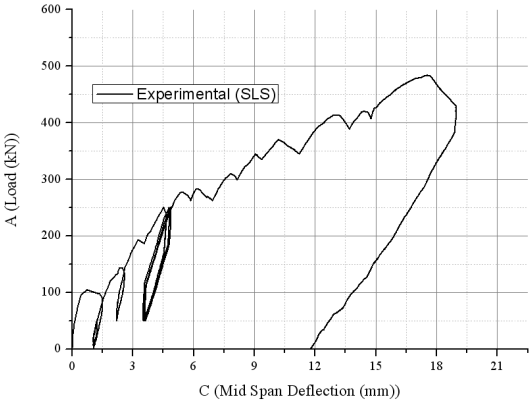

Figure 11. Load-Deflection Experimental Curve to SLS

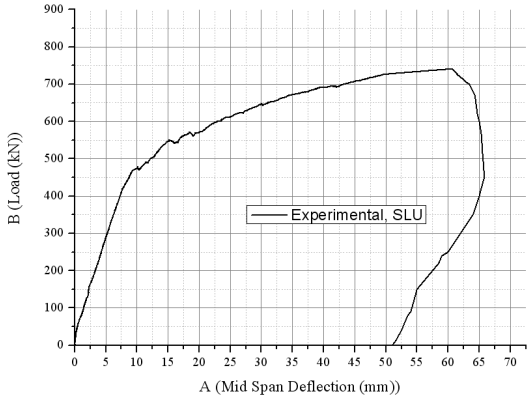

Figure 12. Load-Deflection Experimental Curve to SLU

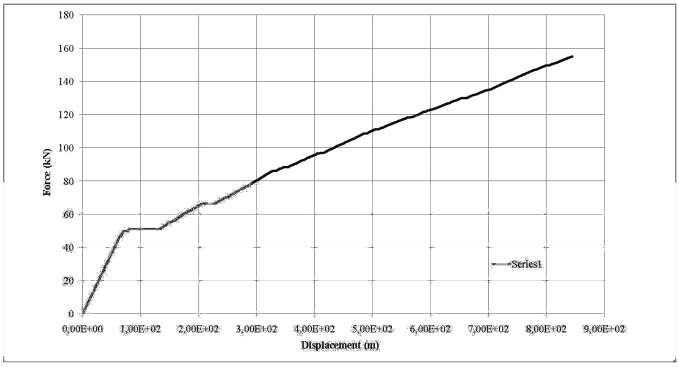

Figure 13. Load-Deflection Curve by Finite Element Analysis

Figure 14. Experimental Crack Patterns, Ax A-B

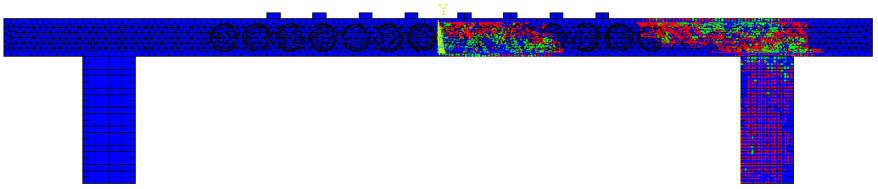

Figure 15. Experimental Crack Patterns by Finite Element Analysis

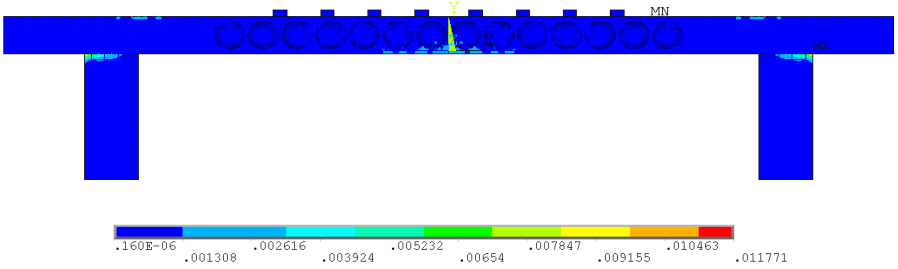

Figure 16. 1stPrincipal Stress by Finite Element Analysis

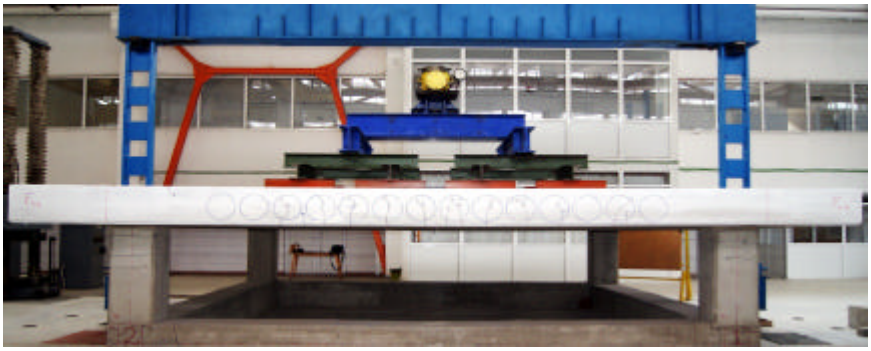

Figure 17. Experimental Crack Patterns, Ax 2-1

3. CONCLUSIONS

This paper has presented the FEA of the spherical voided bi-axial concrete floor slabs in different variant of modeling for an experimental model, where these variant have economical benefits also adequate for structural uses. The following findings are drawn from this work:

- The finite element model was able to simulate the model. Where the load-deflection relation and strain distribution along the section's depth results have good agreements with experimental results;

- Nonlinear finite elements analysis predicted the ultimate capacity and the crack patterns like the experiments. Also indicated the failure types;

- The present finite element model can be used in additional studies to develop design rules for spherical voided bi-axial concrete floor slabs.

References

1. ACI Committee 318, *Building Code Requirements for Reinforced Concrete (ACI 318-08) and Commentary (ACI 318R-08),* American Concrete Institute, Detroit, 2008.
2. Akram, Sh.M., Shatha, S.K., *Nonlinear Finite Elements Modeling of Hybrid Reinforced Concrete Beams*, M.Sc. Thesis, Anbar University, Iraq, 2010.
3. Calin, S., Asavoaie, C., Florea, N., *Issues for achieving an experimental model concerning concrete slab with spherical gaps*, Buletinul IPI, Tomul LVI (LX), Fasc. 2, 2010.
4. Desayi, P. and Krishnan, *Equation for stress-strain curve of concrete*, ACI J.,61, pp. 345-350, 1964.
5. Kachlakev, D., Miller T., Yim, S., *Finite Element Modeling of Reinforced Concrete Structures Strengthened with FRP Laminates*. Oregon Dept. of Transp., USA, Res. Group, Final Report SPR 316, May 2001.
6. Kheyroddin, A., Naderpour, H., *Nonlinear Finite Element Analysis of Composite RC Shear Walls.* Iranian J. of Science & Techn., 32, B2, 79-89, 2008.
7. Kwan, A.K.H., Dai H., Cheung Y.K., *Non-Linear Sesimic Responce of Reinforced Concrete Slit Shear Walls*. J. of Sound a. Vibr., 226, 701-718, 1999.
8. Mac, Gregor, J.G., *Reinforced concrete Mechanics and Design*, prentice – Hall, Inc., Englewood Cliffs New Jersy, USA, 1997.
9. Raongjant, W., Jing, M., *Finite Element Analysis on Lightweight Reinforced Concrete Shear Walls with Different Web Reinforcement,* The Sixth PSU Engng. Conf., May 8-9, 2008.
10. Terec, L., Bugnariu, T., Pastrav, M., *Analiza Neliniara a Cadrelor din Beton Armat cu Pereti Turnati în Situ.* Romanian J. of Materials, 40, 214-221, 2010. (in Romanian)
11. Wolanski, J.A., *Flexural Behavior of Reinforced and Prestressed Concrete Beams Using Finite Element Analysis*, M.Sc. Thesis, Marquette University, Milwaukee, Wisconsin, 2004.

Artificial aggregate from the different types of fly ash

Vít Cerný[1], Rostislav Drochytka[2]
[1, 2] *Faculty of Civil Engineering, Brno University of Technology, Brno, 662 37, Czech Republic*

Summary

Electricity production with solid fuels combustion is currently still one of the main sources of energy. But it is not only single product of these plants. There are formed also so-called energy by-products, which are often the high-quality substitutes source. Due to in progress or completed innovation of various energy equipment, is it obvious that the production decline of these potential raw material is not awaited. It is therefore appropriate to always seek new ways to use it in building materials.

This paper deals with suitability verification of the energy by-products of selected producers to sintered artificial aggregates production. Results of laboratory tests show that the fluidized fly-ashes have a larger perspective for use in technology of artificial aggregate production with using the method of cold way of production. On the contrary, high-temperature fly-ashes can guarantee getting much better aggregate mass by using the method of sintering, thanks to higher percentage of glass phase and minimal percentage of CaO.

KEYWORDS: fly ash, environment, heating plant, building material.

1. INTRODUCTION

Production of artificial aggregates from fly-ash has long been, both at home and abroad, considered as one of the technologically very advantageous ways of using these by-products in building industry. Options for using them in the building production sphere are very numerous, primarily in production of lightweight concretes. There is a considerable interest in the public use provided that the aggregate will be delivered at convenient prices and its use will be beneficial and profitable for building organizations.

Yet known and commonly used production technology of, for example, ash-agloporit is however characterized by high production costs which do not allow production of the aggregate at the desired low price level. To re-establish the production of artificial aggregates from fly ashes in the Czech Republic, it is necessary to find the optimal raw material composition and, of course, the

appropriate production technology in order to maximize the use of the potential of the produced fly ashes.

2. EXPERIMENTAL VALIDATION OF FLY ASHES SUITABILITY

2.1 Characteristics of the fly ash tested

For basic assessment of the characteristics of the tested fly ash samples, it is necessary to consider the physic-chemical properties such as mainly the loss of annealing, bulk density and content of free CaO. For the experimental activities, there have been the basic types of by-products of heating plant Plzen chosen. These samples demonstrate major differences in the nature of ashes from classical combustion and fluid combustion. The following table shows the results of the main parameters with the requirements, given by the Standard of CSN 722072-6 - Fly-ash for production of artificial aggregate by using the method of sintering.

Table 1 Physic-chemical properties of fly-ash samples tested

Name of the test	Unit	CSN	Classical	Fluid
Loss on annealing	[% Wt.]	max. 15	5,51	2,03
Loss on drying	[% Wt.]	max. 5	0,02	0,01
Content of sulphate sulphur	[% Wt.]	max. 15	0,27	7,03
Content of free CaO	[% Wt.]	max. 15	<0,1	6,39
Bulk density in bulk	[Kg.m^{-3}]	min. 600	585	645
Bulk density shaken off	[Kg.m^{-3}]	min. 800	695	755

These properties clearly show that domestic ashes have a low proportion of combustible substances, expressed as loss on annealing, due to effectively adjusted combustion technology. Due to the nature of coal combustion in fluidized furnaces, the table clearly shows the higher content of sulphate sulphur and free lime in the fluid ashes. Likewise, these products typically achieve the lower pouring weight too.

2.2 Pre-drying of the ash mixtures samples

Preparation of raw material batch for sintering charge grid represents the need of adding technological water for the purpose of granulation. In the subsequent process of self-burning, it is thus necessary to spend some energy on the process of pellets drying. If there is the fluid ash used in the mixture, it often causes increasing the need of adding the water for chosen consistency up to the double

amount compared with the mixture of purely high-temperature ash, due to the impact of chemical composition and messy structure.

For maximum utilization of energy which leaves the furnace in the form of flue gases, it is very suitable to use the energy for pre-drying of the raw material batch. When encountering the increase of fluid ash in the mixture, it can also be expected that a batch with higher manipulation strength will be created.

Test samples will be pre-dried in the laboratory drying oven at the temperature of 170°C for the time period of 1 hour. These parameters of pre-drying are chosen on the basis of expected parameters of the new technology. For the purpose of comparison, the following illustration provides strengths in compression related to the dried samples of ash mixtures. In the case of using the classical ash only, it was not possible to determine the parameters of dried samples due to insufficient strength of the tested items.

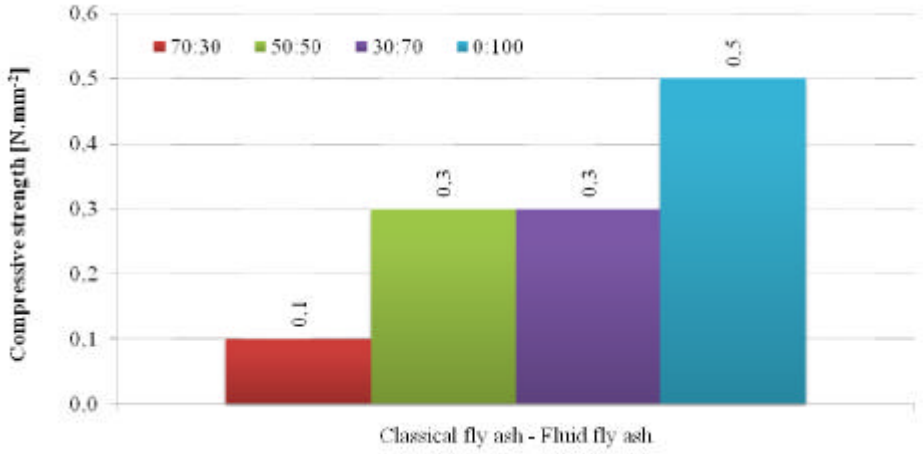

Figure 1. Compressive strength of the dried samples of fly ash mixtures

The results of compressive strength of the fly-ash mixtures samples show the fact that there is the increase of the tested items strength depending on the increasing proportion of fluid ash. This feature is caused mainly by chemical composition of the various types of ash.

2.3. Test burnings in laboratory furnace

This section focuses on monitoring selected physical-mechanical properties of the tested samples of fly-ash mixtures after the process of burning. Test samples will be burned in a muffle furnace with a relatively steep temperature curve of burning which is consistent with the very high speed of burning on the sintering

grid. Burning time is characterized by the initial temperature of 25 °C, maximum burning speed which can be ever achieved in the muffle furnace (approx. 8.0 °C/min.) and isothermal duration at the temperature of 1,200 °C for the time period of 10 minutes, which together determines the burning time of 160 minutes ± 2 minutes.

As expected, after burning the samples in the muffle furnace there were various volume changes caused by characteristics of individual ashes and their mixing ratio. Therefore, it is also important to mention the rate of shrinkage of the individual test samples.

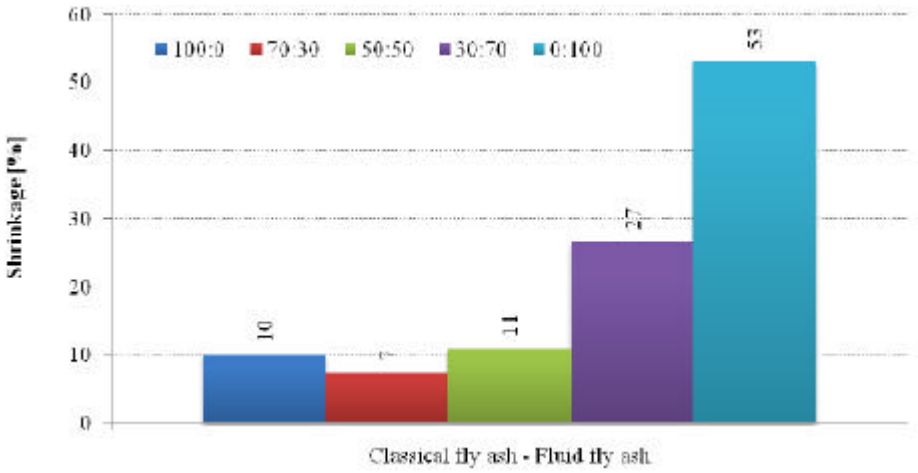

Figure 2. Rate of shrinkage of the burned fly ash mixture samples

The figure shows that the increasing proportion of fluid fly-ash in the mixture causes the increasing of the shrinkage rate of test samples mainly due to the content of free lime as a flux material. In the following pictures there will also be mentioned other important parameters of the burned samples of the fly-ash mixtures to verify the influence of shrinkage on other properties of tested items.

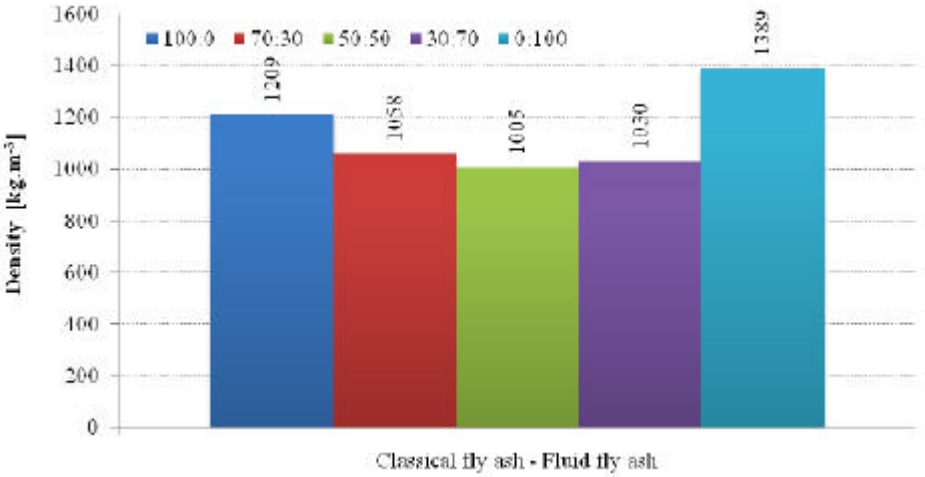

Figure 3. Density of the burned fly-ash mixture samples

Results of the density determination of the burned samples of the fly-ash mixtures show that, in terms of characteristics of the individual types of the fly-ashes, mainly the bulk density and content of free CaO are very important. In the first case, the fly-ash with higher density increases the bulk density of the burned samples too. In the second case, the higher content of CaO causes higher rate of shrinkage and thus it also increases the bulk density.

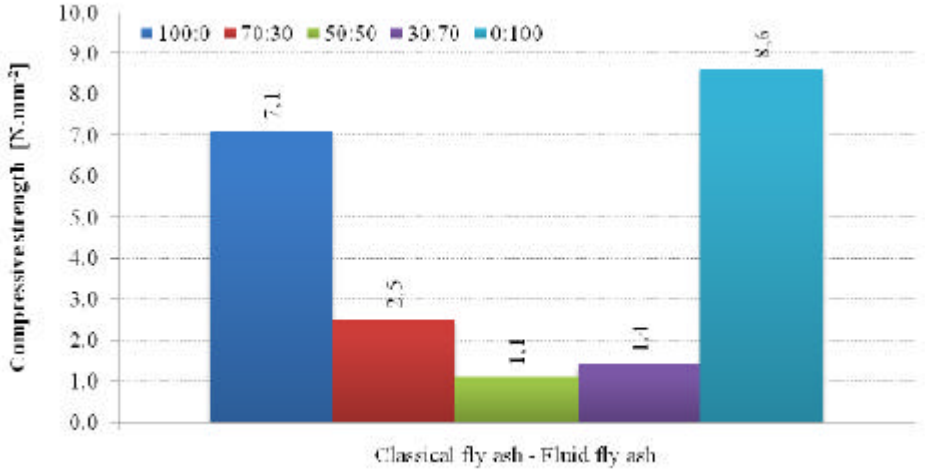

Figure 4. Compressive strength of the burned fly-ash mixture samples

The results related to the determination of compressive strength of the burned samples of the fly-ash mixtures show that the higher strengths are achieved mainly by samples with higher content of ash taken from the classical method of combustion, due to better response in the solid phase. Higher shrinkage of the samples with a predominant proportion of the fluidized ash causes a slight increase in strength. On the other hand, it does not reach such values like the samples with only the standard ash do. Compared to high-quality response in the solid phase, there is the decomposition of hydration products occurring when burning the mixtures with fluid fly-ash. These are the hydration products appearing either during storage of the raw material in the production plant or subsequently during wet process of preparing test items. This process causes weakening of the micro-structure.

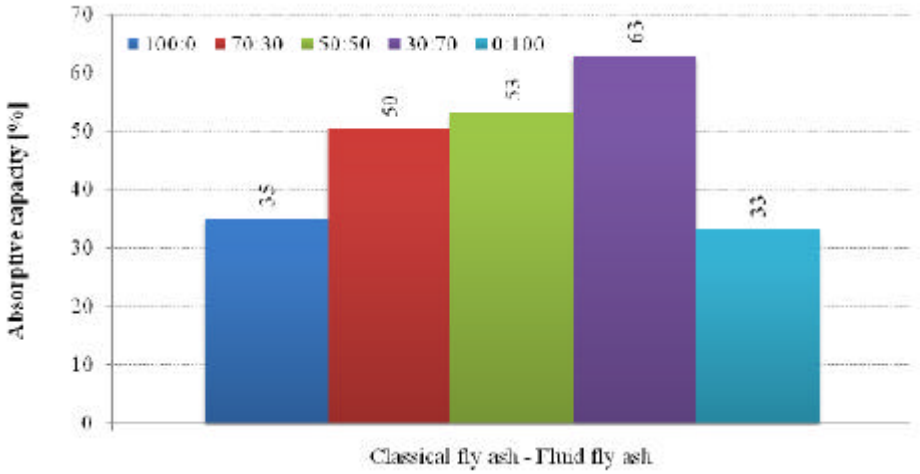

Figure 5. Absorptive capacity of the burned fly-ash mixtures

The main factor that affects the absorption is the nature of fluid ash and its proportion in the mixture. On one hand, its micro-structure and chemical composition cause higher absorption of the material. On the other hand, this trend is influenced by increasing shrinkage of the samples of burned ash mixtures, which results in decrease of the absorption.

3. CONCLUSIONS

Possibilities of using fly-ashes from energy production are now really widespread. It is often about replacement of cement and other binders with using primarily pozzolanic properties of fly-ashes which arise at high temperatures. However, suitability of fly-ashes for these types of processing is considerably reduced. Production of artificial aggregates is a good way of using of even low-quality fly-ashes in maximally possible amount. Results of laboratory tests show that the fluidized fly-ashes have larger perspective of the use in production technology of artificial aggregate by using cold ways of preparation. The technology of their production would therefore be limited to granulation, storing and maturing in humid environment. When preparing the aggregate by using the method of self - burning, there is the negative impact of both its chemical composition but also the disordered micro-structure which reduces quality of the resulting fragment (cullet).

On the other hand, ashes from the classical method of burning guarantee getting much better aggregate by using the method of sintering, due to the higher percentage of glass phase and minimal percentage of CaO. Using the ashes for producing the aggregate by the cold ways is also possible. However, it is required to add a binding material which stimulates the pozzolanic properties.

Acknowledgements

This paper was produced with the research intention MSM 0021630511 with the name “Progressive construction materials with the use of secondary raw materials and their influence on the service life of constructions” with the financial support from funds of the state budget through the Ministry of Industry and Trade within the project FR-TI2/351 with the name “New technologies of high-value porous aggregate from various types of ashes”.

References

1. Cerný, V.; Drochytka, R. Vliv vstupních surovin na kvalitu umelého kameniva ze spékaných popílku. In *Construmat 2010.* Kocovce, Slovak Technical University in Bratislava. 2010. pages 70 - 72 ISBN 978-80-227-3297-0. (In Czech)
2. Cerný, V.; Drochytka, R.; Kulísek, K. Environmental impact analysis of artificial aggregate burning process. In *New Computational Concepts in Civil Engineering.* Iasi, Romania, Editura Societatii Academice "Matei - Teiu Botez". 2010. pages 165 - 172 ISBN 978-973-8955-87-5.
3. Kulísek, K.; Cerný, V. Preparation of Artificial Aggregates based on Self-burning of Coal-wastes. In *17. Internationale Baustofftagung.* Weimar, Bauhaus-Universität, Weimar, Germany. 2009. pages 1293 - 1298 ISBN 978-3-00-027265-3.Clough, R.W., Penzien, J., *Dynamics of Structures*, McGraw-Hill, New York, 1993.
4. Melichar, T., Procházka, D.; Cerný, V. Studium fyzikálne-mechanických parametru lehkých vysokopevnostních betonu s pórovitým kamenivem na bázi spékaných popílku. *Beton TKS* 2010. The tenth (4/2010). pages 54 - 60 ISSN 1213-3116. (In Czech)

The Influence of Contact Algorithm Parameters on the Results for the Case of Static Frictional Contact When Using ANSYS 12

Andrei – Ionut Stefancu[1], Sergiu Baetu[1], Silviu - Cristian Melenciuc[1] and Mihai Budescu[1]

[1]*Department of Structural Mechanics, The "Gheorghe Asachi" Technical University of Iasi,700710, Romania*

Summary

A problem is nonlinear, in structural mechanics, if the stiffness matrix or the load vectors is displacement dependent. Nonlinearity can be classified as geometric nonlinearity – associated with significant changes of structure geometry or material nonlinearity – associated with changes of material properties (such as plasticity or hyperelasticity).

Contact nonlinearities, or boundary conditions nonlinearities occurs when the contact surface between two solids is load dependent, one of such cases this being the case of frictional contact. Described here are two basic theories that, although different in their approaches, offer the desired solutions for such problems. One of the theories is known as the penalty function method, and the other as the Lagrange multipliers method. The papers presents the influence of input parameters for the case of two methods on the results when using the software ANSYS 12.

KEYWORDS: contact algorithm, frictional contact.

1. INTRODUCTION

A linear analysis presumes that the structural response is directly proportional to the loading. This type of analysis can accurately describe real behaviour of structures or less accurate when a series of simplifying hypothesis are applied. A linear analysis assumes that large displacements do not occur, supports do not fail, the stress – strain relationship is linear, the loads are constant etc. The equilibrium equations KD=R are solved taking into consideration the initial boundary conditions. The displacement $D=K^{-1}R$ are obtain via a single step analysis. A lot of the simple engineering problems may be solved using linear approaches [7].

Nevertheless, there are a lot of cases when the hypothesis present above do not fully describe the initial conditions, such as:

- adjoining parts may come in/out of contact;

- the contact area may vary with loading;
- the elastic materials may start to behave nonlinear if the stress – strain curve has nonlinear characteristics;
- displacements and rotations may become excessively high thus requiring the equilibrium equations to be rewritten, taking into considerations the new boundary conditions;

Consequently a problem may evolve from a linear to a highly nonlinear one.

In structural mechanics, a problem is nonlinear if the stiffness matrix or the load vector depends on the displacements. In heat transfer, nonlinearity may arise from temperature-dependent conductivity (which makes the coefficient matrix depend on temperature) and from radiation (which makes the radiative heat flux a nonlinear function of temperature) [6].

Nonlinearity in structures may be classified as:

- geometric nonlinearity - when the nonlinear behavior of the problem is given by significant changes in the geometry of the structure. This case includes, beside others, large displacements/strains analyses [9], [17], extrusion [10] and material welding or forming [12];
- material nonlinearity – is associated to the nonlinear behaviour of materials and includes the case of plastic materials [1] or hyperelastic materials [4];
- contact nonlinearity – occurs when the contact surface between two parts changes during the analysis. This case includes frictional contacts.

Nonlinearity makes a problem more complicated because the equations that describe the solution must incorporate conditions not fully known until the solution is known – the actual configuration, loading condition, state of stress and support conditions. The solution of the problem cannot be obtained in a single step analysis.

Nonlinear problems are describes using differential equations derived from continuum mechanics. Solving these equations leads to understating the studied process. Very often the solution of a set of differential equations may be hard to find. In this cases numerical method are used to provide an approximate solution to the given equations. Approximate methods include the finite element method (F.E.).

Over the last decades a large number of software packages that solve nonlinear problems using the F.E. have developed. One of these programs is ANSYS [2]. ANSYS is a comprehensive general-purpose finite element computer program capable of performing static, dynamic, heat transfer, fluid flow and electromagnetism analyses [11].

The hereby paper presents the influence of input parameters for the case of two different F.E. formulations of contact problems when using the software ANSYS 12.

2. F.E. FORMULATIONS OF CONTACT PROBLEMS

There are briefly presented two basic theories that, although different in their approaches, offer the desired solutions to body contact problems. One of the theories is known as the penalty function method, and the other as the Lagrange multipliers method.

The main difference between them is the way they include in their formulation the potential energy of contacting surfaces. The penalty function method, due to its economy, has received a wider acceptance. The method is very useful when solving frictional contact problems, while the Lagrange method, based on multipliers, is known for its accuracy.

The main drawback of the Lagrange method is that it may lead to ill-converging solutions while the penalty formulation may lead to inaccurate ones.

The normal Lagrange formulation as well as the augmented Lagrange methods will be presented.

2.1. Penalty method

The penalty method involves adding a penalty term to enhance the solving process. In contact problems the penalty term includes the stiffness matrix of the contact surface. The matrix results from the concept that one body imaginary penetrates the another [15], [16].

The stiffness matrix of the contact surface is added to the stiffness matrix of the contacting body, so that the incremental equation of the F.E. becomes:

$$\left[K_b + K_c\right] \cdot u = F \tag{1}$$

The magnitude of the contact surface is unknown [14]; therefore, its stiffness matrix $\mathbf{K_c}$ is a nonlinear term. The total load and displacement values are

$$F^{tot} = \sum \Delta F \tag{2}$$

$$u^{tot} = \sum \Delta u \tag{3}$$

To derive the stiffness matrix, the contact zone (encompassing the contact surface) is divided into a series of contact elements. The element represents the interaction

between the surface node of one body with the respective element face of the other body. Figure 1 shows a contact element in a two dimensional application. It is composed of a slave node (point S) and a master line, connecting nodes 1 and 2. S_0 marks the slave node before the application of the load increment, and S marks the node after loading.

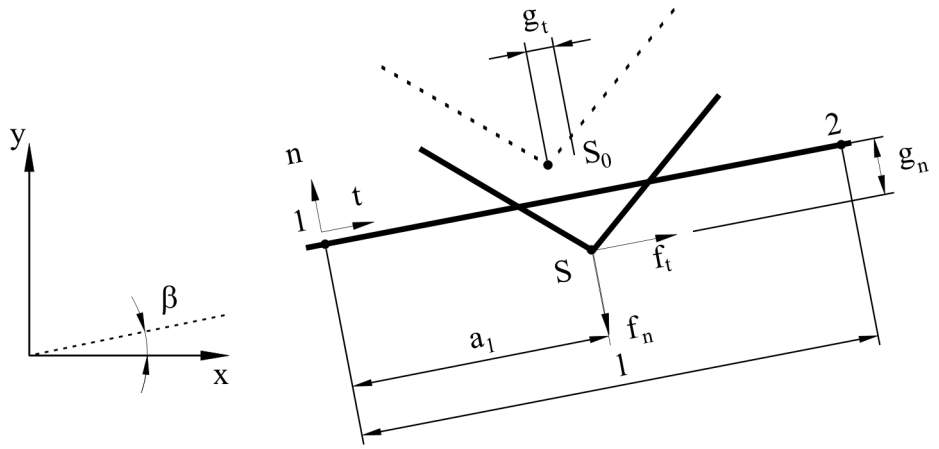

Figure 1. Contact element – penalty method formulation

The two cases of friction namely sticking and sliding friction modes of friction will be presented separately. The expresion of the potential energy will be presented as obtained from a variational analysis

2.1.1. Sticking mode of friction

In this case the first variation of the potential energy equals

$$dp_c = d\,g^t k g = k_n g_n d\,g_n + k_t g_t d\,g_t \tag{4}$$

and the second variation is:

$$d\left(dp_c\right) = d\,g^t k d\,g = k_n\left[d\,g_n d\,g_n + g_n d\left(d\,g_n\right)\right] + k_t\left[d\,g_t d\,g_t + g_t d\left(d\,g_t\right)\right] \tag{5}$$

where k_n and k_t are penalty terms used to express the relationship between the contact force and the penetrations along the two direction for the case of a 2D contact.

2.1.2. Sliding mode of friction

The main difference between the two cases is that now the tangential force acting at the contact surface has equals magnitude friction force hence the first variation of the potential energy of a contact element is:

$$d\Pi_c = f_n d g_n + f_t d g_t = k_n g_n d g_n + \operatorname{sgn}(g_t) m_d k_n g_n d g_t \tag{6}$$

where f_n equals:

$$f_n = k_n g_n \tag{7}$$

2.2. Lagrange multiplier method

The Lagrange multiplier method pertains to adding a linear term that includes constraints multiplied by unknown variables — the Lagrange multipliers. The added linear term is the potential energy of contact surface

Along with the classical Lagrange method, which is limited to the sticking mode of frictional the augmented Lagrange method will be presented.

2.2.1. Classical Lagrange method

In the case of classical Lagrange the contact forces are expressed by Lagrange multipliers. The method is applicable to frictionless contact. However, with certain modifications, it can be applied to sticking-friction contact [8].

The contact elements, in the case of Lagrangian methods it presented in figure 2.

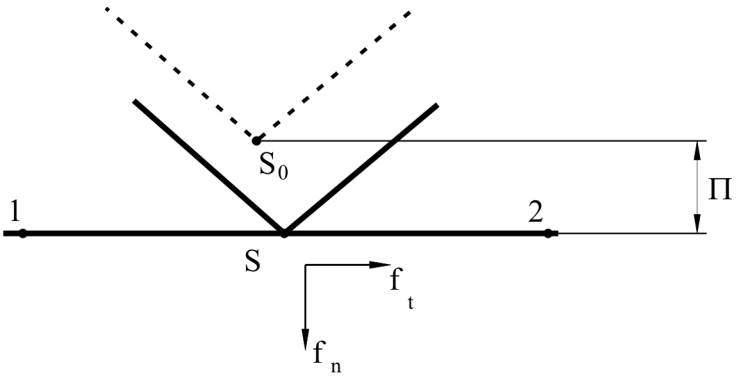

Figure 2. Contact element – Lagrangian methods

The contact problem involves the minimization of potential ? by equating to zero the following:

$$\Pi(u, l_n, l_t) = \Pi_b(u) + \sum_k \left(l_n^k g_n^k + l_t^k g_t^k \right) \tag{8}$$

where $?_n$ and $?_t$ are Lagrange multipliers and g_n and g_t are the displacement along the two direction.

2.2.1. Augmented Lagrange method

In this case the regularization of classical Lagrange method is performed by adding a penalty function from the penalty method [5] [13]. This method, unlike the classical one, can be applied to sticking friction, sliding friction, and to a frictionless contact.

In matrix form, equation 8, for the case of augmented Lagrange method, is:

$$\Pi(u, \Lambda) = \Pi_b(u) + \Lambda^T g + \frac{1}{2} g^T k g \tag{8}$$

3. PARAMETRIC ANALISYS OF STATIC CONTACT

In order to point out the way that the contact formulation may influence the results a parametric analysis is performed. The purpose is to view how various input parameters can alter the results.

The model used comprises of two solids made up of structural steel-like materials. The larger solid has its lower surface fixed while at the upper end interacts with the smaller solid via a frictional contact. A normal force is applied on top of the smaller solid

Input parameters

- Young's modulus for the two solids E1 – for the bigger solid and E2 for the other one. The two, range between $2 \cdot 10^{11}$ Pa and $2 \cdot 10^{12}$ Pa;
- the normal contact stiffness factor (ARG1) that varies between 0.01 and 1;
- the number of finite elements used for the surface belonging to the smaller solid ES1 (can take the value 3 or 4) and the larger solid ES2 (can take the value 5 or 6);
- F.E. formulation (ALG). This parameter can take three values: 0 (augmented Lagrange method) 1 (pure penalty method) and 4 (classical Lagrange method);

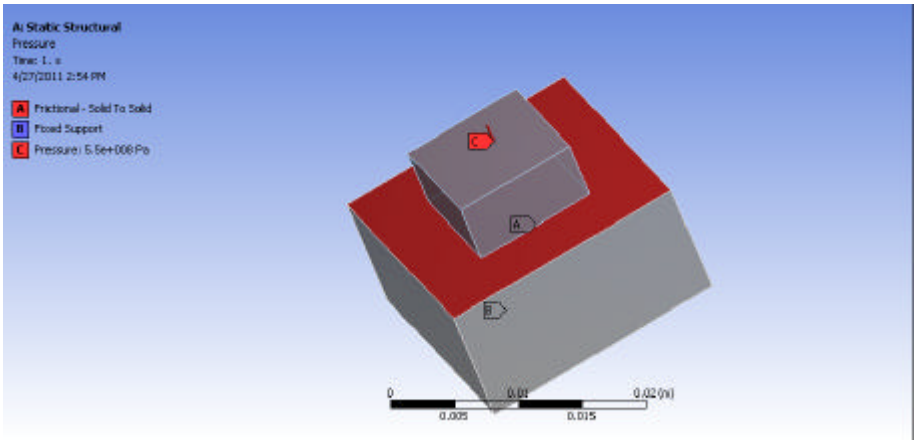

Figure 3. The model used in the parametric analysis:
a) frictional contact; b)fixed support; c) loading surface.

Output parameters:

- the maximum value of the frictional stress (FSM);
- analysis run-time (RT) – the time need to solve the problem**.**

3.1 Variation of FSM

In this part the variation of FSM with E1, E2 and ALG will be presented

3.1.1 Variation of FSM with E1 and E2

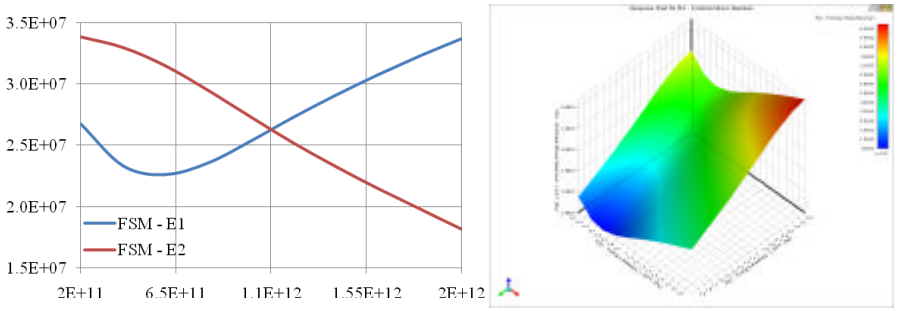

a) b)

Figure 4. The variation of FSM with E1 and E2 for ALG=0:
a) individually with each parameter; b) with both E1 and E2.

The way FSM depends on E1 and E2 will be presented only for the case of augmented Lagrange method (ALG=1). The graphs remain the same when the pure penalty formulation is used for the contact. The differences are small in terms of extreme values of the FSM. This is because the contact conditions are expressed both times based on the principle of imaginary penetrations.

The maximum value of FSM is influenced by both E1 and E2. This is given by the fact that the slave node and the master surface can be alternatively located on the surface of the two bodies.

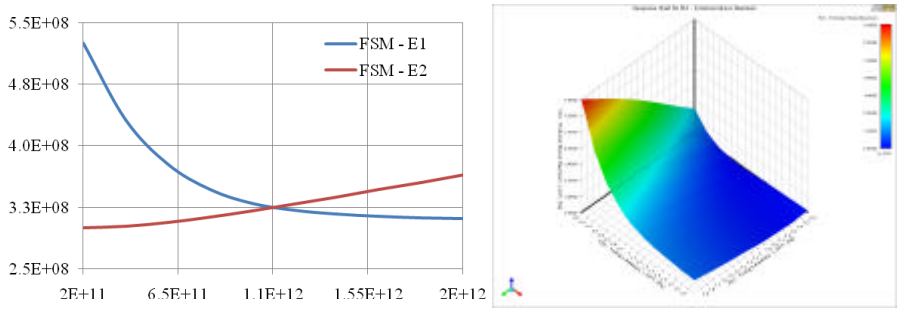

a) b)

Figure 5. The variation of FSM with E1 and E2 for ALG=4:
a) individually with each parameter; b) with both E1 and E2.

3.1.2 Variation of FSM with ES1 and ES2

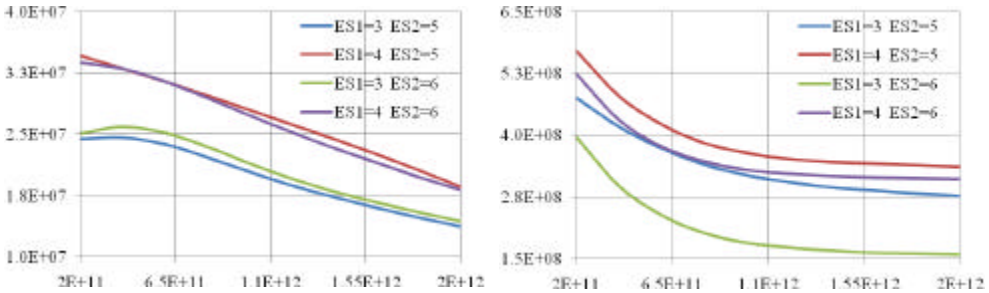

a) b)

Figure 6. The variation of FSM with ES1 and ES2
a) FSM vs. E2 for ALG=0; b) FSM vs. E1 for ALG=4.

Given the fact that for ALG=0 the maximum value of FSM is given by E2 and for ALG=4 by E1 figure 5 presents the variation of FSM with ES1 and ES2 accordingly.

It can be stated, based on the figure 6, that the maximum value of FSM is obtained for the combination ES1=4 and ES2=5. The explanation is that for ALG=4 the errors due the increase of element surface (ES2=5) while for ALG=0 the accuracy of the formulation is improved when increasing the number of elements (ES1=4).

3.1.3 Variation of FSM with ES1, ES2, E1 and E2

Based on the facts stated above the variation of FSM with the four factors is presented in figure 7.

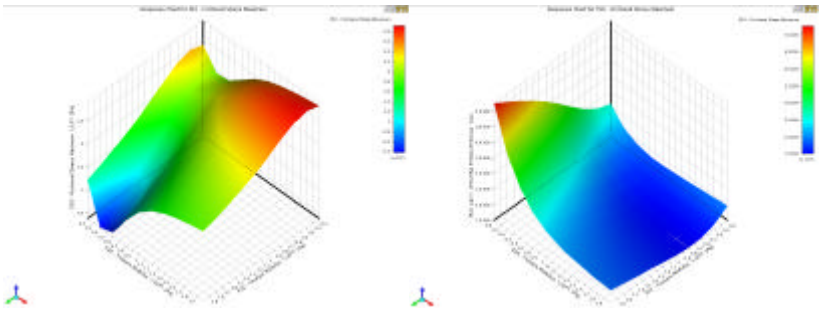

a) b)

Figure 7. The variation of FSM with E1 and E2 when ES1=3 and ES2=6
a) ALG=0; b) ALG=4.

For the rest of the ES1 and ES2 combinations the graphs do no change their shape for neither of the formulations. The only difference may be represented by slight variations of the maximum values of the FSM.

3.2 Variation of RT with ARG1

Another factor influenced by the type of contact algorithm as well as by the input parameters is the analyses run-time. This is the time needed by the program to solve the given problem taking into consideration the initial boundary condition. Besides parameter such as material characteristics, amplitude of loading, support conditions, are the the normal contact stiffness factor and the tangential contact stiffness factor. Given the fact that this is a static analysis the influence of the tangential stiffness will not be presented. The variation will be presented only for the pure penalty and augmented Lagrange formulation since the classic Lagrange method does not need a contact rigidity.

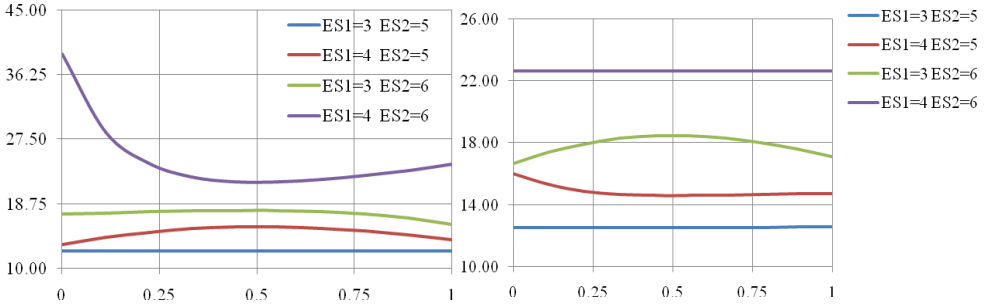

a) b)

Figure 8. The variation of RT with ARG1
a) ALG=1; b) ALG=0.

From figure 8.a can be concluded, that the analysis run-time is independent of the normal stiffness for the case of a small number of finite elements. It can be seen choosing a proper value for the normal stiffness can compensate the increase of the number of finite elements.

Figure 8.b confirms the fact that the augmented Lagrange formulation leads to faster converging solutions due to the optimization function added than the pure penalty method.

Because the way the normal Lagrange method formulate the contact condition this method is independent of the normal contact stiffness factor.

The conclusion that emerges is that the augmented Lagrange method leads to the lowest average run times when solving static frictional contact problems.

4. CONCLUSIONS

When there is the need for an accurate evaluation of the stress state of a frictional contact the classic Lagrange method is providing the best solution.

The main drawback of the classic Lagrange method is the fact that the analysis run-time increases when compared to the other method. It is recommended to use this formulation to partially solved problems (when solving coupled analyses)

When the behavior of the materials during the analysis can be predicted it is recommended to use asymmetric contact. This along with the conclusions pointed out in chapter 3.1.1 can enhance the use of penalty formulations. For further information regarding the asymmetric contact please refer to ANSYS documentation [3].

When the analysis run-time is an issue it is recommended to use the augmented Lagrange method along with a low value of normal contact stiffness factor (such as 0.01) and an appropriate number of finite elements. The lower values of normal contact stiffness factor are required so that the Newton –Raphson method converges more rapidly.

References

1. Anandarajah, A., *Computational Methods in Elasticity and Plasticity: Solids and Porous Media*, Springer, 2010;
2. ANSYS Inc., *ANSYS Workbench 2.0 Framework Version: 12.0.1*, 2009/a;
3. ANSYS Inc., *Theory Reference for Mechanical APDL and Mechanical Applications, Contact Technology Guide, Surface-to-Surface Contact, Designating Contact and Target Surfaces, Asymmetric Contact vs. Symmetric Contact*, 2009/b;
4. Bonet, J., Wood, R. D., *Nonlinear continuum mechanics for finite element analysis*, Cambridge University Press, 1997;
5. Chaudaray, A.B., Bathe, K.J., *A solution method for static and dynamic analysis of contact problems with friction*, Computer and Structures, 1986.
6. Cook, R. D., Malkus, D. S., Plesha, M. E., *Concepts and applications of finite element analsys,Third Edition*, John Wiley & Sons, 1989;
7. Cook, R.D., *Finite element modeling for stress analysis*, John Wiley & Sons, 1995;
8. Crisfield, M.A., N*on-linear Finite Element Analysis of Solids and Structures, Vol. 2, Advanced Topics*, John Wiley, 1997
9. Iu, C. K., Chan, S. L., *A simulation-based large deflection and inelastic analysis of steel frames under fire*, Journal of Constructional Steel Research, 2004;
10. Lebaal, N., Schmidt, F., Puissant, S., *Design and optimization of three-dimensional extrusion dies, using constraint optimization algorithm*, Finite Elements in Analysis and Design, 2009;
11. Moaveni, S., *Finite element analysis – Theory and application with ANSYS*, Prentice Hall, 1999;
12. Osswald, T. A., Turng, L. S., Gramann, P. J., *Injection Molding Handbook*, Hanser Verlag, 2008;
13. Simo, J.C., Laursen, T.A., *An augmented Lagrangian treatment of contact problems involving friction*, Computer and Structures., 1992;
14. Stein, E., Ramm, E., *Error-controlled adaptive finite elements in solid mechanics*, John Wiley and Sons, 2003;
15. Wriggers, P., Vu Van, T., Stein, E., *Finite element formulation of large deformation impact-contact problems with friction*, Computers and Structures, 1990;
16. Wriggers, P., Simo, J.C., *A note on tangent stiffness for fully nonlinear contact problems*, Communications in Applied Numerical Methods., 1985
17. Zienkiewicz, O.C., Taylor, R.L.,*The Finite Element Method, Fifth edition, Volume 2: Solid Mechanics*, Bluetterworth Heinemann, 2000

"Computational Civil Engineering 2011", International Symposium
Iasi, Romania, May 13, 2011

Strengthening of masonry walls with FRP composite

Jerzy Szolomicki[1], Piotr Berkowski[1] and Jacek Baranski[1]
[1]*Department of Civil Engineering, Wroclaw University of Technology, Wroclaw, Poland*

Summary

Analytical model and analysis of numerical calculations results for masonry walls strengthened with FRP composite are presented in a paper. In the recent years, the importance of structural interventions in the area of masonry structures for repair and strengthening increased considerably. Structural weakness or overloading, dynamic vibrations, settlement, in-plane and out-of-plane deformations, can cause failure of masonry structures. In-plane resistance of masonry walls without reinforcement is based on mortar strength and brick proportions. If the forces are strong enough to exceed the in-plane strength capacity of masonry wall, a shear failure will occur. This failure mode is characterized by brittle tensile cracking through the mortar and the masonry unit and by a sudden loss of lateral load capacity. As an alternative for use of traditional reinforcement methods advanced FRP composite can be used, that offer excellent physical and mechanical properties. Fibre reinforced polymers are particular typology of composite materials made of high resistance fibres impregnated with polymeric resins. FRP materials are characterized by excellent tensile strength in the direction of the fibres and by negligible strength in the direction transverse to the fibres. Their function usually consists in adsorbing tensile stress due to shear and flexural actions. Among the reachable advantages there is also the increase of the overall stiffness and ductility. The tensile behaviour of FRP material consisting of one type of fibre material is characterized by a linearly elastic stress-strain relationship until failure. The tensile strength and stiffness of an FRP material is dependent of several factors. Because the fibres in an FRP material are the main load-carrying constituent, type of fibres, orientation and quantity, primarily govern the tensile properties of the FRP material.

KEYWORDS: masonry walls, strengthening, FRP composite.

1. INTRODUCTION

In the recent years, importance of structural intervention in the area of masonry structures for repair and strengthening has increased considerably. It is not only

because of destruction caused by natural disasters, but also because a lot of masonry typical structures have achieved their service life-time, and as well it is a result of many revitalization design actions during that there must be realized structural strengthening. Structural weakness or overloading, dynamic vibrations, settlement, in-plane and out-of-plane deformations can cause failure of masonry structures. Seismic loadings induce out-of-plane bending of walls between the restraining floors. Analysis of the failure modes must take into account many different factors, such as boundary conditions, wall compressive strengths, joint tensile strengths, wall stiffness, and applied loadings. In-plane resistance of un-reinforced masonry walls is based on mortar strength and brick proportions. If the forces are great enough to exceed the in-plane strength capacity of the wall, a shear failure will occur. This failure mode is characterized by brittle tensile cracking through the mortar and the masonry unit and a sudden loss of lateral load capacity.

Among the traditional methods used to repair masonry structures there are:

- filling of cracks and voids using grout injections,
- stitching of large cracks and other weak areas with metallic,
- application of reinforced grouted perforations to improve the cohesion and tensile strength of masonry,
- external jacketing by shotcrete or by cast-in-situ concrete,
- external or internal post-tensioning with steel ties, in order to tie structural elements together into an integrated three-dimensional system.

Advanced FRP materials which offer excellent physical and mechanical properties can serve as an alternative for use of traditional methods. Fibre reinforced polymers area particular typology of composite materials, made of high resistance fibres impregnated with polymeric resins. FRP are characterized by excellent tensile strength in the direction of the fibres and by negligible strength in the direction transverse to the fibres. Their function usually consists in adsorbing tensile stress due to shear and flexural actions. Often, among the reachable advantages, there are also the increase of the overall stiffness and ductility. The tensile behaviour of FRP materials consisting of one type of fibre material is characterized by linearly elastic stress-strain relationship until failure. The tensile strength and stiffness of FRP material depends on several factors. Because the fibres in FRP material are the main load-carrying constituent, type of fibres, orientation and quantity, primarily govern the tensile properties of the FRP material [1, 2, 3, 4, 5].

The main aims of the presented analysis are: to compare numerically behaviour up the ultimate conditions of walls strengthened by different types of fibres (CFRP and GFRP ones [12, 13]), having different strip widths and by placing the reinforcement in different positions, to formulate analytical models able to predict

the ultimate strength in agreement with the observed failure mechanisms. The application of FRP strips modifies the static behaviour of walls because the fibres can bear the stresses occurring at the tensed edges. It has been observed that the distance between strips and their width can influence on the mechanism of failure [6, 7, 8, 9, 10, 11, 12, 13].

2. APPLICATION OF FRP LAMINATES

Fibre reinforced polymers (FRP) are a particular typology of composite materials, made of high resistance fibres impregnated with polymeric resins. The mixing result is a material with properties between fibre and resin. FRP materials are characterized by excellent tensile strength in the direction of the fibres and by negligible strength in the direction transverse to the fibres. Their function usually consists in adsorbing tensile stress due to shear and flexural actions. Often, among the reachable advantages, there also are the increase of the overall stiffness and the ductility. FRP products are commercialized in different shapes as rods, tendons, laminates and three-dimensional components [14].

In presented numerical analysis, the Authors used strips of rectangular cross-sections to reinforce the masonry walls. It is a sample of FRP laminate. Lamination technology is based on the joining or bonding of two or more layers to form a laminate. The materials can vary in type and mechanical properties in addition to property specific orientation. All laminate constructions utilize relatively high strength and stiffness materials.

3. IN-PLANE BEHAVIOUR OF MASONRY WALLS STRENGHTENED WITH FRP LAMINATES

The in-plane resistance in load-bearing unreinforced masonry walls is provided by the shear bond strength of the mortar and the friction shear due to the vertical load. The shear strength of a bearing wall, in the case of a sliding failure mode, can be determined as:

$$\tau = \tau_0 + \mu \sigma_n \tag{1}$$

where:

τ - shear stress at the shear bond failure, τ_0 - shear bond strength at zero normal stress due to adhesive strength of a mortar, μ - coefficient of friction between brick and mortar, σ_n - normal stress.

Fibre reinforced polymer composites can provide viable solutions for the strengthening of walls subjected to stresses caused by wind or earthquake loads.

4. NUMERICAL ANALYSIS OF MASONRY WALLS STRENGTHENED BY CFRP AND GFRP LAMINATES

The walls which dimensions – 3.65 m x 1.2 m x 0.125 m – and loading conditions are shown in Figure 1, were the subject of the analysis. Numerical FEM analyses were performed using LUSAS code. The walls were modelled by means of solid elements (HX16).

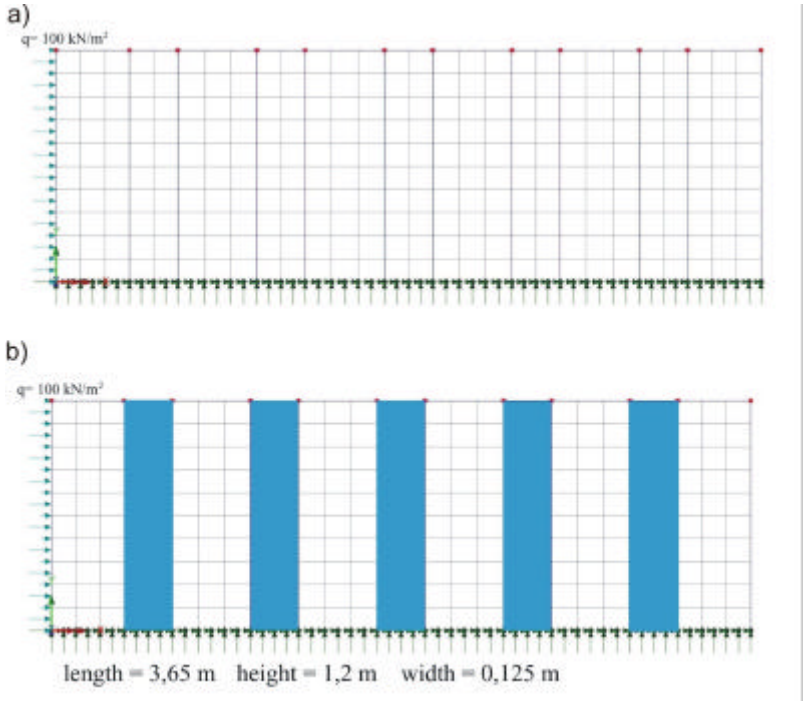

Figure 1. Scheme of the analyzed masonry wall (front view):
a) model of wall without strengthening; b) model of wall strengthened with CFRP and GFRP.

Calculations were conducted for three cases:

1) wall without strengthening,

2) wall strengthened with CFRP strips (5x0.26 m; epoxy TB650 + HS Carbon),

3) wall strengthened with GFRP strips (5x0.26 m; epoxy TB650 + E-Glass Fabric).

In the cases 2) and 3) the walls were strengthened with 5 strips. In all the cases the walls were loaded with horizontal uniformly distributed loading) with increments 20 kN/m^2 until final value 500 kN/m^2. In cases 2) and 3) the composite strips (carbon and glass laminates) were bonded with an epoxy resin on the faces of the walls.

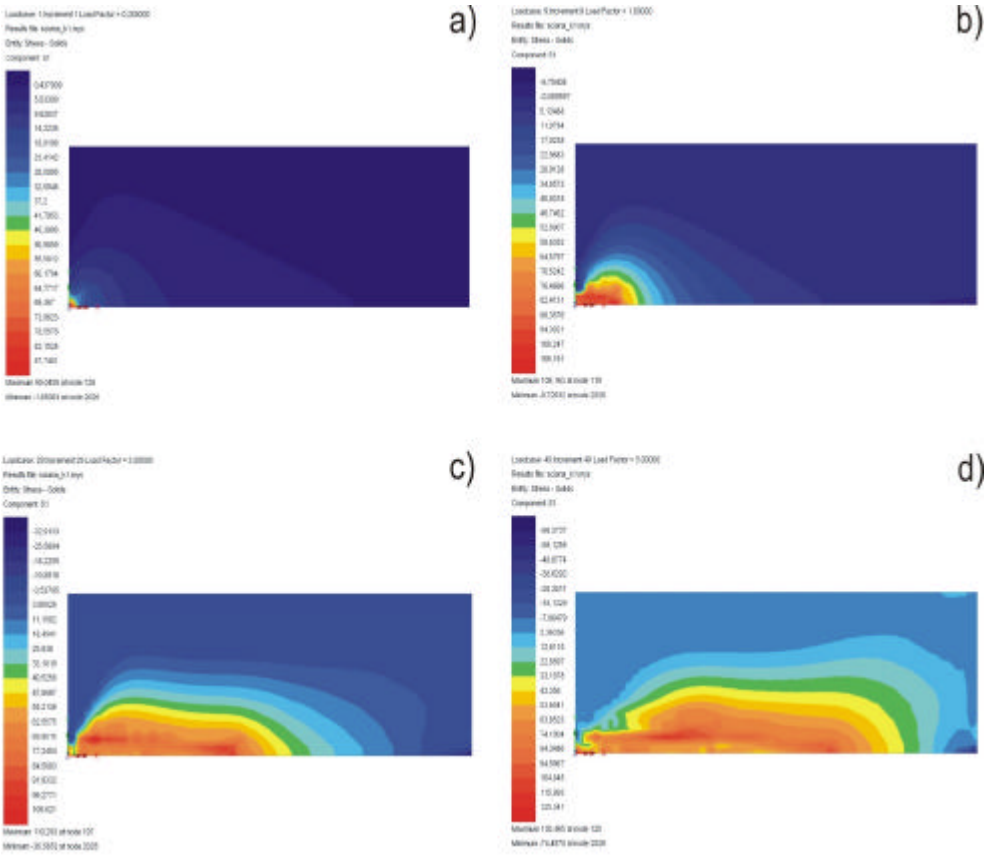

Figure 2. A diagram of principal stresses S1 in the wall without strengthening for different levels of load factor increment: a) l.f. = 0.2; b) l.f = 1.0; c) l.f. = 3.08; d) l.f. = 5.0.

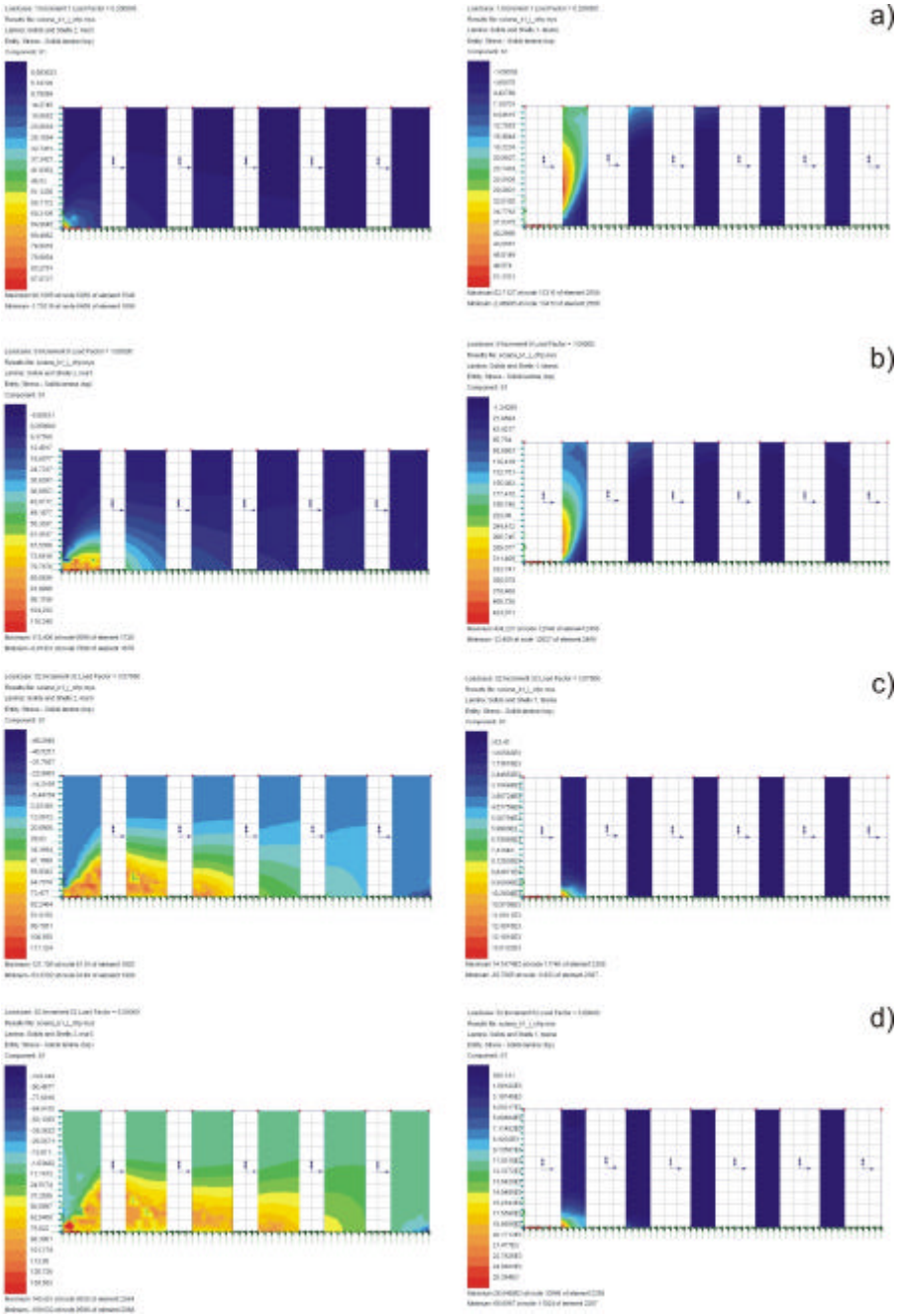

Figure 3. A diagram of principal stresses S1 in the wall strengthened with CFRP strips for different levels of load factor increment. Left side - distribution of stresses in a masonry wall; right side - distribution of stresses in a top layer of CFRP strips. Load factor increments: a) l.f. = 0.2; b) l.f = 1.0; c) l.f. = 3.08; d) l.f. = 5.0.

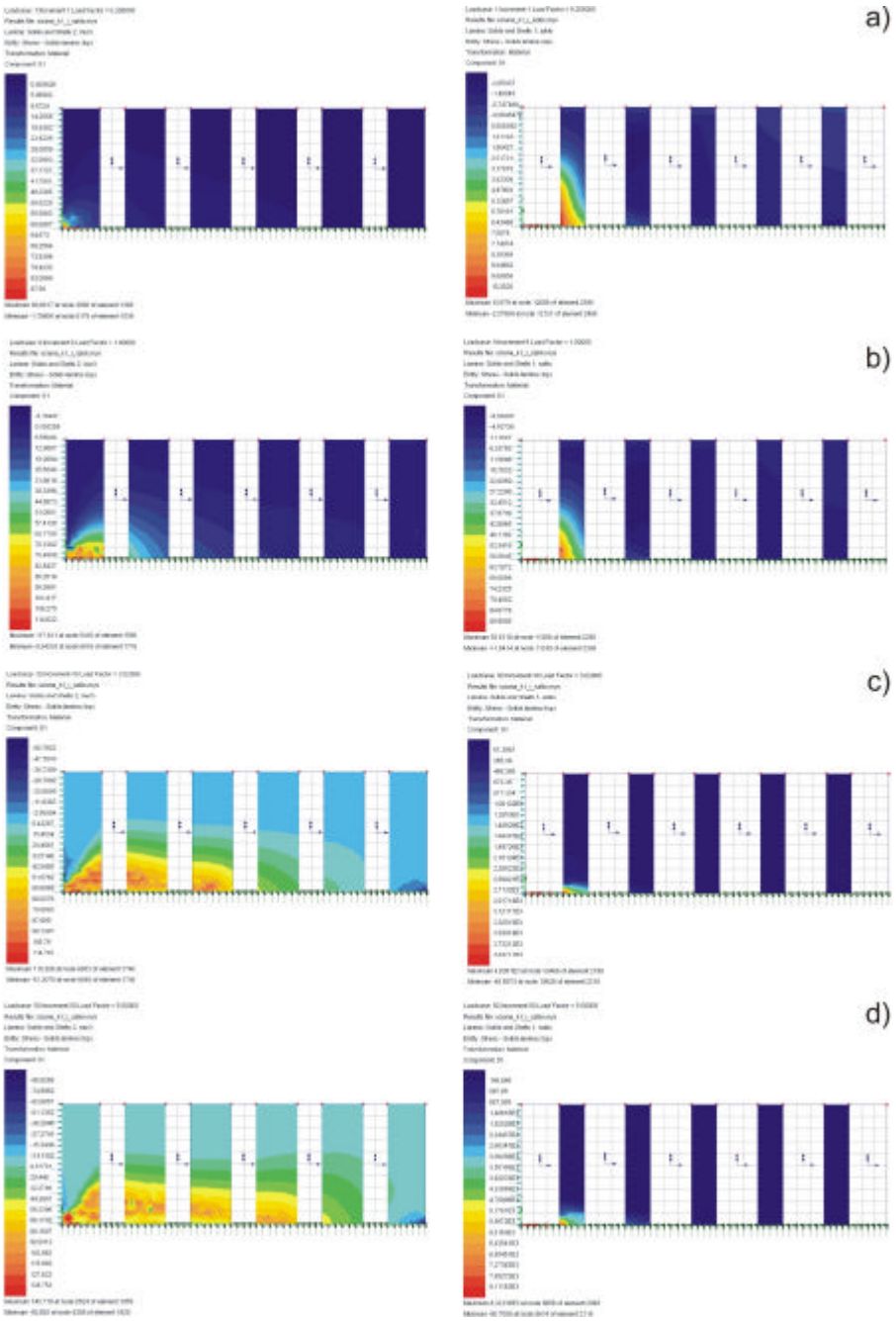

Figure 4. A diagram of principal stresses S_1 in the wall strengthened with GFRP strips for different levels of load factor increment. Left side - distribution of stresses in a masonry wall; right side - distribution of stresses in a top layer of GFRP strips. Load factor increments: a) l.f. = 0.2; b) l.f = 1.0; c) l.f. = 3.08; d) l.f. = 5.0.

5. CONCLUSIONS

Load model of the wall was assumed as in order to observe the behaviour of the wall from the initial state (not damaged one – Figure 2) to the state of its destruction. For such model stress distribution analyses in the wall without reinforcement and in the walls strengthened with CFRP (Figure 3) and GFRP (Figure 4) strips, were conducted. For the walls strengthened with CFRP and GFRP strips it can be clearly seen that the tensile stresses are transferred to these stripes, that leads to a significant reduction of theses stress in the wall. With the increase of the loads a zone of the maximum tensile stress appears in the analyzed case only in the first FRP tape and moves downwards. Tensile stress in the wall without reinforcement causes appearance of cracks and with their further increase provokes wall's destruction, of course. In the case of walls strengthened with CFRP and GFRP fibres stress S_1 distribution is similar. However, it should be noted, that more efficient for the transfer of unfavourable tensile stress are the CFRP strips.

In addition, a careful consideration of the boundary conditions should be realized in order to identify the critical factors that may affect the bending strength of masonry walls. The presented analysis show that both CFRP and GFRP composites offer great advantages in strengthening of masonry walls by a great increase in their bending strength. In the analyzed cases the Authors wanted to verify how the non-reinforced and composite reinforced walls behave during the full load cycle, from the initial, not damaged state until the total destruction. In the future, it is planned to determine numerically the effectiveness of FRP strengthening of already damaged wall, as well some laboratory and in-situ examinations will be executed.

References

1. Aiello, M. A. , Pecce, M. , *Experimental bond behavior between FRP sheets and concrete*, Proceedings of the International Conference Structural Faults and Repair, London, UK [CD-ROM version] (2001).
2. Aiello, M. A., Sciolti, S. M., *Bond analysis of masonry structures strengthened with CFRP sheets*, *Construction and Building Materials*, 20 (1-2), 90–100 (2006).
3. Ceroni, F, Pecce, M, Manfredi, G., Marcari, A., *Experimental bond behavior in masonry elements externally reinforced with FRP laminates*, Proceedings of International Conference: Composites in Constructions – CCC 2003, Cosenza, Italy, Eds. D. Bruno, G. Spadea, N. Swamy, Editoriale Bios, 313–318 (2003).
4. Liu, Y., Dawe, J., McInerney, J., *Behaviour of GFRP sheets bonded to masonry walls*, Proceedings of the International Symposium on Bond Behaviour of FRP in Structures (BBFS 2005), Hong Kong, China, 473-480 (2005).
5. Panizza, M. , Garbin, E., Valluzzi, M. R., Modena, C., *Bond behaviour of CFRP and GFRP laminates on brick masonry*, Proceedings of the 6th International Conference on Structural Analysis of Historical Construction, Bath, UK, 763-770 (2008).
6. Foster, P. , Gergely, J., Young, D. , McGinley, M., *Strengthening masonry buildings with FRP composites*, Proceedings of the 11th International Conference: Structural Faults & Repair, Edinburgh, UK, 183 (2006) [CD-ROM version].

7. Garbin, E., Valluzzi, M. R., Modena, C., Galati, N., Nanni, A., In-plane design for masonry walls strengthened by FRP materials, Proceedings of the 11th International Conference: Structural Faults & Repair, Edinburgh, UK, 184 (2006) [CD-ROM version].
8. Hamilton, H. R., Dolan, C. W., Flexural capacity of glass FRP strengthened concrete masonry walls, *ASCE Journal of Composites for Construction*, 5(3), 170-178 (2001).
9. Hanoush, S., McGinley, M., Mlakar, P., Scott, D., Murray, K., Out of plane strengthening of masonry walls, *ASCE Journal of Composites for Construction*, 5(3), 139-145 (2001).
10. Kiss, R. M., Kollar, L. P., Jai. J, Krawinkler, H., *Masonry strengthened with FRP subjected to combined bending and compression*, Part II: Test results and model predictions", *Journal of Composite Materials*, 36(9), 1049-1063 (2002).
11. Mosallam, A. S., Out of plane flexular behaviour of unreinforced red bricks walls strengthened with FRP composites, *Composites Part B: Engineering*, 38 (5-6), 559-574 (2007).
12. Nanni, A., Tumialan, G., Fiber-reinforced composites for the strengthening of masonry structures, *Structural Engineering International*, 13(4), 271-278 (2003).
13. Valluzzi, M. R., Strengthening of masonry structures with Fibre Reinforced Plastics: From modern conception to historical building preservation, Proceedings of the 6th International Conference on Structural Analysis of Historical Construction, Bath, UK, 33-45 (2008).
14. Morbin, A., Strengthening of Masonry Elements with FRP Composites. University of Missouri-Rolla, pp. 192.

Assessment of the residual bearing capacity of reinforced concrete road bridges

Cristina Romanescu[1] and Constantin Ionescu[2]
[1]*Highway Bucharest-Comarnic Direction, Romanian National Company for Motorways and National Roads, Bucharest, 010873, Romania*
[2]*Department of Structural Mechanics, Faculty of Civil Engineering and Building Services, Iasi, 700050, Romania*

Summary

Bridges have been assessed in Romania until now using simple methods of analysis, without use of site specific data. This type of bearing capacity evaluation is conservative and doesn't satisfy the current necessity of knowledge in road bridges management domain. Because the number of damaged bridges located on national roads and motorways network from Romania is in constant growth, an impressive number of bridges were classified as deficient as a result of visual inspection, it is therefore very important to evaluate bearing capacity as accurate as possible. To determine the most accurate bearing capacity of a bridge the best model is the bridge itself, but at design time this model was not available. During operation period testing can be made on real model and with actual traffic loads and can be used in evaluation of the bridge.

In this respect the Romanian National Company for Motorways and National Roads is concerned with in situ checking of bridges using the latest equipments and assessment of residual bearing capacity on real models.

This paper presents realized tests for the maximum values of vertical deflection obtained by calculation comparing to using laser flexigraph, by measuring vertical movements in several specific sections of the new built passage on National Road 1 at km 55+720.

KEYWORDS: bridges; nondestructive testing; residual bearing capacity; actual traffic loads; weight restriction.

1. INTRODUCTION

Evaluation of residual bearing capacity of bridges is an assessment that is based on scientific principles. The analysis refers to the structure and processes of degradation over time of the constituent materials. Calculation of the initial bearing

capacity, respectively the residual one requires a large amount of information about the structure, such as:

1. Standards and regulations applied during the bridge design and actual ones (calculation loads and real loads, calculation method of bending moment produced by the calculation loads for different forms of cross section for elements)
2. Properties of the constituent materials will be determined by physical and chemical analysis at initial moment (based on results of tests conducted on the site) and at the time of the assessment (determined by nondestructive methods: resistances, static and dynamic elasticity modules, area of reinforcement before and after the effect of corrosion)
3. As built drawings of the bridge, including formwork and reinforcement plans (containing geometry data for elements and reinforcement, distances between and its arrangement)
4. History of maintenance and rehabilitation works.

For the recalculation of the bearing capacity of elements and reinforced concrete structures exposed to degradation processes is it necessary to know the actual, real characteristics of the component materials.

Determination of physical-mechanical characteristics (strength, stiffness and ductility) of the structures may be performed by calculation, if one has all the necessary information on physical and mechanical characteristics of materials and actual condition of the bridge or whether they can be estimated with sufficient accuracy or by testing when the above requirements are not met.

Currently, in Romania, bearing capacity is calculate by the strength limit state method, working with calculation loads pondered by the overload factors and calculation strengths of concrete and reinforcement. There are bridges which were calculated by the allowable resistance method, using normated loads and strengths of concrete and reinforcement. A first step in establishing the operating conditions of the bridge is to calculate the bearing capacity by the limit state method and to make comparison to the loads in service.

Faster or slower evolution in time, of degradations is a hypothesis that should be taken into account. Analysis of all degradation and monitoring its evolutions [1] reduces the risk to fall below the allowable bearing capacity required by the actual traffic. To each structural degradation, function of type and severity of structural damages one may attach a reduction coefficient of the characteristics of structure components. Also, location of damages may influence on the distribution of loads and therefore a new structural behavior.

Another issue of concern is the evolution, both in structure and intensity of the traffic on the bridge because a lot of bridges designed for lower loading classes are now trafficked by heavier convoys.

From the entire range of defects only a part of defects are affecting the structural capacity [2], and some of them even if they do not affect it may be an imminent risk of collapse for the structure: rust stains on concrete surface, geometric imperfections of the concrete surface, segregation of concrete, infiltrations, efflorescence, stalactites, carbonation of concrete, concrete corrosion, brittle concrete, scaling concrete, honeycomb fissures of concrete, fissures or cracks in concrete, corrosion of reinforcement, uncoated reinforcement, inappropriate connections between precast elements, large deformations of the superstructure, cumulus to an superstructure element of several degradations (corrosion of concrete and steel reinforcement, scaling, fissures, cracks, etc…), overloading of bituminous pavements, patching and potholes in bituminous pavements, wrong location of the drainage tubes, infiltrations in expansion joints area and damaged expansion joints.

Influences of the defects on the bearing capacity are the following:

- modification on geometrical characteristics of section [degree of reduction on reinforcement area (reduced stiffness due to corrosion of reinforcement), reduction degree of concrete section (low durability of concrete due to corrosion, delamination, wear, carbonatation, other chemical phenomena), loss of bonding (adhesion) between concrete and reinforcement, including the reduction or lack of reinforcement anchorage at the ends of the element];
- modifications of the efforts condition in element and real loads redistribution on each element;
- increase of the dynamic effect due to relaxation and growing deformations of reinforcement and due to the increase of live loads (loads from those used for design).

For the evaluation it was proposed [3] a noninvasive methodology which consists of following steps:

1. Determination of physical-mechanical characteristics of concrete by nondestructive methods:

- determination of compressive strength of concrete using a method or combined methods by testing in situ;
- experimental determination in situ of the static and dynamic module of elasticity of concrete (ultrasonic pulse method);
- measurements of the dimensions of elements that compose the superstructure.

2. Determination of reinforcement characteristics by nondestructive methods (pahometer, radiography, thermography, etc…):

- determination of the path of rebar;
- determination of concrete cover thickness;
- determination of reinforcement area (comparison to the diameter from reinforcement plans if available, to find out how much was reduced due to corrosion A_a).

3. Necessary data concerning convoys: axle weight, axle and wheel position to the elements of resistance structure of the bridge and the speed of the convoy
4. Calculation of the capable moment of the bridge deck without degradation and then degraded bridge, after loading convoys tests
5. Evaluation of the current solicitation level of the superstructure's beams, highlighting the potential reserves of bending moment for the designed class load of the bridge and according to Eurocode convoys, taking into account the real dynamic coefficient

- the designed charging schemes having test loads;
- reading, of the measuring devices before loading, after completion of each loading scheme and after each discharge.

6. Comparing obtained test results by the proof method of superstructure to those obtained by laser flexigraph.

In 2009, the National Company of Motorways and National Roads from Romania (CNADNR) acquired under a project funded by European Union, PHARE Project RO 2006/018-147.03.10 "Improvement of safety and quality services in transport sector" (a project undertaken by Center for Road Technical Studies and Informatics - CESTRIN, subunit CNADNR) quality control equipment for road works. Among others, there were purchased two laser flexigraph, conception of the "Laboratoire Central des Ponts et Chaussées" in France in order to use this equipment for the assessment of bridges. Given the worldwide trend to use the latest equipment began an extensive testing program for bridges with these devices have begun. In this respect, CESTRIN designed a tests program which consists of comparative studies between the results obtained by classical methods and with modern devices. In 2007 the project to widen the National Road 1 on a length of 12.850 km (route containing five bridges) financed by the Romanian State Budget, amounting to approximately 40 million Euro has started. On this road at km 55+720 there is located a passage over the railway, in the Brazi village. The project involved extending the implementation of a passage in this section parallel to the existing one. Given that this passage was completed this year, action was necessary to test it by test loads and was included in the comparative testing program. The newly built passage crosses nine railway lines and is 196.00 m long and it has seven openings. The superstructure is made in the static scheme simply supported beams in the central opening and continuous beam in the other openings. Cross section are arranged in four prestressed precast beams with post-tension reinforcement and in the central opening, over the railway line group are arranged six beams with the same cross section. The width of passage carriageway has 7.80 m with a sidewalk width of 1.50 m. Lamellar shaped piles are oriented in the direction of the railroad. Abutments are choked with elevations on three walls, secured to the top of the bearing seats and the guard walls.

2. MEASUREMENT OF DEFLECTIONS USING LASER FLEXIGRAPH

Laser flexigraph was used to measure vertical displacements at several points of the bridge under static, respectively dynamic loads and the deflections are determined in mm and are presented in Table 1.

Table 1. Maximum deflections measured under static, respectively dynamic loads

Opening	Static/dynamic	Temp.	Time	Registration 1	Registration 2	Maximum deflection (mm)
1	ST	26	15	779	779	**7.88**
	DYN10	27	5	3949	3974	**3.24**
	DYN20	26	5	2699	2674	***99.25***
	DYN30	27	5	2724	2724	**1.61**
	DYN40	28	2	2024	2024	**3.45**
	DYN50	28	5	3199	3199	**3.55**
2	DYN10	21	5	4099	4149	**5.4**
	DYN20	21	2	1324	1349	***90.61***
	DYN30	21	5	5099	5049	**5.75**
	DYN40	21	5	3024	3024	**8.39**
	DYN50	22	5	3349	2399	**5.82**
3	ST	19	30	1079	1036	***28.01***
	DYN10	19	5	2499	2574	**6.07**
	DYN20	19	2	1774	1774	**8.33**
	DYN30	19	5	3149	3199	**6.31**
	DYN40	20	5	2999	3024	**6.26**
	DYN50	20	2	2349	2399	**7**
4	ST	23	30	963	963	**7.01**
	DYN10	23	10	6974	6999	**2.85**
	DYN20	23	10	8324	8349	**3.56**
	DYN30	24	5	5524	5549	**2.58**
	DYN40	24	5	4724	4749	**2.71**
	DYN50	24	5	3374	3399	**2.87**

Dynamic measurements were made at different speeds of the convoy respectively 10, 20, 30, 40 and 50 km / h, passing it over a threshold of wood, as is provided in Romanian Standard 12504-86 “Railway bridges, road bridges and footbridges. Superstructure proof tests”. From analyzing the charts for opening 1 DYN20, the opening 2 DYN20 and opening 3 ST show that the measurements were disturbed so they are wrong and cannot be taken into account for the analysis.

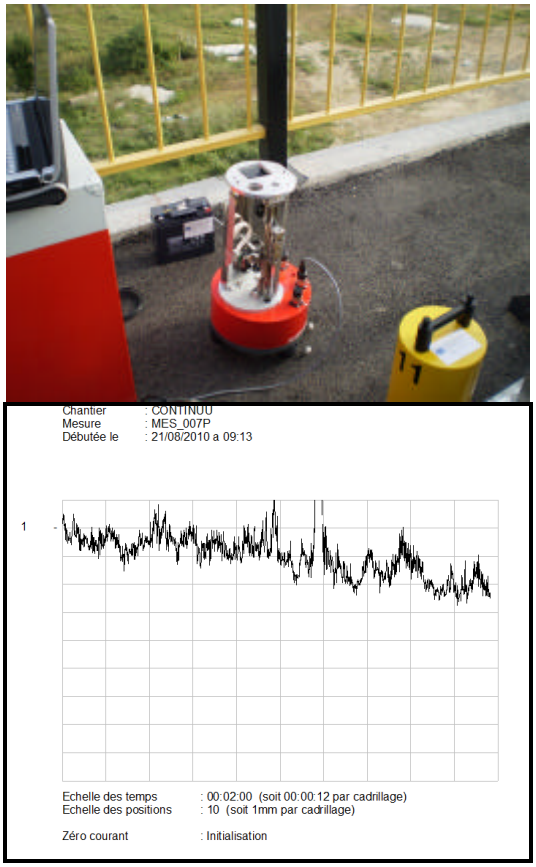

Figure 1. Measurements of deflections with laser flexigraph - passage situated on Road 1 at km 55+720 at Brazi village (dynamic measurement graph made with the laser flexigraph in opening 3 at speed of 50 km/h)

For comparing the maximum deflection values obtained using laser flexigraph were performed calculations according to limit states method, as follows:

$$M = \mathrm{M} * S \tag{1}$$

where M is the amount resulting from the calculations of 1648 kNm, S is equal to 0.775, so it follows M = 1277.2 kNm.

$$f = \frac{5ML^2}{48EI} \tag{2}$$

where: L = 35.25 m, E = 35 000 N/mm^2, I = 0.2652 m^4.

3. CONCLUSIONS

So, maximum computed deflection has a value of 18 mm, and the measurements of the laser flexigraph are 8.39 mm. In conclusion, the maximum deflections obtained by measurements are below the calculation ones, of 18 mm. Comparison of measured characteristics to the calculated ones is very useful to improve design calculating methods and for the efficiency of certification of repair works of the defects.

References

1. Prof. Dr. W. Rücker, Dipl. eng. F. Hille and Dipl. eng. R. Rohrmann, B., *Guideline for the Assessment of Existing Structures*, SAMCO Final Report, Federal Institute of Materials Research and Testing, Berlin, Germany, 2006.
2. Prof. Dr. F. Burtescu, *Experimental study on the contribution of collaboration between existing superstructures and new concrete in assessing of actual bearing capacity of the superstructure*, Technical University of Civil Engineering Bucharest, 1997. (in Romanian)
3. Eng. C. Romanescu, *Doctoral Thesis: Scientific research on deterioration states of reinforced concrete bridges using nondestructive investigation and evaluation of influence on load carrying capacity*, 2010. (in Romanian)

Shielding Testing of Barite Blocks

David Procházka[1], Tomáš Melichar[2] and Vít Cerný[3]
[1] *Institute of building Materials and Components, Faculty of Civil Engineering , Brno University of Technology, Brno, 662 00, Czech Republic*
[2] *Institute of building Materials and Components, Faculty of Civil Engineering , Brno University of Technology, Brno, 662 00, Czech Republic*
[3] *Institute of building Materials and Components, Faculty of Civil Engineering , Brno University of Technology, Brno, 662 00, Czech Republic*

Summary

Concrete products are highly prized commodity, both from manufacturers and user's perspective. Their advantage is versatility, price, durability and ease of assembly. They include a wide range and variety from vegetation blocks through interlocking pavement, shaft rings or concrete blocks for walling.

The product range is growing ever bigger. First of all in response to customers request and the purpose of use. This gives rise to special products such as barite concrete blocks used primarily for harmful ionizing radiation shielding. As is known, the blocks very ease and speed building process of vertical structural units. In the case of special structures, such as the construction of masonry shielded rooms for hospitals and nuclear plants the blocks are often more suitable option than on-site production. Mortar or concrete production with heavy aggregate has its specifics and requires experienced staff.

The presented article describes barite blocks applicability for use in construction units proposed primarily for personal protection against ionizing radiation.

KEYWORDS: barite shielding, ionizing radiation, concrete blocks

1. INTRODUCTION

In the development of medical X-ray rooms or their additional redevelopment the projector must always solve the shielding problematics. He must verify the shield degree quality in relation to the ionizing radiation source and to propose adjustments when needed. The design should naturally follow the relevant laws and regulations on nuclear safety. These documents are valid not only for nuclear power plants but generally for places where people work with ionizing radiation. Thus, even for medical X-ray workplaces.

Good design should be based on the measurement of dose rate, the amount of energy absorbed per unit weight for a certain period of time (unit is the gray per second - Gy·s-1). Respectively the dose equivalent, which reflects the effect of radiation on living tissue (unit sievert – Sv). According to these values the kind of "containment" and its thickness should be designed. Due to the fact that many X-ray devices are adjustable for varying intensity, it is obviously necessary to work with the expected maximum values. It is better to overdimension the protection than additionaly identify deficiencies and costly carry out additional modifications. It is perhaps necessary to remark that special emphasis should be placed on the x-ray control room. The annual dose equivalent for personnel may not necessarily be completely meaningless.

The X-ray workplace containment is mostly based on the barite shielding system. The barite is a mineral of high density and in these systems replaces usually used aggregate for masonry mortars, concrete or plasters.

Together with building of new workplaces additional adjustment of existing sites or rebuilding of primarily nonradiological sites can be found. In such cases, the designer may have relatively limited possibilities. Additional treatment of floors, walls and ceilings can be quite complicated if we take into account the limited lay-out or constructions carrying capacity. If those adjustments are already made the increase in floor layers and construction of additional walls may be the simplest.

2. DESIGN AND TESTING OF BARITE BLOCK

For the construction of thin walls as additional radiation protection the block – filling mortar system is probably the most suitable. This system is technologically simple and enables quick working procedure. In advance, the block production proceeds in concrete block making machine with vibration. Filling mortar should

be sufficiently flowing, to completely fill the block. It is important to maintain the desired bulk density, which is a prerequisite for successful shielding. As for block, there is less need for consistency because of vibropressing (Fig. 1).

Figure 1. Block making machine with vibration

For own blocks production, common mobile block making machine with vibration was selected. After mixture design for the block the pilot test was performed. It showed that experimental batch has too plastic consistency for vibropressing (Fig. 2).

Figure 2. Initial design. Too plastic mortar after vibropressing

Consequently the amount of water and admixtures was revised so that the mortar had reached a suitable consistency and needed strength. The final formula is given in Table 1, the appearance is shown in Figure 3.

Table 1. Designed mortar formula

Parameter		Value
Composition [%]	Cement	12
	barite sand 0-4 mm	88
	admixtures	1,12
Dry mass Volume weight of the dry mixture in shaked state [kg·m^{-3}]		2 830
Water-cement ratio [-]		0,29
Bulk density of concrete [kg·m^{-3}]	fresh mixture	3 140
	after 28 days of maturing	3 070

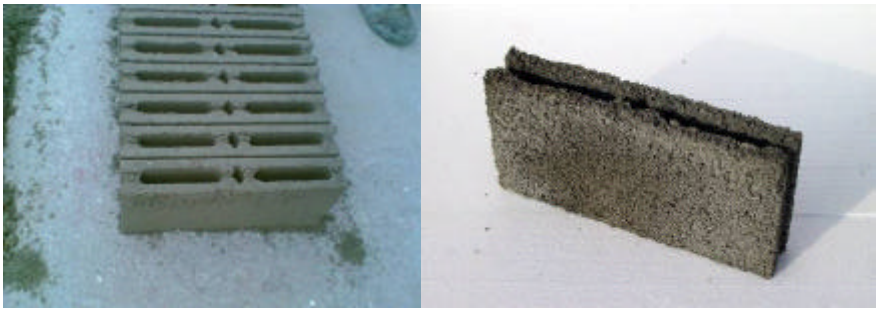

Figure 3. The block according to final formula

Tests of technological properties were conducted on prisms 40 x 40 x 160 mm. Due to stiff consistency for vibropressing it was necessary to vibrate the prisms.

Table 2. Hardened mortar properties

Parameter		Value
Water-cement ratio [-]		0,29
Bending tensile strength [MPa]	after 1 day	1,6
	after 28 days	3,3
Compression strength [MPa]	after 1 day	6,6
	after 28 days	22,4

One day strength is sufficient for materials handling. Not very high 28-day strength of the samples is due to stiff consistency. The samples, despite the vibration were not thoroughly compacted. Vibropressed samples would have surely higher strength due to pressure presence.

Shielding capabilities of material for blocks have been tested on a specially made plates of thicknesses from 10-50 mm. Radiation intensity was changed by voltage changing on the X-ray tube. Measured physical value was the dose rate.

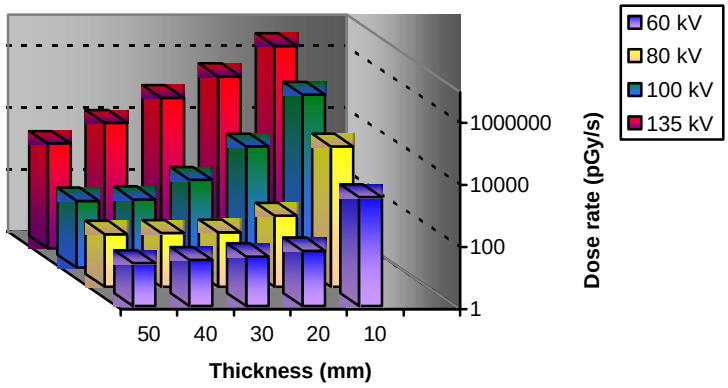

Figure 4. Shielding of barite mortar for blocks production

The block alone was not tested on X-rays. The shielding efficiency (unfilled) corresponds to approximately 40 mm slab.

Shielding of the block was then tested with previously proposed filling mortars [2, 3]. Figure 5 shows shielding of the block filled with fine (f-70) and coarse-grained (c-70) filling mortar. Shielding capability would correspond roughly to 70 mm slab. The significant decrease in dose rate is shown in Figure 6, where the comparison of filled barite blocks with fine and coarse mortar is stated. For comparison lead plates and slabs from Figure 4 are added.

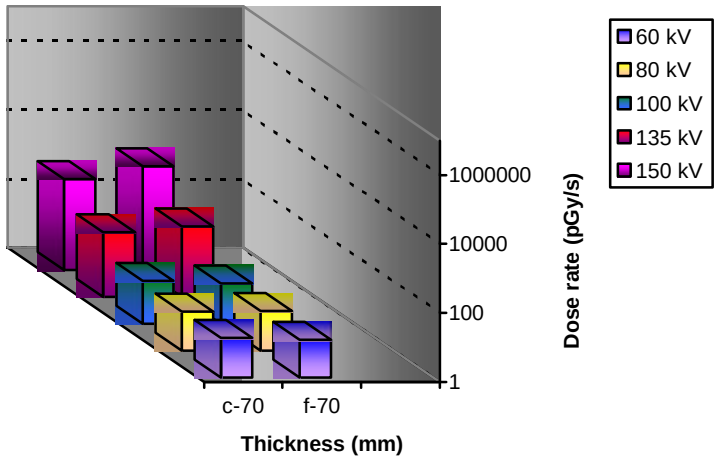

Figure 5. Barite block with coarse (c-70) and fine (f-70 filling mortar

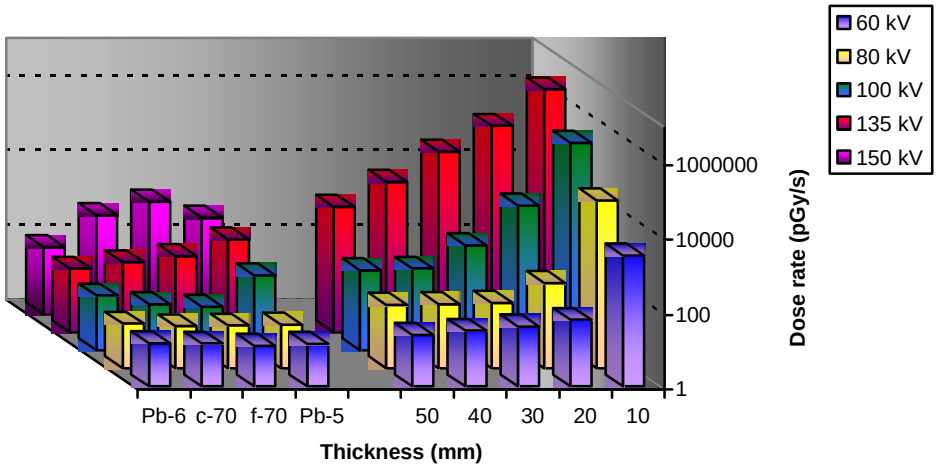

Figure 6. Comparison of various thickness of shielding materials (from left: 6 mm lead, block with filling mortars, slabs from mortar for the block)

Filled Blocks shielding capability (thickness of 70 mm) corresponds to the lead plates of about 5-6 mm. Adding to this barite plaster of 20 mm and of 3 000 kg·m^{-3}, we get protection, which is for shielding of most workplaces, in most cases sufficient.

3. CONCLUSIONS

Barite mortar and concrete is due to its high density suitable alternative to commonly used shielding materials. Their advantage is relatively modest production, friendly price and good anti-radiation efficiency. The advantage may be even that the resulting element in structure can have virtually any shape given by formwork.

Using barite concrete is particularly suitable for sophisticated workplaces, where it is necessary to build a strong shielding containment. Most often it is of course a nuclear plant, where it is necessary to eliminate the most harmful effects of ionizing radiation produced during the fission reactions. Another such place may be e.g. medical department, where ionizing radiation is worked with too.

With additional protection increasing in hospitals a simple system of thin brick walls can be used. Here will find application especially the barite mortar. The

article simply described the block-filling mortar system, which is probably for this purpose the most suitable. Two variants of filling matter (fine and coarse) were proposed and tested previously. It remained only to design mortar for block production. Here were used the findings from previous research. In addition mortar for block production was tested for compressive strength, which showed its applicability for supporting structural elements. After it, shielding tests against X-ray were performed for filling mortar and on filled block. Tests showed sufficient shielding capability for most X-ray workplaces, if used 70 mm block and 20 mm barite plaster.

Acknowledgements

The work was supported by the projects: *FAST-S-11-44: Efficiency of high volume of fine admixtures in current concrete mix design in the Czech Republic* and project *1M0579, within activity of research center CIDEAS.*

References

1. Pospíšilová, P., Fridrichová, M. Betony s kamenivem na bázi síranu barnatého, *Speciální betony*, Sekurkon, Praha, 2007. (in czech)
2. Procházka, D., Brožovský, J., Cerný, V. Shielding Mortar Design for Protection of Rooms Exposed to X-Ray, *Computational Civil Engineering 2010*, Iasi, România.
3. Procházka, D., Beneš, D. Gamma Radiation Shielding, Computational Civil Engineering 2008, Iasi, România.
4. Pospíšilová, P., Fridrichová, M., Hoffmann, O. Systém stínicích barytových smesí, *Ekologie a nové stavební hmoty a výrobky*, Vustah, Telc, 2007. (in czech)
5. Hönig, A., Zapletal, V. Nedestruktivní zkušebnictví, VUT v Brne, 1982. (in czech)

Numerical modeling on behavior under loads of self compacting concrete floors with hollow space

Gabriela Dascalu and Ciprian Asavoaie
Department of Concrete Structures, Building Materials, Technology and Management, "Gh. Asachi" Technical University of Iasi, Faculty of Civil Engineering and Building Services, Iasi,700050, Romania

Summary

The hollow space floors emerged from the modern man desire to design structural elements which can allow the structures construction within the earliest time possible and with a lower work effort. Due to the different shape of gaps in the floor, the materials used for implementation of these new constructive systems should offer the opportunity to achieve them without difficulties. Thus, the only type of concrete that is suitable for the construction of these elements is self compacting concrete, a special material characterized in fresh by different properties from those of traditional concrete. Its particularity is that, due to its increased content of paste (cement + fine paste + water) in its composition, the modulus of elasticity has lower values (in average by 11% compared with that of normal concrete), as was noted from experimental tests performed for the same strength class (C16/20). The present paper aims to developing a theoretical study consisting in performing numerical simulation for hollow space floors, made with self compacting concrete, in order to obtain conclusive information regarding specific stresses and strains that occur in their components.

KEYWORDS: finite element method, structural analysis, stress and strain states, modulus of elasticity, strength class.

1. INTRODUCTION

Reinforced concrete is a composite material commonly used in the production of many types of modern construction (civil buildings, bridges). The widespread is justified by the qualities that it have regarding structural strength (a good behavior under gravitational loads and earthquakes, high heat resistance etc.), as well as economic qualities and versatility it has, thus offering the possibility and freedom to achieve special architectural forms.

A structure, regardless of the architectural form it present or the destination for which it was designed, must satisfy certain major criteria: to be aesthetic, to fit

within the environment it was built, to be economic (the economic efficiency assessment should be carried out throughout the lifetime of the building), to answer to basic structural requirements (to provide sufficient strength to withstand the effects of all actions planned, so as not to deform, crack or vibrate in any way), to be resistant to aggressive agents in the environment, to provide the possibility of a light maintenance etc.

Each achieved construction is unique, having a proper design and form, imposed by the destination and technological processes which will take place within it. However, all constructions are based on a skeleton, called the resistance structure of the building, consisting several components, called structural elements, with the role to taking over the applying on structure, to ensure the smooth of the processes taking place in that building. In building and civil engineering, structural elements are beams, floors, columns and foundation. Choosing a structure of resistance in this case is a difficult problem to solve, since the factors involved in the design process are often numerous and contradictory. The main factors involved in establishing an optimal solution for structure are:

- the technologic processes requirements, imposed by the investor, are those who determine the size of the building;
- the loads acting on the structure, influence, mostly, the choice of the structure type, meaning that they must produce uniform and reduced stress. Establishing of loads for a structure, after which result the dimensions for structure elements and also determining the stresses produced by their action, are processes governed by the norms existing in that country;

An important structural element of those set for civil and industrial buildings is the reinforced concrete floor, since, in addition to the functional role of partition of the vertical structure, has an important role, alongside with columns, in providing a rigid space frame to take loads from earthquakes action.

2. MODERN CONCEPTION REGARDING THE USE OF SELF COMPACTING CONCRETE ON HOLLOW FLOORS

Currently, they are many types of reinforced concrete floors, each country, company or constructor engineer wanting to find the correct solution of floor, based on technical and economic criteria specific to that area.

The introduction of hollow space in concrete floors may have advantages not only technical, but also economic. The cost required to achieve a building that is composed with such type of floor can be reduced, more or less, by removing as much material as would have been in place of these hollow space.

Worldwide, the hollow space floors are widely used in various types of construction, regardless of shape voids, due the numerous technical, economic and architectural advantages, such as: fast execution of concrete floors, materials economy, the possibility to achieve concrete floors with span larger than in classical systems, reducing the weight of the floor, the possibility to realize outstanding architectural forms.

Function on shape voids embedded in the floor, these new construction elements can be classified into three types: reinforced concrete floors with bell-shape voids, reinforced concrete floors with cubic voids and reinforced concrete floors with spherical voids (fig. 1).

Fig. 1 Details of constructive systems for reinforced concrete floor with bell-shaped, cubic and spherical voids

Features of constructive design of reinforced concrete floors without beams with space voids, is characterized by reduced thickness of the components elements (ribs and plates) and small diameter for most of reinforced used. All this involve pouring a special type of concrete, such as a concrete with higher fluidity (self compacting concrete), characterized in fresh by different properties from those of the material used in the regular elements and structures.

Especially to the hollow space floors, self compacting concrete is widely used in various country like Austria, Belgium, Denmark, Germany, Iceland, Italy, United Kingdom, Netherlands, but also on other continents, in Canada or USA, because of the essentials qualities such as segregation resistance, ability to spread and influence, increased fluidity, but also a wide range of outstanding properties such as: easy and rapid implementation work ensuring high speed productivity and performance, reduce noise, higher recovery of local materials practically unusable (industrial waste of power plant fly ash, granulated blast furnace slag, limestone filler), achieve a high degree of homogeneity, obtaining a very good apparent surface after removal of shuttering, no compaction by vibration, a competitive price by reducing the cost of putting in work of concrete, which tends to offset the higher cost of materials.

By using the self compacting concrete on these types of concrete floors, should be given by the design engineers an increased attention on this type of concrete deformability, which is mentioned in treatise by many researchers.

Following experimental studies conducted on normal concrete and self compacting concrete with the same strength class was observed the self compacting concrete tend to be somewhat more deformable then normal concrete, resulting a modulus of elasticity for self compacting concrete slightly lower in value than ordinary concrete reference (Fig. 2).

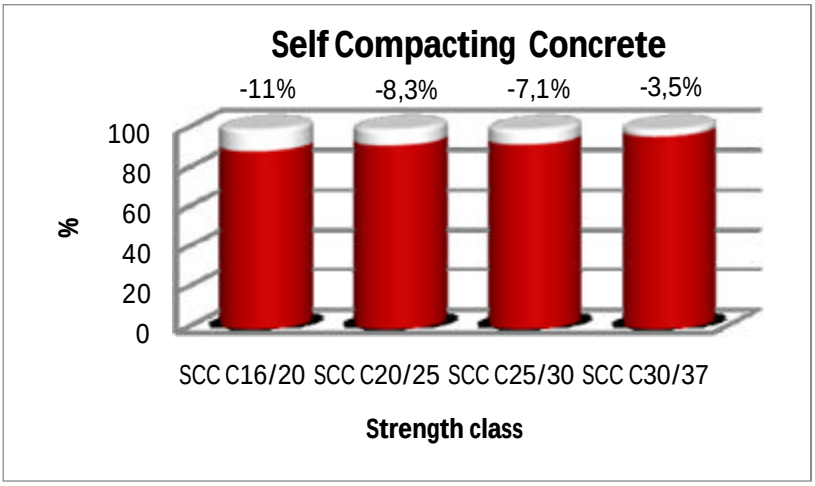

Fig. 2 Loss of modulus of elasticity for self compacting concrete from the values specified in EC2 for normal concrete with same strength class

It is noted that in Romania, currently does not produce and is not used, only sporadically, self compacting concrete, because the existing norms relating to the quality of concrete does not contain separate provisions for self compacting concrete, it can be done only on the basis of books specifications and technical specifications, additional norms, which constitutes an impediment to its use in current practice.

3. ASSESSMENT ON BEHAVIOR UNDER LOADS USING NUMERICAL MODELING

3.1 The concept of modeling

Designing a building supposed to go a certain number of steps, where a particular attention is structural strength analysis and design, as by this stage is to obtain that structures which satisfy the essential requirements, functional and economic and

provides safe operating, that also covers the requirements for strength, stiffness, stability and durability. Given the complexity of the composition of resistance structures, internal and external links, the complexity of the charges and the complexity of the behavior of constituent materials, structural analysis and design will be done on a simplified structural model (perfect model). This implies a schematic strength structure of the building and its components as form, geometric dimensions and constituent materials. Similarly, internal and external links are idealized, reducing to three existing basic types: plain bearing, joint and restraint. Also, actions that require the structure be schematize and reduced to concentrated forces and moments, distributed forces and moments, imposed displacements or temperature variations.

The physical model of a structure is obtained from construction schematization which simplified models were attached to ties, loads and material constitutive behavior. Once obtained, it may be modeling the behavior, which is conducting a process to obtain from the response of the structure parameters (displacements, stresses sectional, voltages, etc.).

3.2 Develop the phisical model of behavior

The principle underlying the modeling performance using specialized programs is the principle of finite element method.

Finite element method is a discretization method that uses a full mathematical model of the phenomenon studied, obtained by using variation methods or weighted residue method.

Key steps to be followed in finite element analysis are:

- idealization - the phase in which the physical model is transformed into a mathematical model. This step is very important to establish, because establish the mathematical model is not an automatic process, but is performed by a human being, who must have extensive and advanced knowledge in the studied field;
- mesh – spatial structure of a mathematical model is described by the degrees of freedom. These values are defined as field trips or derivatives (components of displacements and rotations). If the number of degrees of freedom is infinite, then the system is considered ongoing, but if the number of degrees of freedom is finite, then the item is considered discretized;
- obtaining the solution.

Such a numerical modeling program, using the steps mentioned, is the Ansys program and use of this program is characterized by advantages such as: the

modeling of complex geometry elements, assemblies or subassemblies modeling, modeling all types of materials, modeling of elements with linear and nonlinear behavior, modeling domain uni-, bi-and three-dimensional, modeling of all types of loads (concentrated and distributed forces and moments, accelerations, temperatures), static and/or dynamic analysis and capabilities visualization of results in various forms (fields in color code, animations, deformed state, lists of values, graphs, etc.).

With this program have been performed simulations (modeling) for the physical behavior of hollow floor space covered by research activities.

The followed steps in development of phisical models and achieve modeling solution have mainly focused on the following issues: determining the physical and mechanical characteristics, assessment of loads acting on floor systems, inputting data into the program and obtaining the desired results.

To perform physical simulations using the program, was considered a space frame, fully realized from self compacting concrete and the horizontal element of the structural system (concrete floor) were taken into account two forms of new types of hollow space slabs and namely: spherical voids and cubical (fig. 4), in order to determine differences between the two categories in terms of overall behavior of a structure under loading.

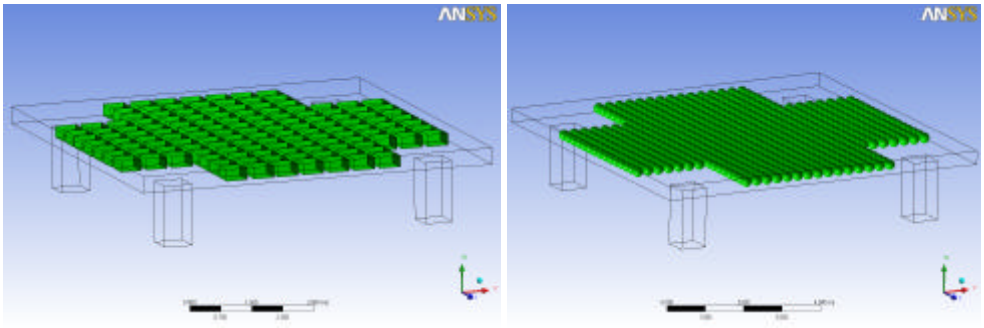

Fig. 3 – Constructive variants of concrete floor with hollows spaces: cubics and sphericals

Geometric dimensions of span and bay are the same for both types of goals analyzed (L=T=9.00 m) and the third dimension, the thickness, will be different depending on study goals type. Thus, the recommendations developed, the thickness of the reinforced concrete floor, in spherical voids case, should not exceed 34 cm, with a 27 cm diameter sphere and for the cubic shape voids, the thickness is 40 cm and cubic void height 28 cm.

To assess loads were taken into consideration the permanent loads, given by the weight of the plate, board floor (cold floor, mosaic) and the action of non-bearing interior walls, and the appropriate variable loading of reinforced concrete slabs.

3.3. Final result

Behavior analysis under loading of a reinforced concrete element is a process that involves determining the values of parameters that describe this phenomenon, namely: displacement, strain, tension, efforts, etc. These parameters can be obtained either by numerical computer simulations, resulting in stress maps, or by mathematical modeling, using analytical methods.

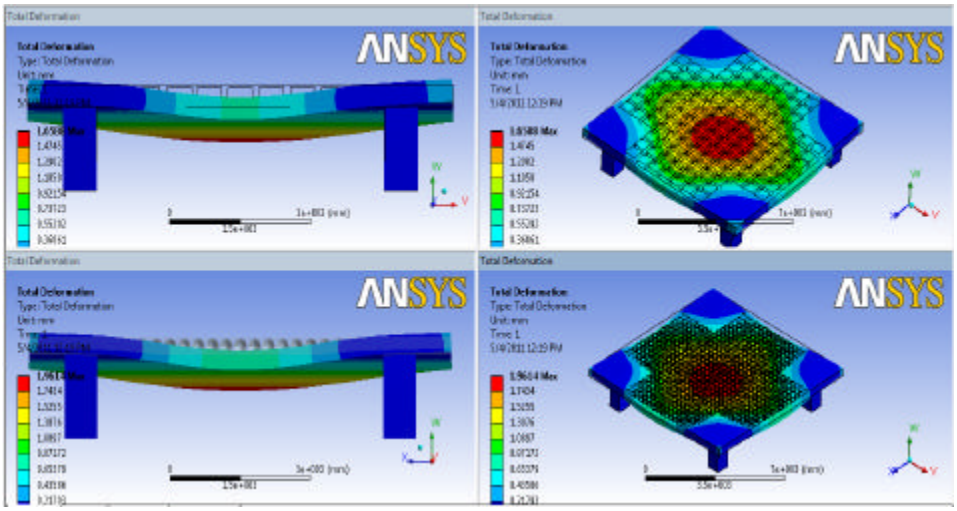

Fig. 5 – Harta deformatiilor specifice

4. CONCLUSION

The ultimate goal of a calculation of strength lies in sizing and verification of building elements so that the whole construction and the individual elements to meet the three conditions imposed by the existing norms and standards: condition of strength, stiffness and stability.

The problem of calculating the resistance elements and structures was, is and will be an important activity in construction, requiring advanced computer knowledge, as construction resulting from these operations must have a certain degree of safety for their beneficiaries.

This meaning has grown today, more demanding requirements, arising from the implementation of diversified construction, with more complex components. Therefore, it requires analysis studies on behavior under load of concrete floor, from which to determine the accuracy and veracity of constructive solutions.

Following the numerical modeling conducted for the two systems of modern floors, it was concluded that the reinforced concrete floor with cubic hollow space, presents a better behavior to the action of gravity type loads (less deformable) than composed with spherical hollow space (fig. 5). Further attention should be paid on the value of SCC modulus of elasticity (especially for small strength classes, where the loss modulus is somewhat higher, this difference reduced to less than 5% for self compacting concrete of high strength), based the class of concrete used, it having values lower than normal concrete with the same strength class, the explanation for this trend of self compacting concrete being given by higher content of fine component parts as compared with normal concrete.

Currently in Romania there are no suitable methods for calculating these types of reinforced concrete floors and any programs specialized in designing these new constructive systems (ANSYS program proving currently the only program to viable automatic calculation of such numerical simulations) considering it to be useful to prioritize design and execution such structural systems in our country-specific conditions, but considering the recent practical achievements of various countries and relevant research results, reported in the treatise.

It is believed that their study, improving the calculation methods used, test methods and their standardization, is important targets for future research.

References

1. Clough, R.W., Penzien, J., *Dynamics of structures*, McGraw-Hill, New York, 1993.
2. Achkire, Y., Preumont, A., Active tendon control of cable-stayed bridges, *Earthquake Engineering and Structural Dynamics*, vol. 25, 1996.
3. Popescu, I., Tanase, R., Asupra modelarii statistice a fenomenului de defectare în cazul podurilor, *Buletinul IPI*, Tomul XLVII, Fasc. 5, 2001. (in Romanian)
4. Magaña, M.E. and Rodellar, J., Nonlinear decentralized active tendon of cable-stayed bridges, *Journal of Structural Control*, vol. 5, 1998.
5. Paunescu, F., Badea-Dinca, N., Stacut., E. *Informatizarea societatii: un fenomen inevitabil ?*, Ed. Siintifica si Enciclopedica, Bucuresti, 1985. (in Romanian)
6. Persson B., *Creep, shrinkage and elastic modulus of self-compacting concrete*, First International RILEM symposium on self-compacting concrete, Rilem Publications, 1999, pp. 239–250;
7. Terec Liliana, Szilagyi Henriette, Filip Mihai, Domsa Julietta, Mircea Andreea, *Elemente Prebabricate din Beton Autocompactant*, în Revista Constructiilor, anul II, Nr. 22, decembrie, 2006, pp. 20-25.
8. Nicolae Florea, Asavoaie Ciprian, Calin Sergiu, Nicolaiciuc Sergiu, *„Tipuri de plansee moderne utilizând beton autocompactant*", Revista Constructiilor, Nr.61, iulie 2010, pag. 46-49.
9. Calin Sergiu, Asavoaie Ciprian**,** *„Plansee cu Goluri Sferice Tip Bubble-Deck–Program Experimental"*, în Revista Constructiilor, Nr.56, februarie, 2010, pp. 42-45.
10. BIBM, CEMBUREAU, ERMCO, EFCA, EFNARC – *The European Guidelines for Self-Compacting Concrete. Specification, Production and Use,* may, 2005.

Spherical Voided Bi-Axial Concrete Floor Slabs - Shortcomings of CAD Models

Sergiu Calin[1], Lucian Ungureanu Constantin[2]
[1]*Department of Concrete Structures, Building Materials, Technology and Management, "Gh. Asachi" Technical University of Iasi, Faculty of Civil Engineering and Building Services, Iasi, 700050, Romania, e-mail: sergyu_kalin@yahoo.com*
[2]*Department of Concrete Structures, Building Materials, Technology and Management,"Gh. Asachi" Technical University of Iasi, Faculty of Civil Engineering and Building Services, Iasi, 700050, Romania, e-mail: lucianungureanuconstantin@yahoo.com*

The designing of the voided slabs is difficult because of the gaps area. For the designing of these types of slab some simplified methods are used. The use of the simplified methods is helpful for the structural engineers, offering them an easy and efficient way for computing these types of structural elements but they must know the shortcomings of using them.

This paper intends to detail and analyze the shortcomings between the real model slab and the one used in numerical analysis. Emphasizing them is made by modeling a structure in ANSYS – model closest to the real one and in AXIS VM – model made using simplified methods.

KEYWORDS: equivalence area, voided slab, coffered ceiling, finite element method, hypothesis analysis.

1. INTRODUCTION

The new tendencies in the reinforced concrete practice are evidenced through the use of modern floors which leads to a series of clearly superior advantages compared to the classical solutions. This paper aims to add more information on the topic through the detailing of some computational methodologies specific to these modern floor systems.

Realizing these objectives leads to a decrease in material consumption, a reduction of the self weight of the floors and an increase of structural performances, as a result of the possibility of enlarging the distance between supports.

To remove the concrete from the median zone of the slab where it cannot be efficiently used because the stress degree is reduced, some empty spaces of large dimensions [11], compared to the thickness of the element, are realized.

To this purpose filling bodies are employed, as light as possible, under the form of lost or reusable formworks of diverse shapes and ways of making [4]. With these, a

meshed structure is obtained [6], [8], whose component elements (networks and plates) are special due to their thinness of few centimeters.

The team of BMTO Department of Faculty of Civil Engineering and Building Services Iasi set to elaborate specific computing methods; this article represents just a synthesis of elaborated methods and a review of the encountered problems.

2. HYPOTHESIS OF MODELING

Finite Element Modeling (FEM):

- nonlinear analysis by ANSYS 12.0 [9].
- linear analysis by AXIS VM10.0 [2], [10].

2.1. Hypothesis I – Ideal hypothesis

Nonlinear finite element analysis helps researchers to conduct more detailed investigations on the behavior of reinforced concrete structural elements. Three-dimensional finite element structural model are made in order to predict the nonlinear behavior of spherical voided bi-axial concrete floor slabs, Figs. 1 and 2.

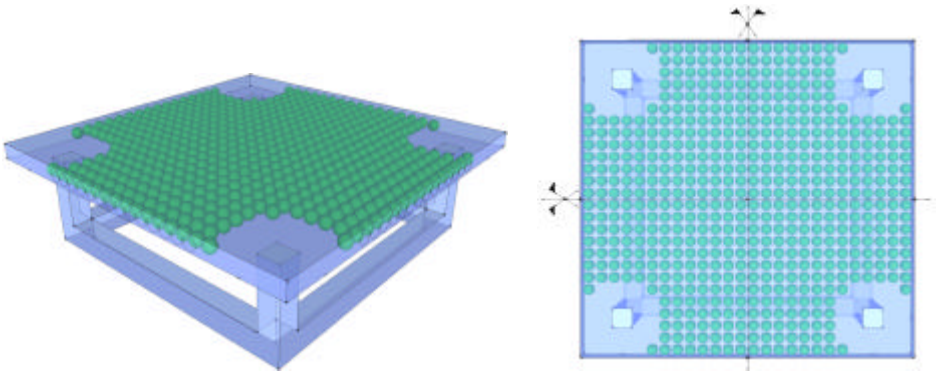

Figure 1. Drawing of Experimental Model in 3D - Hypothesis I

The analysis is made on an experimental model at a real scale. In the program there have been introduced only a corner of the slab for which there have been marked symmetry axes, the number of the finite elements go over 1 million which consist a serious problem but not impossible to run. For a regular PC (Dual Core 5600+, 2.91GHz, 4GBRAM) unconvincing results have been obtained and for best results requesting a running time of 5-6 months, as conclusion the method is inefficient.

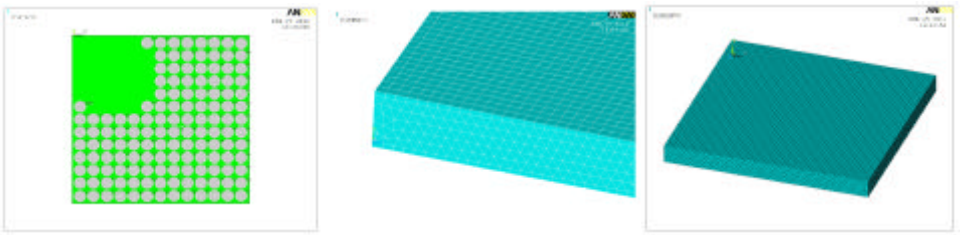

Figure 2. Nonlinear finite element analysis of Experimental Model

2.2. Hypothesis II – Beams network

This version aims at a fast analysis, linear analysis with designing program AxisVM 10.0, for the design of these floors, thus, a division of the floor into several component elements was done: a superior plate and an inferior one, ribs and column heads [7].

An equivalent of the vertical ribs' area with small beams having the cross section as in figure 3 was done and the empty space is intersection between two cylinder, figure 4. These small beams are displayed along two orthogonal directions, forming a beam network, which works particularly advantageous when taking the efforts, figures 7 and 8. It will be displayed, both at the bottom and at the upper part, a plate having a thickness resulting from calculations, the sizes and the dimensions varying depending on the thickness of the used floor. In the bearing plate on pillars are arranged the column heads embedded in the plate. In that area there are no gaps [1], [3].

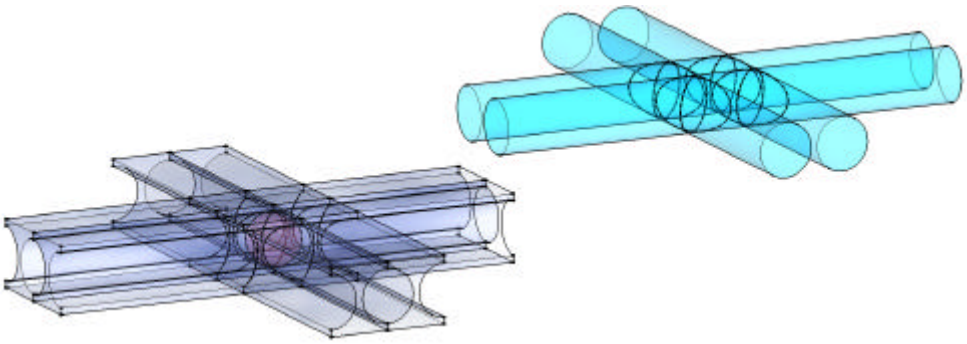

Figure 3. Intersection detail of small beams and cylinders - Hypothesis II

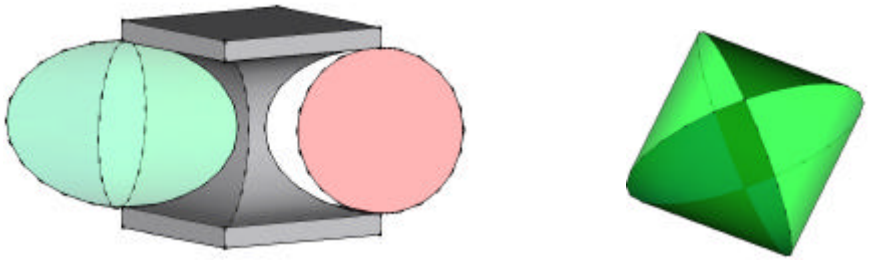

Figure 4. The equivalence of the sections, new concept - Hypothesis II

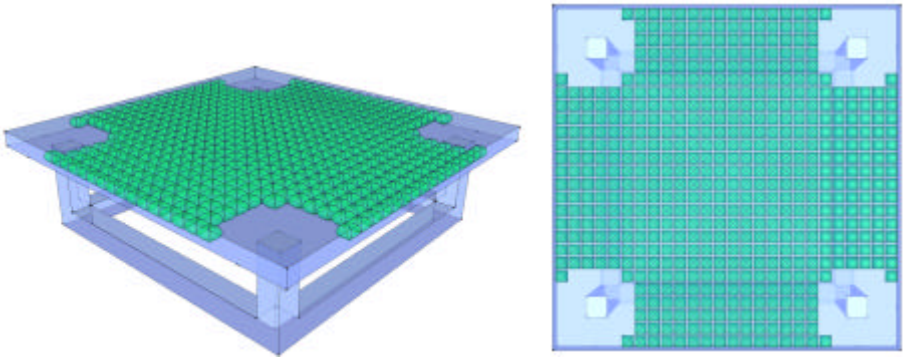

Figure 5. Drawing of Experimental Model in 3D - Hypothesis II

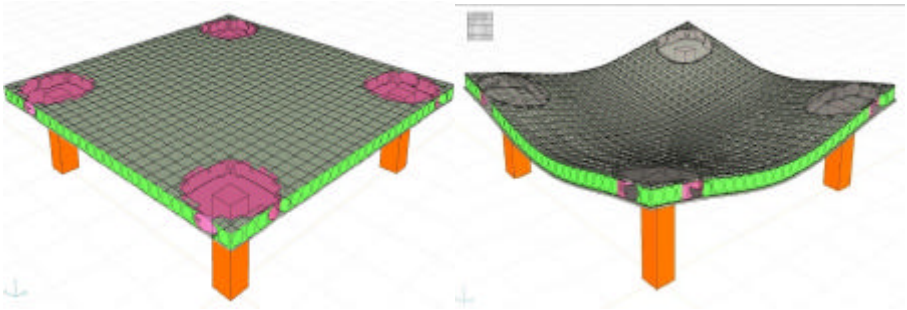

Figure 6. The Experimental Model in the Computation Program - Hypothesis II

Loads were placed on the slab, and after performing the static calculations, resulted effort diagrams for each rib and effort maps for the upper and lower slab and how the elements are deformed, figures 6, 7 and 8**.**

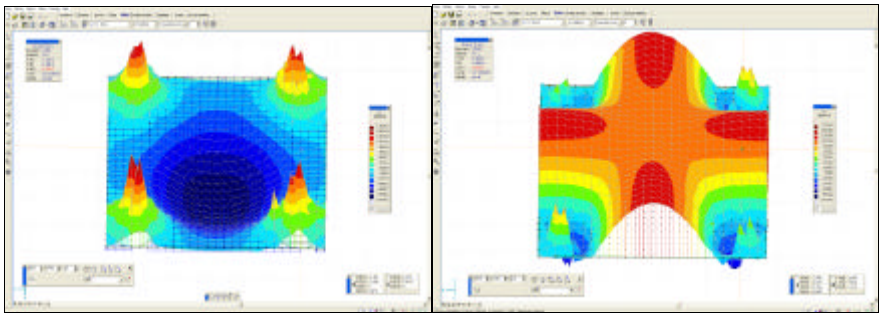

Figure 7. Tension Map N1 for the Upper and Lower Slab - Hypothesis II

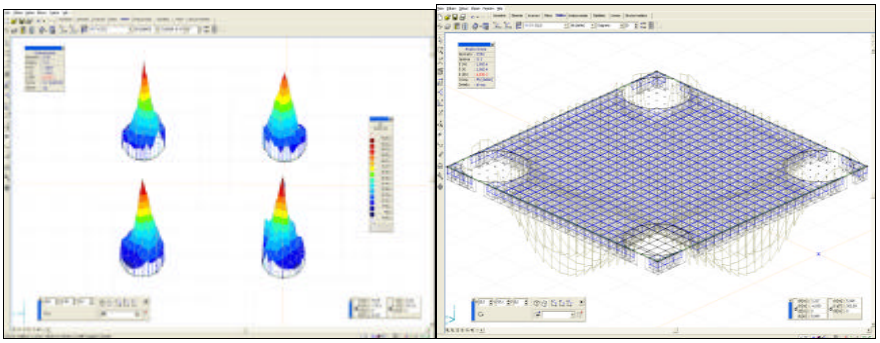

Figure 8. Obtained Results for Column Heads and Ribs - Hypothesis II

2.3. Hypothesis III – Simplified method

Due to the spheres' contour, the ribs' cross section has a special form which leads to a series of difficulties when introducing the data into computational programs. The equivalence was done by replacing the spherical gaps with gaps shaped as cubes. Adopting this solution resulted in a double T section for the ribs, ribs which have been displayed along two orthogonal directions, thus realizing a floor with very dense ribs forming practically a coffered ceiling [5]. After establishing the shape of the cross section for the ribs and the computation of the equivalent areas was done, the floor model was introduced in the design program, figures 9 and 10.

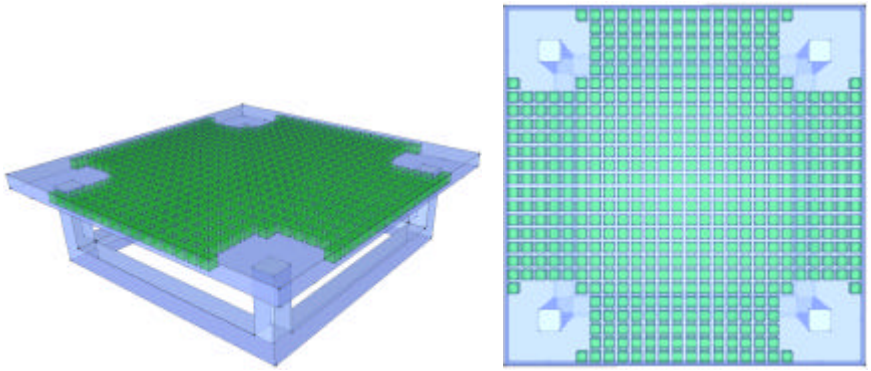

Figure 9. Drawing of Experimental Model in 3D - Hypothesis III

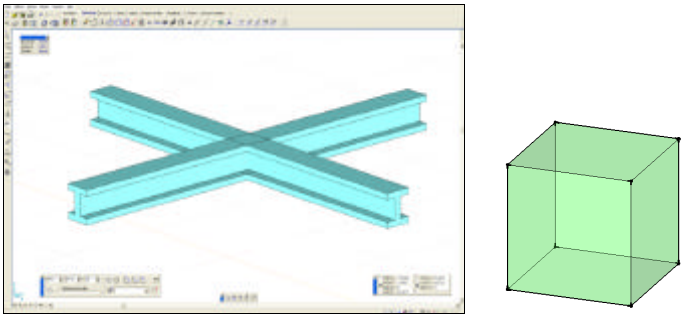

Figure 10. The intersection detail of small beams, hollow cube - Hypothesis III

After establishing the shape of the cross section for the ribs and the computation of the equivalent areas were done, the floor model was introduced in the design program, figure 11.

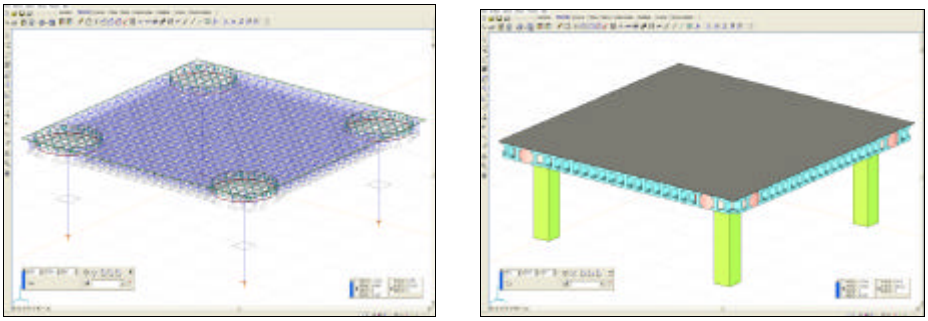

Figure 11. The Experimental Model in the Computation Program - Hypothesis III

3. HYPOTHESIS ANALYSIS

Table 1. Hypothesis analysis table

Hypothesis	Pros	Cons	Difficulty level
I	Detailed analyze, failure mechanisms, the possibility of making the ideal gaps shapes	Difficult to carry out, long design program running time, difficult to implement	III
II	Quick run, known designing program	Gaps close spherical shape, close to the real behavior	II
III	Quick run, known designing program	Big differences between behavior due to cubical shape	I

4. CONCLUSIONS AND RESEARCH DIRECTIONS

It has been aimed to meet specialists who wish to use this relatively new constructive system by detailing some new specific methods of calculation. The studies and methodology is described in this article reveal the behavior under the action of static loads, leading to accurate results and encouraging and justifying their implementation in practice in our country and beyond. However, careful examination of these methodologies and their tools has to be done in order to choose the optimum design solution regarding the numerical modeling of these systems.

It is considered that the study of the concrete floors with spherical gaps, improving the calculation and test methods and their standardization are important goals for future research.

This paper come in help to understanding the deficiencies between the models made using the simplified methods and the real ones. Future research directions will emphasize the differences at efforts, tensions and displacements level concluding certain equivalent coefficients.

References

1. Agrement Tehnic 007-01/120-2007. (in Romanian)
2. Axis VM *Finite Element Analysis & Design Program*, V9r3, 2009.
3. EN 1992-1-1:2004 *Eurocode 2:* Design of Concrete Structures.
4. Kristian, S., *Impact Load Tests on Reinforced Concrete Slabs*, 6th International PhD Symposium in Civil Engineering, Zurich, p. 130-131, 2006.

5. Mihai, P., *Reinforced Concrete Structures*, Ed.Matei-Teiu Botez, Iasi, 2010.
6. Plug, R., *Benelux BV, Parkeergarage Sint Antonius Ziekenhuis, Nieuwegein. Nemetschek, Engineering, Category 7: CAD Engineering, Engineering work and special structures*, p. 258-259, 2009.
7. SR EN 13747:2006 *"Produse prefabricate de beton – Predale pentru sisteme de plansee"*. (in Romanian)
8. Von Emilie Veillon UEFA, *Verwaltungsgebäude in Nyon Eine runde Sache,* Nr. 4, Freitag 29, 2010.
9. www.ansys.com/Products/ANSYS+13.0+Release+Highlights
10. www.consoft.ro/axisvm/
11. Zoltán K., Attila P., Karoly B. *Plansee performante pentru cladiri multietajate,* Simpozionul National - Noi reglementari pentru Beton, Ed. Conspress, Bucuresti, p. 94-102, 2009.

Air exchange rates of a wind ventilated façade using CFD simulation

Claudiu Romila[1], Georgeta Vasies[1]
[1]*Department of Civil and Industrial Engineering, "Gheorghe Asachi" Technical University of Iasi, Iasi, 700050, Romania*

Summary

Passive ventilation solutions for façades and roofs can remove the excess of heat and water vapors. Ventilation of the façade elements depends on several factors among which wind direction and pressure differences on the height of the façade. Air exchange rates vary accordingly with the intensity of the ventilation. CFD analysis is an effective method to determine the physical properties mentioned above that otherwise would be difficult to be obtained by in situ observations. This article presents a method for calculating air exchange rates for a ventilated façade of a residential building using the finite element program ANSYS 12.

KEYWORDS: ventilated façade; wind direction; air exchange rates; CFD analysis.

1. INTRODUCTION

Ventilated façades include beside the bearing wall an airspace which, if ventilated, brings some advantages: reduced energy consumptions for cooling or heating, increased drying capacity, better sound insulation and suitability for thermal rehabilitation works.

Channel air circulation is caused by both pressure and temperatures differences at the openings. In order to analyze the hygrothermal behaviour of ventilated façades the air exchange rates must be known. Bigger exchange rates with the exterior mean that larger quantities of heat and water vapours are extracted from the walls.

Full scale measurements of air velocities in ventilated channels and air exchange rates have been performed on site for real buildings and in laboratory on wall elements. On site measurements results are influenced by the meteorological conditions and their reliability is diminished. Laboratory measurements are more accurate but they cannot take into account wind-flow pattern around the building. Channel ventilation can be conveniently studied also by using finite Computational Fluid Dynamics (CFD) programmes, apart from on site measurements and laboratory testing.

Field experiments and CFD simulations were made by Saelens and Hens [1] in an intensive study on a double skin façade located in Vliet, Belgium. They concluded that CFD calculations don't correspond completely with the field measurements. Especially the wind pressure distribution on the envelope was difficult to be estimated.

Stovall and Karagiozis [2] employing CFD simulations found no significant difference in the mass flow rates between channel thicknesses of 19 and 50 mm. On the other hand, when the size of the slots was doubled the air flow also doubled.

Coupled and decoupled simulations on narrow ventilated faces were done by Nore and al. [3]. It was concluded that there are limitations of the CFD simulations especially when reproducing turbulent flow in the channel. Field studies of ventilated façades have been undertaken by Finch [4], Hansen [5] and Nore [6].

To the knowledge of the authors, there are only a few CFD studies on air exchange rates of a narrow ventilated cladding made for real buildings. This paper presents an investigation of wind induced airflow in ventilated façade with a 12 mm thick channel for an isolated low-rise building based on CFD simulations.

2. REAL AND NUMERICAL MODEL

2.1. The real building

The investigated building is located in the village of Bârnova, near Jassy. It has the following dimensions: L = 20.10 m, W = 10.20 m and H = 7.55 m. The building is isolated and positioned on a flat, uniformly rough terrain (Figure 1).

Figure 1. Frontal view of the south façade

The outer cladding is made of painted softwood boards fitted tongue and groove. The ventilated channel is 12 mm thick and has resulted from the chipboard panel thickness on which the boards are fixed. The ventilation openings are circular with a diameter of 10 mm. Protection nets barriers for insects have been mounted in the opening thus reducing ventilation area. The constructive system divides the entire ventilated air space into several 1 m thick channels.

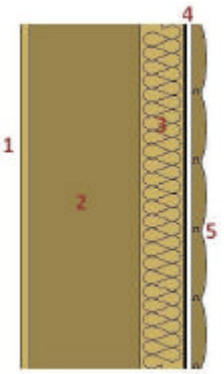

Figure 2. Cross section of the ventilated façade with 1) 12.5 mm gypsum board, 2) 24 cm thick autoclaved aerated concrete blocks, 3) 10 cm mineral wool with wind barrier, 4) 12 mm ventilated air channel and 5) 20 mm softwood boards fitted tongue and groove

2.1. The modeled building

The numerical simulation was made using the finite element program ANSYS 12 CFX [7]. The used scale for the model was 1:1. The building was completely immersed in the computational domain (Figure 3), according to specifications [8, 9, 10] from the scientific literature.

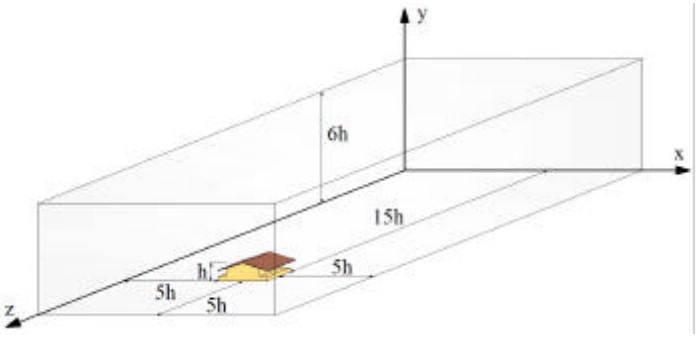

Figure 3. The numerical model and the computational domain

The numerical simulations were realised for an average wind speed for the region of Jassy of 4 m/s, an average turbulence of 5% and for different wind directions on the south façade (0º, 45º, 90º and 135º).

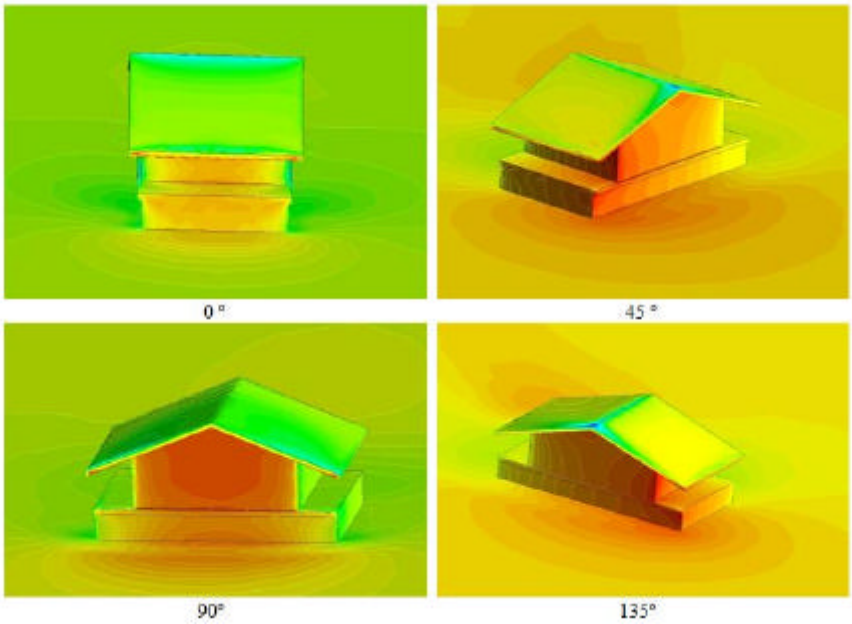

Figure 4. Pressure distribution on the façades depending on wind direction

For each particular case the wind pressures on the façades have been established. Pressure measurements for the south/north façades were taken in 28 points while on the east/west façades in 20 points coresponding to the position of the ventilation openings (Figure 5). The lower ventilation grids are positioned 15 cm above the ±0.00 level while the upper ones are located 15 cm below the eaves.

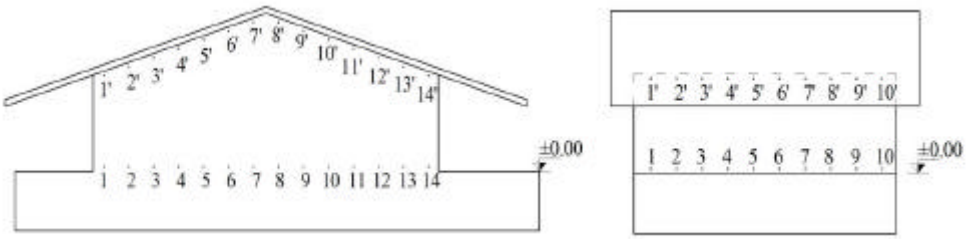

Figure 5. Pressure points on south/north façades (left) and east/west façades (right)

3. RESULTS

CFD analysis was used to find the effective pressure on the façades and thus the pressure differences on the height of the ventilation channels were computed. Air flow inside the channel can be computed using Reiher equation [11] if the pressure difference and the geometry of the channel are known:

$$D_a = 2\frac{A_c}{h^2}\left(\frac{\Delta p}{h}\right)^{2/3} \tag{1}$$

where : D_a – air flow (m^3/h), A_c – flow area (m^2), h – height of the channel (m), *?p* – pressure difference (Pa).

If the air flow is known the air exchanges rates can be computed:

$$n = \frac{D_a}{V} \tag{2}$$

where : n – air exchange rates (h^{-1}), V– channel volume (m^3).

The obtained pressure differences and air exchange rates on the façades for each wind direction scenario are represented below:

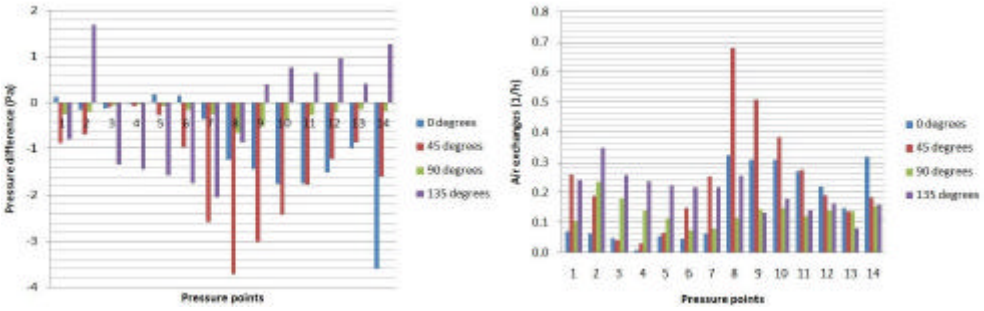

Figure 6. Pressure difference (left) and air exchange rates (right) for the south façade

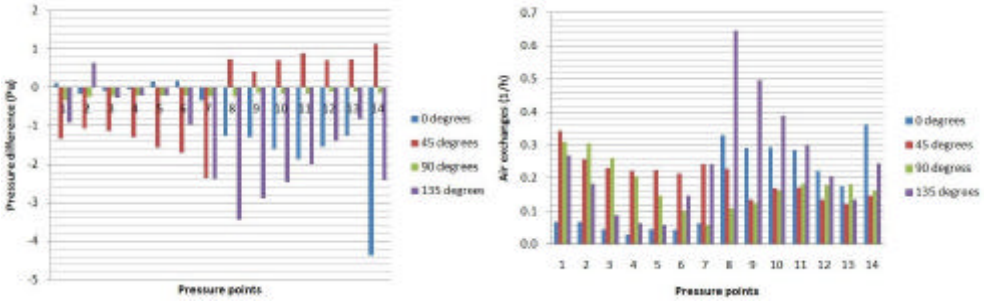

Figure 7. Pressure difference (left) and air exchange rates (right) for the north façade

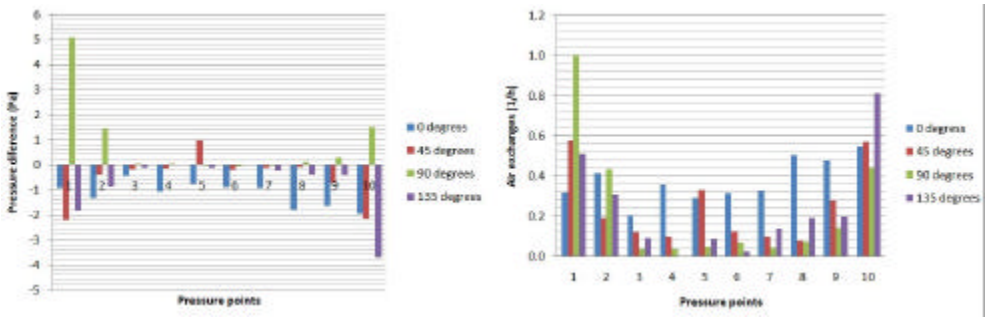

Figure 8. Pressure difference (left) and air exchange rates (right) for the east façade

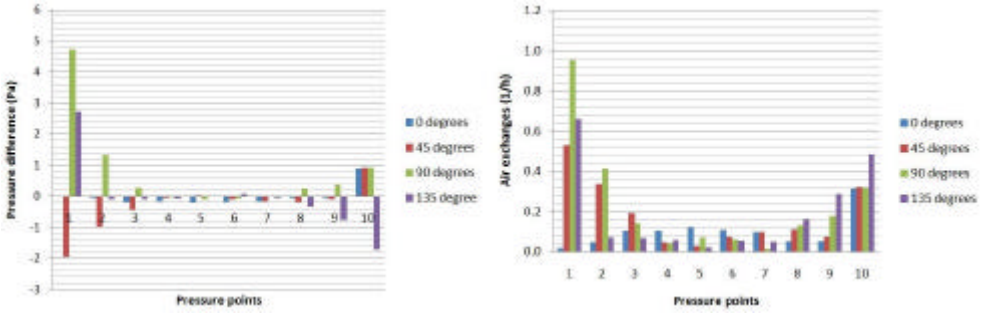

Figure 9. Pressure difference (left) and air exchange rates (right) for the west façade

Ventilation is the effect of both buoyancy and wind action. While buoyancy is the prevalent force, the wind effects can be considerable when they act. Buoyancy makes the air flow upward, while the wind induced airflow can be in both directions. For the examined building and for an average 4 m/s wind speed, airflow was mainly downward as it can be seen in Table 1. The effect of buoyancy is not considered.

Table 1. Percentage of the airflow direction in the channels on the façades

Flow direction	South	North	East	West
Upward	19.5%	19.5%	22.5%	30%
Downward	80.5%	80.5%	77.5%	70%

The air exchange rates differ on the façade for each separate channel, but average rates can be computed for an entire façade.

Table 2. Average air exchange rates on the façades

Air exchange rate	South	North	East	West
n (h^{-1})	0.185	0.198	0.182	0.176

4. CONCLUSIONS

Ventilation caused by the effect of wind can be evaluated by on site measurements and also using CFD analysis that can be a reliable tool for assessing pressure distribution on the façade which is needed to determine air flow and air exchange rates in the ventilated channel.

This study is presenting the airflow due to wind action in the ventilated channels for an isolated low-rise building. Average pressure differences varied between – 1.60 and 1.40 Pa. Peak values of – 4.40 and 5.10 Pa have been obtained (Figure 8). The average wind induced air exchange rate computed for an average wind speed of 4 m/s was below 0.2 h^{-1}.

Ventilated façades allow that the excess water vapors to be eliminated. Although smaller rates are required in order not to drain heat in the cold season, they must be sufficient enough to transport the water vapors. In the presented study the obtained air exchange rates are not high consequently the condition mentioned above is satisfied. On the other hand bigger air exchange rates in the warm season can lower the temperature on the bearing wall thus increasing thermal comfort and decreasing energy demand.

Future work should emphasis the relation between the thermal buoyancy and wind action. Other limitations of the study are summarized below:

- no air diffusion into the wall and façade;
- no air leakages;
- only average wind speed, no gust effect and no perturbations;
- wall and façade roughness were not modeled;
- thermal and moisture buoyancy were not considered.

Acknowledgements

The authors *acknowledge* the support from the Ministry of Education and Research (Romania), CNCSIS – UEFISCU, through PN II-Ideas, Grant No. 603/19.01.2009, *CNCSIS* Code ID-327.

The authors would like to acknowledge the assistance of the scientific coordinator, professor Adrian Radu.

References

1. Saelens, D., Hens, H., *Experimental evaluation of airflow in naturally ventilated active envelopes,* Journal of Thermal Envelope & Building Science, vol. 25, 2001.
2. Stovall, T.K., Karagiozis, A., *Airflow in the ventilated space behind a rain screen wall,* Buildings X International Conference - Thermal Performance of the Exterior Envelopes, US, 2007.
3. Nore, K., Blocken, B., Thue, J.V., On CFD simulation of wind-induced airflow in narrow ventilated façades cavities: Coupled and decoupled simulations and modeling limitations, Building and Environment 45: 1834-1846, 2010.
4. Finch, G., Straube, J.F., *Ventilated Wall Claddings: Review, Field Performance and Hygrothermal Modeling*, Buildings X International Conference - Thermal Performance of the Exterior Envelopes**,** US, 2007.
5. Hansen, M.H., Nicolajsen, A., Stang, B.D., On the influence of cavity ventilation on moisture content in timber frame walls, 6th Symposium on Building Physics in the Nordic Countries, Norway, 2006.
6. Nore, K., Thue, J.V., Time, B., Rognvik, E., Ventilated Wooden Claddings – A field Investigation, 8th Nordic Symposium on Building Physics, Danemark, 2008.
7. Ansys Inc., *Ansys 12 user's guide*, U.S., 2010.
8. Franke, J., et al., *Recommendation of the use CFD in wind engineering,* Proceeding of the International Conferences on Urban Wind Engineering and Building Aerodynamics, Belgium, 2004.
9. Bloken, B., Carmeliet J., *Wind Building Aerodynamic,* An international course-workshop, Leuven, 2007.
10. Blocken, B., Stathopoulos, T., Carmelit, J., *CFD simulation of the atmospheric boundary layer – wall function problems*, Atmospheric Environment 41 (2): 238-252, 2007.
11. Stefanescu, D., Velicu, C., *Fizica constructiilor*, Editura Societatii Academice „Matei-Teiu Botez", Iasi, 2009. (in Romanian)

The influence of wind direction on the solar panels placed on flat roofs, using CFD simulations

Georgeta Vasies[1], Elena Axinte[1] and Elena Carmen Teleman[1]
[1]*Department of Civil and Industrial Engineering, "Gheorghe Asachi" Technical University of Iasi, Iasi, 700050, Romania*

Summary

Solar energy is one of the principal sources of renewable energy, it is efficient, cheap, clean and accessible The photovoltaic panels and solar collectors being more and more used placed individually or in several parallel rows, on the ground or on the top of the buildings determine specific alteration of the urban aspect. Placing the solar collectors on the roofs of the current buildings is a very wise decision, because they are plane, rigid and safe as a support, in the same time, exposing their surface to sun for a long period of daily time. The security in exploitation of these „solar" building services is not possible to be insured unless a thorough knowledge of the wind effect has upon them. Wind gust speeds, the angle of inclination of the panel and the relative position of the panels with respect to the roof itself are important factors that model the behavior of the air flow around the structure of the solar panels.

The paper presents the study using Computer Fluid Dynamics Simulation of the influence of the wind direction of action with the respect to the position of the building upon the air flow field developed in a group of solar collectors placed on a flat roof of a building. Two ways of placing the solar collectors were studied: in separate groups and in compact group. Also, to determine peak loads, there were considered the four angles of the wind action in relation to the building.

KEYWORDS: wind direction, solar panel, flat roofs, CFD simulation, ANSYS 12 CFX

1. INTRODUCTION

During the last several years, photovoltaic panels and solar collectors are gathering more and more attention from all over the world's most potential users and also, by designers in real estate industry domain, because of their promising advantages of energy saving in parallel with the possibility of easy mounting on facades and a secure exploitation during the service life.

The main design loads acting directly upon the solar collectors determine a rather complex combination: gravitational force, temperature variation and snow but also wind and accidentally, seismic force. Wind action is by far the most important because it is a variable action basic for the design. In the case considered here, the wind action depends on three factors: wind speed, the height of the roof and the particular position of the solar panel on the roof (may be in the plane of the roof or as a protuberance that will increase the local turbulence of wind bursts). In the literature dedicated to the evaluation of wind effects on buildings and mainly, in the codes dealing with the design to wind action these particular aspects are almost absent and for this reason, tests on scaled physical models in wind tunnel had to be run and for a more acurate analysis numerical modeling was also considered a good alternative. The present design national standard SR EN 1991-1-4, which is concordance with the Eurocodes, does not contain any direct indication what so ever upon the evaluation of wind loads on the solar collectors and a general description of the wind pressure on buildings surfaces is discarded in three main factors: wind referrence presure, pressure coefficient and exposure factor, depending on the terrain roughness. The value and sign of the pressure coefficient (called also aerodynamic coefficient) depends on the geometry of the building and on the obstacles situated in the vicinity of the building. For obtaining the optimum value of wind loading for the design of the solar panels, a thorough examination of the complex air flow field resulted from the interaction between the wind blow and the building itself must be performed.

The solar panels exposed to wind strong blowing or to local gusts of important intensity would from the start rise the problem of the energetic efficiency, an increase of wind speed being a source of important loses of the heat gathered by their surfaces. In the same time, the sustaining skeleton and the supports of the solar panel systems will be affected by the increase in the spectral power of the wind, developing a dynamic behavior (vibrations, maybe even resonance) on the steel consumption and the solar energy collected. The constructive solutions must consider all these aspects in order to insure a safety design for the service life and in the same time to optimize both the steel consumption and the solar energy collected [1].

2. STUDIES IN THE DOMAIN

The techniques of collecting and converting the solar energy are constantly developing. The evaluation of the forces that really acting on the solar panels are transferred to the supporting system, is the object of numerous research studies, all over the world. The behavior of these panels when being placed in the aerodynamic field was studied experimentally, on models in wind tunnels and on prototypes, at site.

In Romania, the first researches regarding wind dynamic action on solar panels and systems were developed from 1979, at the Institute of Constructions in Bucharest. These studies aimed the determination in wind tunnel using experimental methods of the pressure coefficients for the solar collectors placed near the ground level. From 1984, in the atmospheric boundary layer wind tunnel, at the Technical University "Gheorghe Asachi", a number of research programs were designed to obtain the local pressure coefficients resulting from the complex forces that act on the solar panels placed on the flat roofs of the residential buildings situated in urban environments [1].

Worldwide, the year 1979 is marked by experiments on the solar collectors at the A&M University in Texas [2] followed by Colorado State University in 1980 [3]. The so called shelter effect, that is the mutual influence of the solar panels closely situated leads to a benefic reducing of the wind loading [4]. Researches regarding the methods of diminishing the effects of the wind action on the solar panels were run also at the National University Cheng Kung in Taiwan [5] [6].

Due to the fact that both the experiments in wind tunnel and those developed at site, at natural scale are consuming important financial and time resources, a new domain is developed in wind engineering, dealing with virtual modeling, via computer simulation of the air flow. The numerical methods applied are based on the fundamental equations of the Fluids Dynamics (CFD). The continuous increasing power and processing speed of the computers make possible superior refining of the turbulent wind flow field. In order to insure a reliable virtual simulation, the results must cope with the experimental observations on the models placed in the wind tunnel.

3. NUMERICAL SIMULATION WITH ANSYS CFX

The numerical simulation in the study presented here was developed under ANSYS 12 CFX. The building is immersed in the computational domain, its minimal dimensions respecting the specifications from the literature [7].

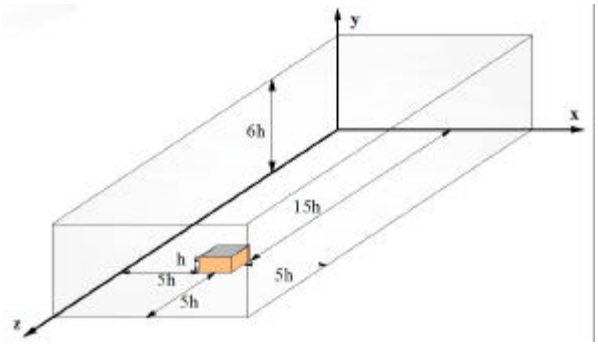

Figure 1. Computational domain

Two cases were analyzed:

- rows of solar collectors placed in one compact group on the terrace;
- two separate groups of rows of solar collectors.

The rows measure 24 m in length and 1.58 m on height, their thickness being of 8 mm; the pitch has an angle of 30º. In both cases the space between two running rows is 1.0 m. In the case of the panels placed in separate groups, the distance between the two groups is 3.0 m.

For the two situations three exposure angles were considered: 0º, 45º and 90º.

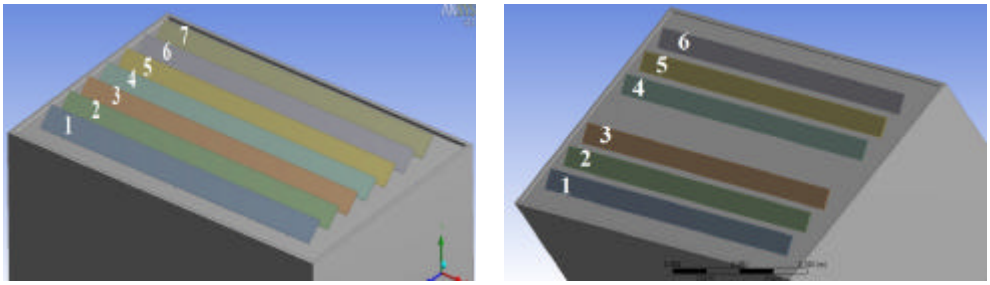

a. b.

Figure 2. The solar panels studied positions on the roof: a. rows of panels placed in a compact group, b. rows of panels placed in separate groups

The building equipped with solar collectors on the roof is a regular one, 30m x 20m in plane dimensions and 15 m height; an attic of 0.2 m is placed on the roof perimeter. The solar panels are lifted at 0.3m height from the level of the roof and situated in consecutive rows, respecting the recommendations from the literature: the distance between these rows and the edge of the attic is about $e/10$, where:

$$e = \min(b, 2h) \tag{3.1}$$

The significance of the symbols being:

b - the dimension of the face normal to the wind direction,

h - height of the building.

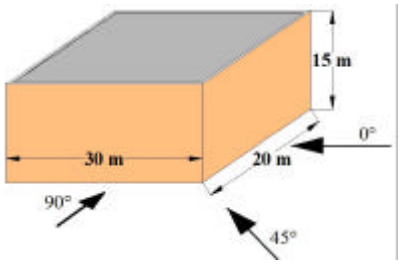

Figure 3. Dimensions of the building and the wind action angles

During the numerical simulation season, the wind speed considered is 14 m/s and the turbulence intensity is 10 %. The scale of both the model of the building and of the wind flow was 1:100. As a result of the numerical simulation for the two analyzed cases and or the wind action angle, the pressures coefficients on both faces of the exposed solar collectors were registered.

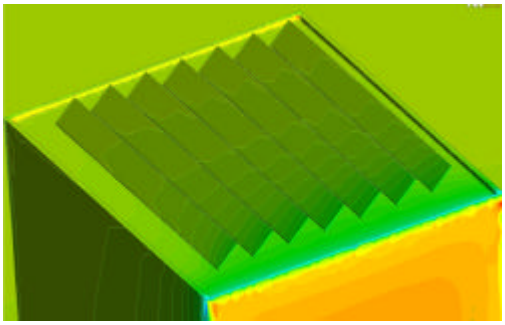

a.

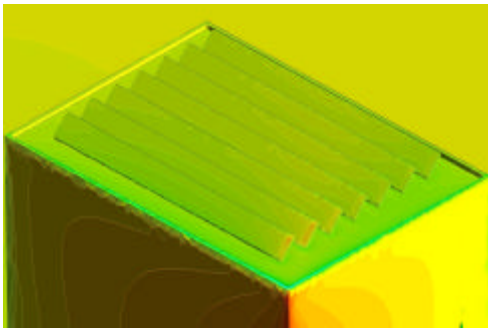

b.

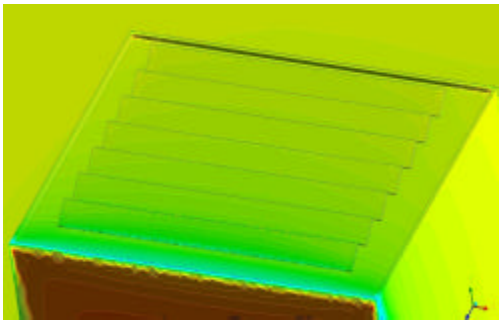

c.

Figure 4. Rows of panels placed in one compact group. Isopleths of the mean wind pressure (obtained from the ANSYS simulation) traced on the windward faces for the wind angles of action: a. 0º; b. 45º; c. 90º

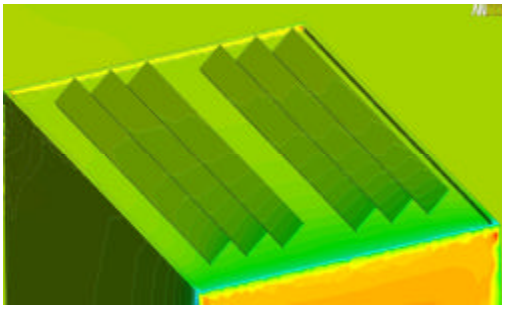

a.

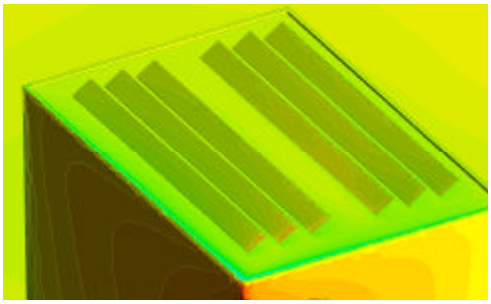

b.

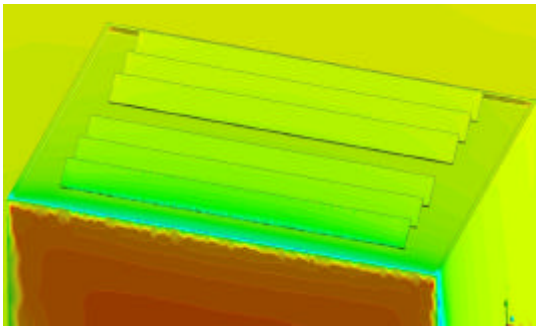

c.

Figure 5. Rows of panels placed in separate groups: Isopleths of the mean wind pressure (obtained from the ANSYS simulation) on the inward face of the building and on the terrace (attic and first rows of panels) for the wind angle of action: a. 0º; b. 45º; c. 90º

4. DISCUSIONS AND RESULTS

According to the standard SR EN 1991-1-4 [10], the evaluation of the global wind forces on the whole structures is determined with the following relationship:

$$F_w = q_{ref} c_f(z) c_s c_d A_{ref} \tag{4.1}$$

where:

F_w – wind cumulated force acting on the whole structure or a part of it, particularly a structural element,

q_{ref} – reference wind pressure at the reference height above the ground level, z,

c_f – force coefficient

c_s c_d – structural coefficient

A_{ref} – reference area for structure or, for a structural element or part of the whole structure

In the case of the plane solar panels, the coefficients c_f, normal to the surface of the building, may be globally evaluated, in this case being used to determine the resultant force that acts on the whole surface of the collector, or local pressure coefficients with which the resultant from a small surface may be obtained. The vectorial characteristics of the normal pressure coefficients (sign and spatial direction) depend mainly on the wind angle of action with respect on the surface of the building [1]. In the case of the plane photovoltaic panels mounted on supports the local pressure coefficients will act on both faces of the panel and the resultant of the normal component will be obtained with the sum:

$$c_{LR} = \pm c_{ns} \pm c_{ni} \tag{4.2}$$

where c_{ns} is the pressure coefficient on the in wind surface of the panel and c_{ni} is the pressure coefficient from the leeward face (Figure. 6b).

The code for design to wind action of structures gives information about isolated mono-pitched canopies, the case of several canopies placed in a row being absent. In the same time, any method of evaluation of the influence of the neighborhood is missing.

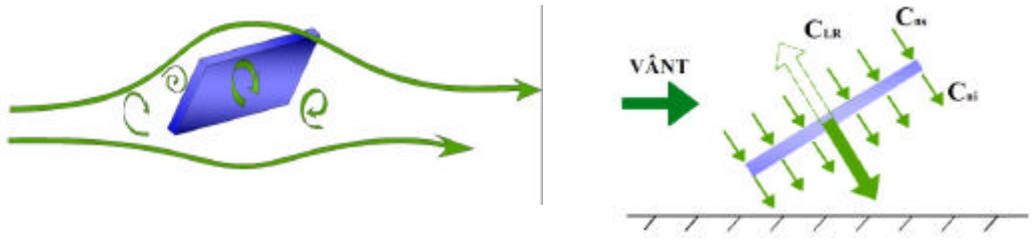

a. b.

Figure 6. The air flow around the plane surface of the collector (a) and the computation of the coefficient c_{LR} (b)

The air flow around the solar collectors is complex (Figure. 7a), being significantly influenced by the geometry and dimensions of the building together with the incidence angle of the wind action.

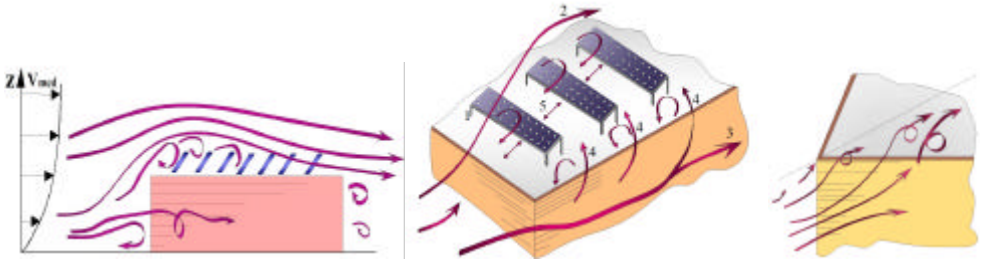

a. b. c

Figure 7. The lines of the turbulent flow above the flat roof equipped with solar collectors: a. - the building immersed in the atmospheric boundary layer, b.-air flow on the roof equipped with solar collectors placed in parallel rows, c.- vortex created by the yaw angle of wind action, 1.- photovoltaic panels, 2. – detached shear layers in the contact with the sharp edge of the roof and local turbulence produced by the collectors, 3. – lateral current lines, 4. – vortices detached at the edge of the roof in the shear layers area, 5. – local turbulent flow under the collectors [4].

The presence of the vortices in the area where the shear layers detach from the edges of the roof (Figure. 7a) and of the corner of the building (Figure. 8.c) intensify the turbulence in the perimeter of area, so the panels must not be placed near the attics [8]. From studies prior developed at the Faculty of Construction and Building Services in Iasi regarding the wind action upon the collectors placed on flat roofs (E. Axinte, A. Radu) it was observed that the local turbulence lifting forces act on the panels as well as pushing forces, their intensity being influenced

directly by the way that these collectors are placed, the speed and the direction of the wind with respect to the building and finally, by the presence of other similar elements placed on the terrace [4] [9].

4.1 Analysis of the results obtained during the numerical simulation:

Pressure produced by wind action was registered on every row of panels in 35 points, placed in 5 respective 7 lines, according to figure 8.

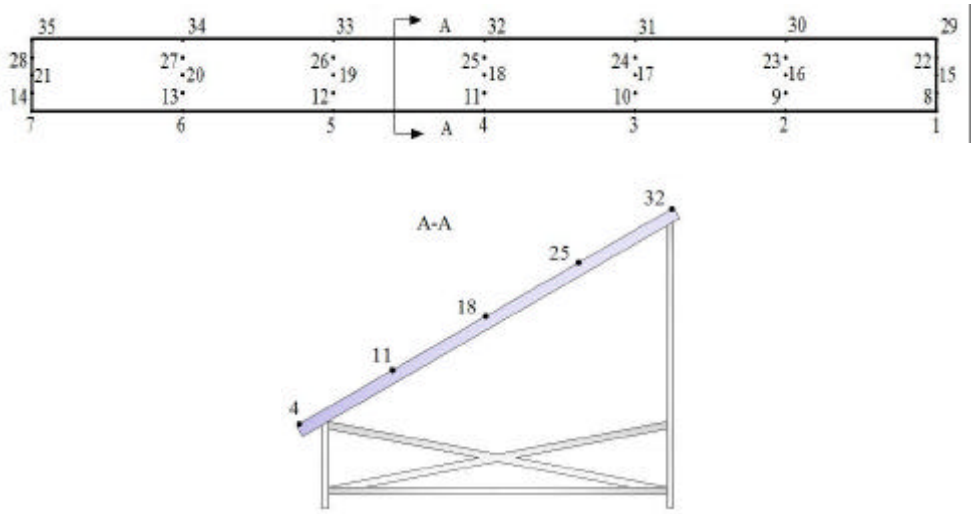

Figure 8. Distribution of the points on the surface of the collector where the local wind pressure was measured

Distance between the points placed on a line is of 4 cm add between the points on a row is of 0.4 cm, at the model scale.

After gathering the values obtained in every point graphics were traced for the observation of the variation of in between the lines with the rows and between the rows.

4.1.1 Solar collectors placed in a compact group

The analysis of the values of local pressures on the exposed faces of the collectors for the tree angles of the wind action put in evidence the following aspects:

The wind angle action 90º (Figure.3. Figure. 9)

The panels placed in the first row are the most exposed to and the most affected by the wind action. Maximum pressures were registered in the middle of the row (in

points 4, 11, 18, 25 and 32) and minimum at their extremities (in points 1, 8, 15, 22, 29, then 7, 14, 21, 28 and 35 respectively); the observation is the same for the second row. Rows 3 and 4 are subjected to a uniform pressure, the differences between the central points and the extremities being rather small. From rows 6 and 7, the flow is modified due to local turbulences and the variation of the wind pressure is different. The smallest pressures registered are still those from the extremities but the maximum values are away from the central point, both sides.

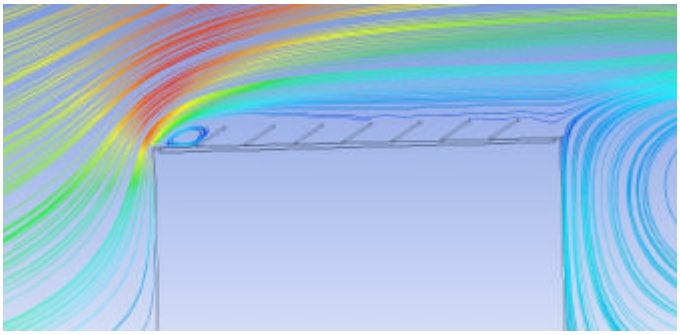

Figure 9. The flow lines above the collectors field for wind action angle of 90º

Another observation is that in the case of all the rows in the points placed in the first line (points 1 ... 7) the pressures are bigger (Figure 10), while the points placed in the first line (points 29....35) experience lower values.

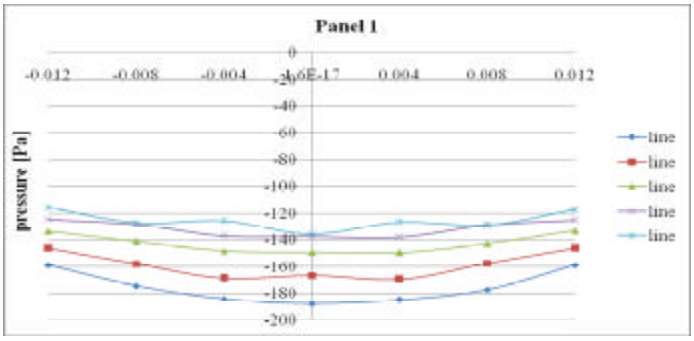

Figure 10.Variation of the pressure on the surface of the first row of collectors for the wind action angle of 90º

The first row of collectors being exposed more exhibits the biggest values of wind pressure (figure. 11) which diminish gradually, in the case of the panel 7 reaching the lowest.

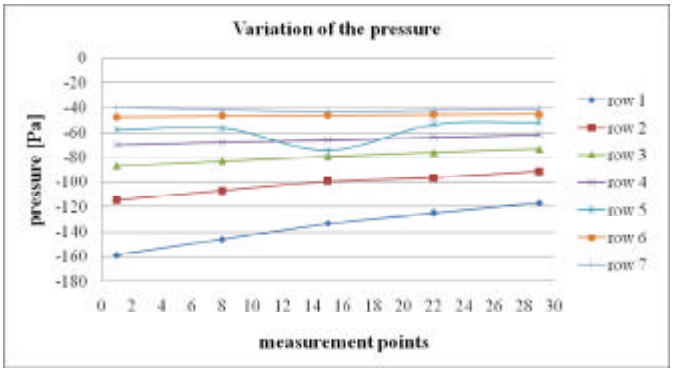

Figure 11. Variation of the wind pressure in the points placed in the first row of every row of solar panels for the wind action angle of 90º

The wind action angle 0º (Figure. 3)

In case of the panels placed in compact group (fig. 4) the following observations are extracted:

- in the case of all the rows of collectors, the biggest values of pressure are registered in points 1, 8, 15, 22 and 29 in marginal area, and the smallest in points 7, 14, 21, 28 and 35, placed in the opposite corner;
- every particular row analyzed show a great variation between the values in its extremities; in the case of the first and the last row (1 and 7) the difference between them is about 30%, and in the case of the rows placed in the central area of the roof the difference is of 26%. In the central area, the rows are more affected by wind pressure than those in the first and the last row;
- unlike the wind angle analyzed before (90º), for the 0º angle the first row is not so exposed (points 1...7) but instead, the last row is far more affected in the vicinity of the edges of panels.

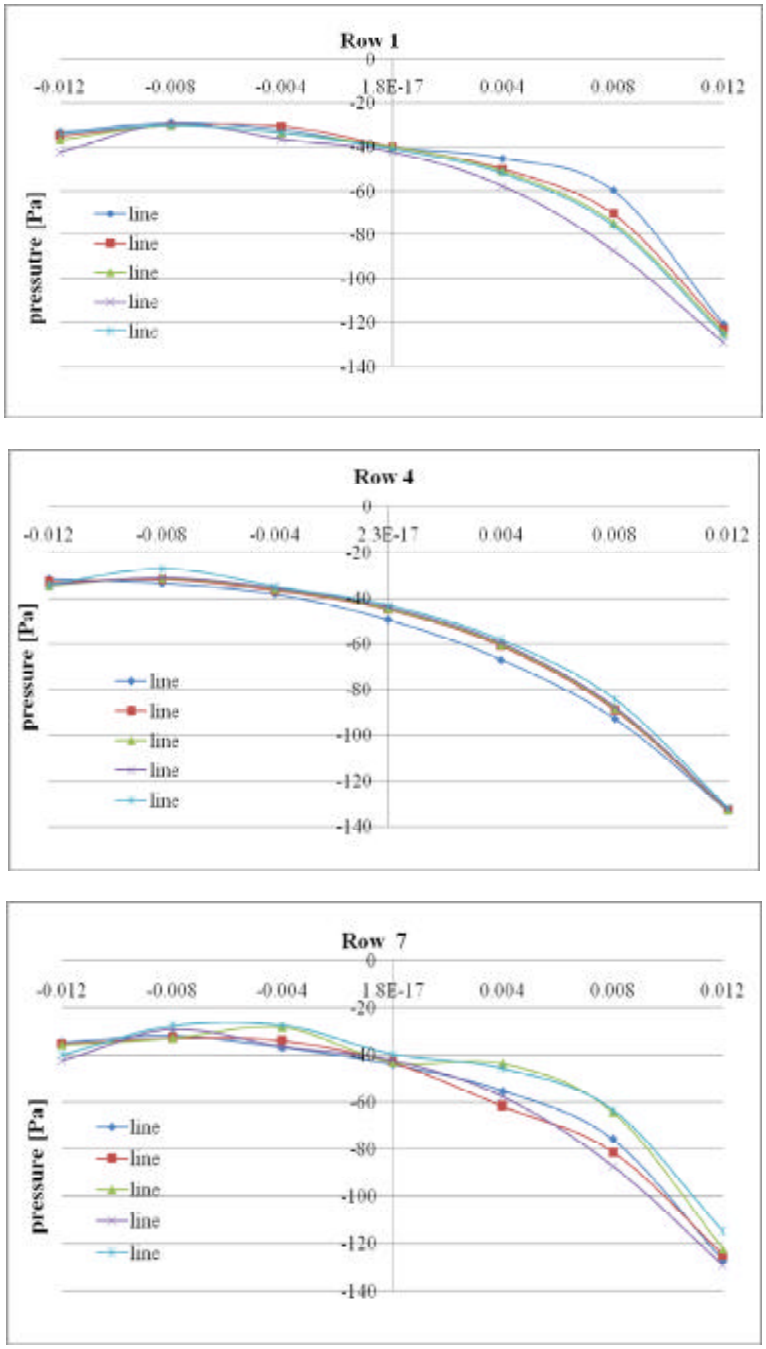

Figure 12. Variation of the pressure on the surface of the rows 1, 4 and 7 for the wind angle of action of 0º

Angle of wind action of 45º (Figure.3)

On the surface of the row 1, being the one the most exposed, the wind pressures are bigger than in the other rows. For the rows 1, 2 and 3, in the points placed in the in the right extremity (first row) the pressures are up to 50% smaller than those in the left extremity. In the central area of the group of panels, (row 4) the differences of pressure between the two extremities are not relevant. In the right extremity of all rows, starting with the row 5 and finishing with the last, pressure rise and drop down at their end.

Tab. 1 Variation of wind pressure in the points situated in the central area and in the extremities of the rows 1, 4 and 7

	Point	Pressure [Pa]	Point	Pressure [Pa]	Point	Pressure [Pa]
Row 1	1	-52.3169	4	-173.755	7	-95.7958
	8	-45.3876	11	-121.01	14	-91.836
	15	-38.2839	18	-109.87	21	-87.894
	22	-37.2229	25	-101.452	28	-85.3064
	29	-36.1043	32	-113.465	35	-82.769
Row 4	1	-74.7144	4	-80.672	7	-70.14
	8	-77.553	11	-68.868	14	-70.637
	15	-80.352	18	-64.307	21	-71.131
	22	-83.3383	25	-58.263	28	-71.918
	29	-86.133	32	-99.652	35	-72.234
Row 7	1	-97.413	4	-73.101	7	-71.733
	8	-95.25	11	-88.215	14	-74.649
	15	-92.9296	18	-88.9115	21	-77.229
	22	-92.204	25	-89.064	28	-74.814
	29	-91.429	32	-61.149	35	-72.48

4.1.1 Solar panels placed in separate groups (Figure. 5)

In this case, the panels are placed in two separate groups of three rows each on the flat roof. The distance between the rows in each group is 1.0 m, and between the groups is 3.0 m.

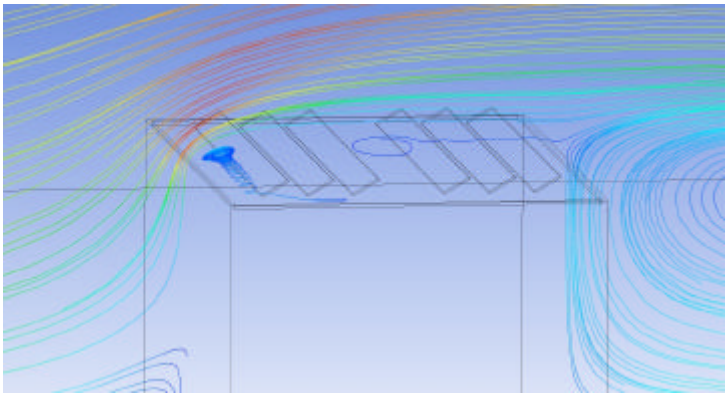

Figure 13. The lines of wind flow over the collectors, placed in the field of two separate groups for wind incidence angle of 90º

The second case of placing the solar collectors analyzed in this study showed similar values in the parallel situations. The first row in the second group in the direction of the incident angle (row 4, Figure. 2b), is however more affected by the wind pressure than in the first case, in one compact group (row 5, Figure. 2a).

5. CONCLUSIONS

The interaction wind- solar panels is influenced by the characteristics of the wind (direction of the flow, frequency of fluctuations, turbulence scale), by the shape of the building and its dimensions and finally by the grid of the solar collectors placed in specific order, inclination and fixings on the surface of the roof. Wind upon one panel cumulates all the effects of its action on the obstacles situated in wind and on the panel itself. All the panels placed on the flat roofs are immersed in a general zone of important negative values of wind pressure that affects the local distribution on the panels. In the case of solar panels placed in consecutive rows, a mutual effect of screening appears, along with the general screening produced by the building itself.

Maximum actions generated by wind action appear on the panels placed in the first row whichever of the angles of wind action might be. The position of solar panels one close to the other in rows reduces the mean wind pressure and contributes to the optimization of steel consumption in the sustaining structure.

The study reveals the fact that the numerical modeling is an important and handy instrument in the evaluation of the wind pressures on the simple structural shapes. A good numerical modeling is the one that copes with the results obtained from a

physical modeling in wind tunnels, both of these methods fulfilling the thorough knowledge of the wind action on the built environment.

Bibliografie

1. Axinte E., *Modelarea fizica a interactiunii vant-structura pentru proiectarea captatoarelor solare*, teza de doctorat, Universitatea Tehnica "Gheorghe Asachi", Iasi, 1988
2. Chevalien L., Norton J., *Wind loadson solar collectors panels and support structure,* Aerospace Eng. Dept., Texas A&M University, 1979
3. Xerikos J., et al., *The aerodynamics of heliostats for solar power plant applications*, Proc. 5th Int. Conf. on Wind Engineering, Pergamont Press, Oxford, 1980
4. Radu A., Axinte E., *Steady wind pressures on solar collectors on flat-roofed buildings*. J. Wind Eng. Ind. Aerodyn. 23, 249-258, 1986
5. Chang K., et al., *Solar water in Taiwan*. Renew. Energy 31, 1299-1388, 2006
6. Chung K., Chang K., Liu Y., Reduction of wind uplift of a solar collector model, J. Wind Eng. Ind. Aerodyn. 96, 1294-1306, 2008
7. Franke J., et al. *Recomandation of the use CFD in wind engineering.* Proceeding of the International Conferinces on Urban Wind Enineering and Building Aerodybamics, Belgia, 2004
8. Axinte E. Teleman E., C., Vasies G., *Actiunea vântului asupra panourilor solare* , Revista Constructiilor, anul VI, nr.57, martie 2010, ISSN 1841-1290.
9. Radu A., Axinte E., Wind forces on structurea supporting solar collectors. J. Wind Eng. Ind. Aerodyn. 32, 93-100, 1986
10. Eurocod 1: *Actiuni asupra constructiilor. Partea 1-4: Actiuni generale – Actiuni ale vântului*, 2006

Seismic modeling of concrete shear walls with irregular openings

Ovidiu Chelariu[1], Ioan Petru Ciongradi[2] and Mihai Budescu[3]
[1]*Department of Structural Mechanics, "Gheorghe Asachi" Technical University, Jassy, Romania*
[2]*Department of Structural Mechanics, "Gheorghe Asachi" Technical University , Jassy, Romania*
[3]*Department of Structural Mechanics, "Gheorghe Asachi" Technical University , Jassy, Romania*

Summary

Concrete shear walls with irregular openings are not recommended in earthquake regions due their incertain post-elastic behavior. However, in some cases they are still permited, conditioned by adequate computational analysis of their behavior.

The paper presents the in-plane analisys of a concrete wall with irregular openings, using the strut-and-tie design method. The next structural codes were used for this analysis: EC2, ACI 318.

At first, the strut-and-tie method and some of the basic principles regarding the practical approach are presented.

Next, a linear elastic analysis is used for the seismic design of the shear wall, according to the structural codes. For this, a "shell" finite element model is developed.

Then, a strut-and-tie model is developed based on the results from the seismic linear elastic design. Importance has been given here to the stress flows and to the code provisions for the wall reinforcement: minimum percentage and rebar placement.

The wall is designed again based on the strut-and-tie model.

The results from the two models are compared, and opinions are given on the influence of the irregular openings on the structural behavior of the shear wall. Some conclusions on the limits of practical using for this type of concrete shear wall are pointed out.

KEYWORDS: strut-and-tie; shear wall; seismic design; finite element model.

1. INTRODUCTION

Concrete shear walls with irregular openings presents itself as a challenge in the seismic areas. The seismic design codes are not encouraging their use, except for the case when openings are placed in some favorable position (ex. staggered) for the load path. The reason is post-elastic incertain behavior of such walls.

However, concrete shear walls with irregular random openings are permitted in earthquake regions conditioned by adequate computational analysis of their behavior. The paper presents the in-plane analisys of such a wall using the strut-and-tie design method.

2. STRUT-AND-TIE METHODOLOGY AND PRINCIPLES

Strut-and-tie design models for structural concrete were proposed in 1987 by Schlaich et all [1] and represents a generalization of the old truss analogy introduced by Ritter and Mörsch. The method was developed later by other authors, getting to be included in the reference design codes such as ACI 318 and Eurocode 2.

The method is oriented towards the design of structural elements with statical or geometrical discontinuities (to which Bernoulli's hypothesis does not apply) like frame corners, corbels, walls or beams with openings/ holes, regions adjacent to abrupt changes in loading at concentrated loads and reactions, etc.

Practical approach using strut-and-tie models usually follows certain steps:

- Identifying B and D regions
- Developing the strut-and-tie model
- Dimensioning (verifying) the struts, ties and nodes

2.1. Identifying B and D-regions

B-Regions ("Bernoulli" or "Beam ") are element regions where Bernoulli hypothesis is valid, and therefore can be designed using any method available for frames. The stress state in such regions is easily determined based on the sectional forces. If desired, these regions can also be designed using strut-and-tie method.

D-Regions (“Discontinuity”, “Disturbance”, or “Detail”) are element regions where Bernoulli hypothesis is not valid, due to statical or geometrical discontinuities.

If D-regions remain uncracked, they can be designed by the linear elastic stress method, applying Hooke's law. In cracked D-regions, it is appropriate to develop strut-and-tie models.

The reason could be that alternative design is:

- traditional approach using more or less empirical principles (often inadequate),

- developing nonlinear finite element models (onerous as a daily design method).

2.2. Developing the strut-and-tie model

The strut-and-tie model is a hypothetical truss, the components being struts, ties and nodes. Struts are idealized compression fields and ties are idealized tension fields. The development of the model is made on the following bases: the experience of the analyst, the load path method or a previous linear elastic stress analysis. Many times can be a combination of them.

In the process of developing the model are to be considered the minimum design code provisions for strut-and-tie models, such as: strut are not allowed to intersect, and the angle formed by any strut with any tie should not be less than 25 ° [4].

The code provisions regarding the type of structural element should also be considered, especially the minimum reinforcement requirements.

Using the strut-and-tie method implies that the structure is designed according to the lower bound theorem of plasticity. Since concrete permits only limited plastic deformations, the model has to be chosen in a way that the deformation limit is not exceeded at any point before the assumed state of stress is reached in the rest of the structure [1].

In order to fulfill the ductility requirements, the struts and the ties should be oriented to the direction and size of the internal forces, especially in highly stressed regions. The consequence would be the need to estimate as accurately as possible the stress fields.

Another recommendation is to have fewer tie bars (or shorter), because they are much more deformable than strut bars.

Geometry and element ductility requirements could draw the need to develop static indeterminate strut-and-tie models. This may lead to an iterative design of strut and tie sections.

2.3. Dimensioning (verifying) the struts, ties and nodes

Dimensioning not only means sizing and reinforcing the individual struts and ties for the forces they carry, but also ensuring the load transfer between them by

checking the node regions. There is a close relation between the detailing of the nodes and the strength of the struts bearing on them and of the ties anchored in them because the detail of the node chosen by the design engineer affects the flow of forces.

The strength of the concrete in struts is reduced according to different design codes considering the follows: strut type, stress state, cracking state, reinforcement type, also the type, load and sectional forces of the structural element.

The axis of steel reinforcement must coincide with the axes of the tie in the model. The strength and the anchorage of reinforcement need to be checked.

Checking the node regions is done considering its geometry. For a planar structure, the statical equilibrium is reached when a minimum of three forces converge in the nodes. Nodes are classified by the type of forces that meet at the node. Thus a C-C-C node anchors three struts, a C-C-T node anchors two struts and one tie, a C-T-T node anchors one strut and two ties.

The concrete strength in the nodal zone is reduced according to different design codes considering the follows: node type, reinforcement type, number of ties entering the node and stress state (plane or three-dimensional).

3. SHEAR WALL ELASTIC ANALYSIS

Fig. 1 shows the shear wall geometry and finite element (shells) meshing. The model is used for linear elastic stress analysis. It is a two level structural concrete wall, each level having a heigh of 3.1m. The vertical loads are distributed along the wall lenght at each floor level.

The seismic action is considered to act horizontally, inplane of the wall and in both senses (fig. 2-5). The seismic forces are acting equivalent static at the floor levels. The reduction seimic coefficient value for inelastic structural response is estimated to be equal to 2. The value corresponds to a preventive design, altought some authors consider such shear walls (with irregular random openings) as having a good ductility if proper reinforced.

Specificed strength values:

- concrete compressive strength: 11,25 N/mm^2
- concrete tensile strength: 0,82 N/mm^2
- reinforcement strength: 300 N/mm2

In some regions (fig. 3, 5), the tensile principal stresses exceed the concrete tensile strength, leading to partial wall cracking. In fact, wall cracking was already

assumed when the decision to use inelastic structural response was made. Thus, strut-and-tie is proposed as design method.

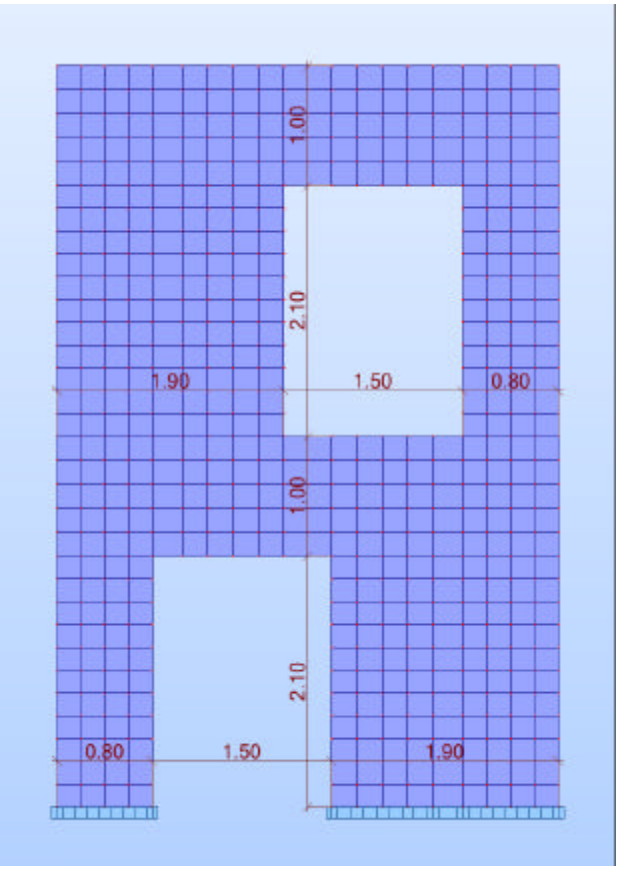

Fig. 1. Shear wall geometry and meshing (dimensions are in m). Wall thickens is 0.15 m.

3. STRUT-AND-TIE MODEL

For start, B and D regions of the wall are identified (fig. 6). Dividing lines between B and D regions are drawn based on Saint-Venant principle.

For design simplicity, the B regions of the wall are idealized as single truss elements in the strut-and-tie models (fig. 7, 8). Another reason is that B regions of the wall are more flexible and there is a possibility to redistribute forces toward stiffer regions based on the structural ductility.

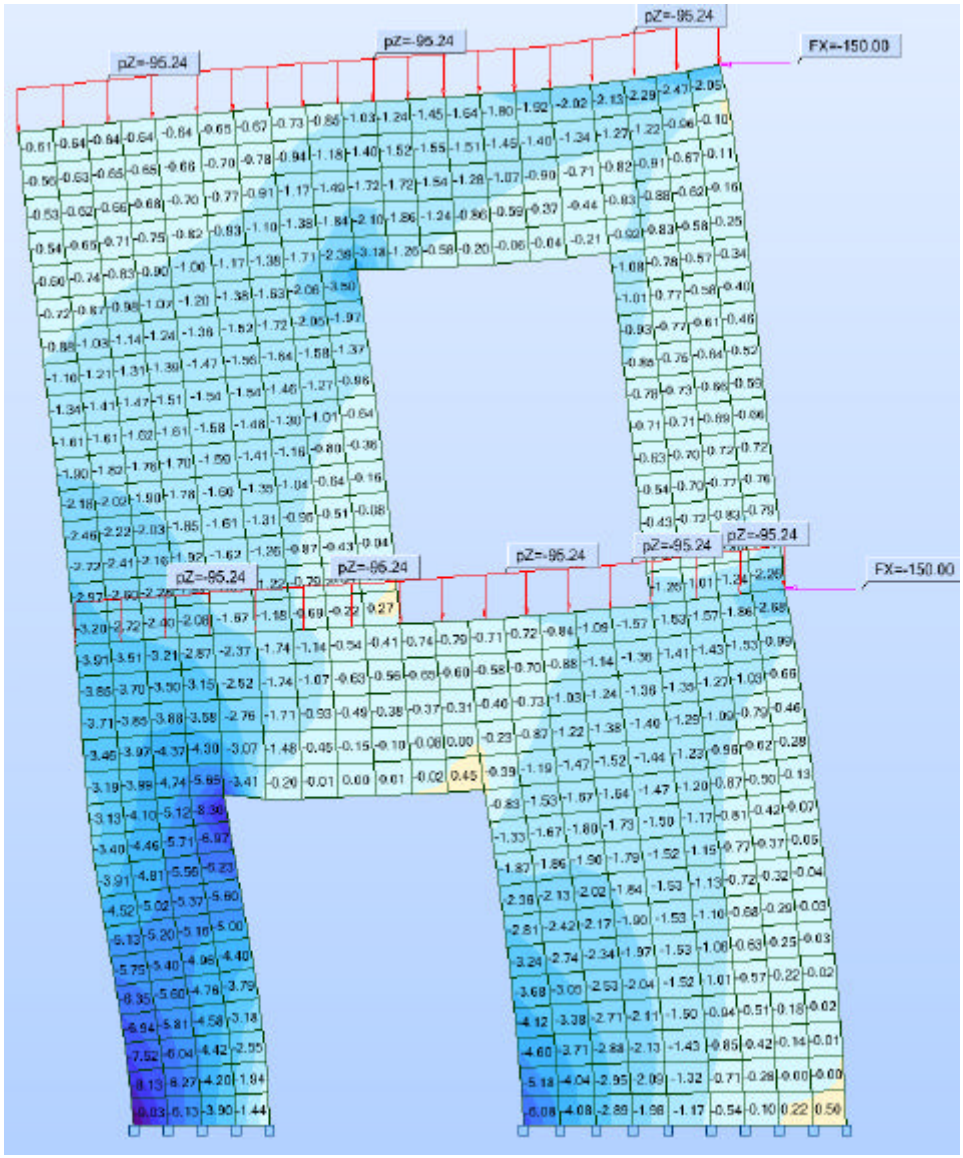

Fig. 2. Load case with seismic forces acting from right. Wall deformation and compressive principal stress fields. Units: KN (point loads); KN/m (distributed loads); N/mm2 (stresses)

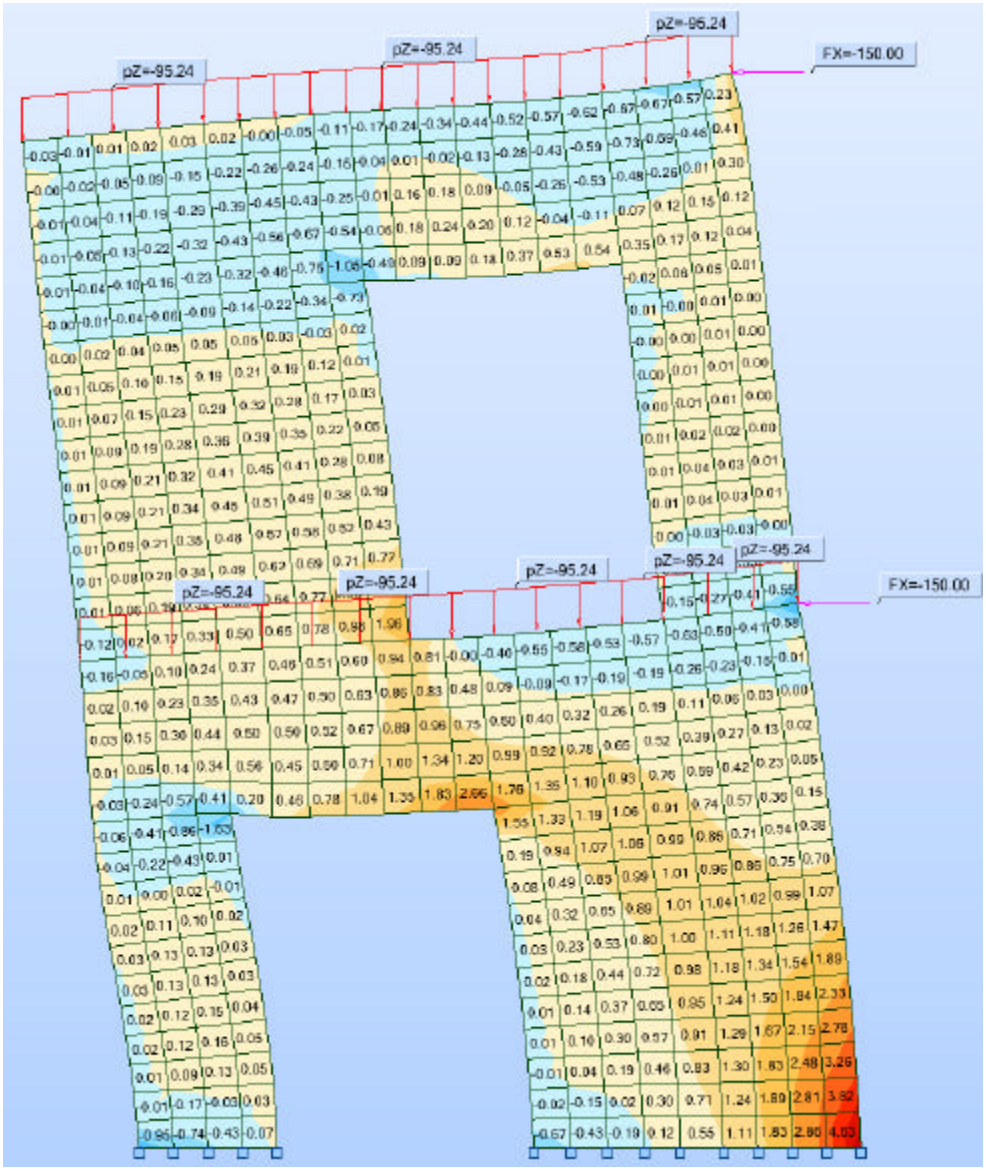

Fig. 3. Load case with seismic forces acting from right. Wall deformation and tensile principal stress fields. Units: KN (point loads); KN/m (distributed loads); N/mm2 (stresses)

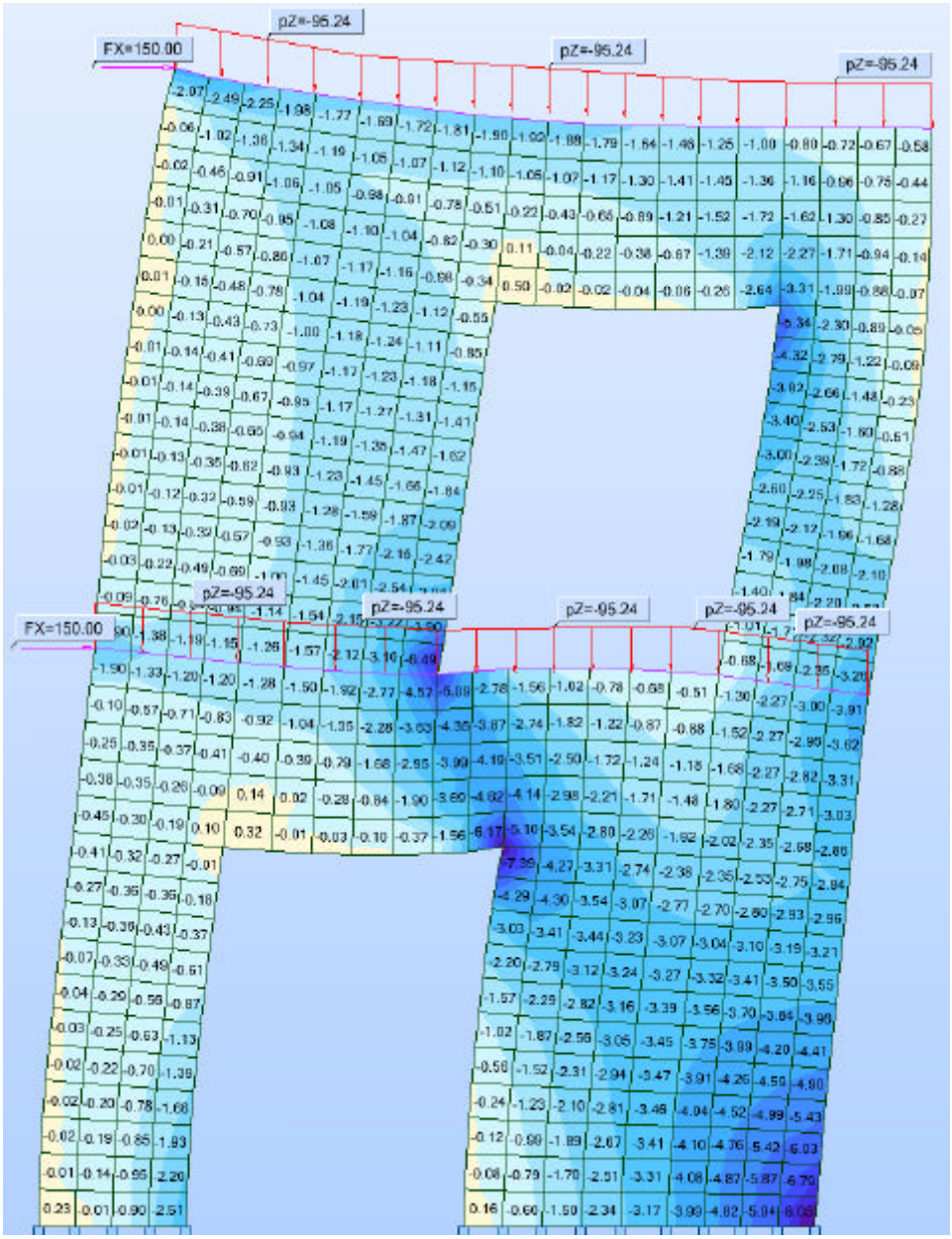

Fig. 4. Load case with seismic forces acting from left. Wall deformation and compressive principal stress fields. Units: KN (point loads); KN/m (distributed loads); N/mm2 (stresses)

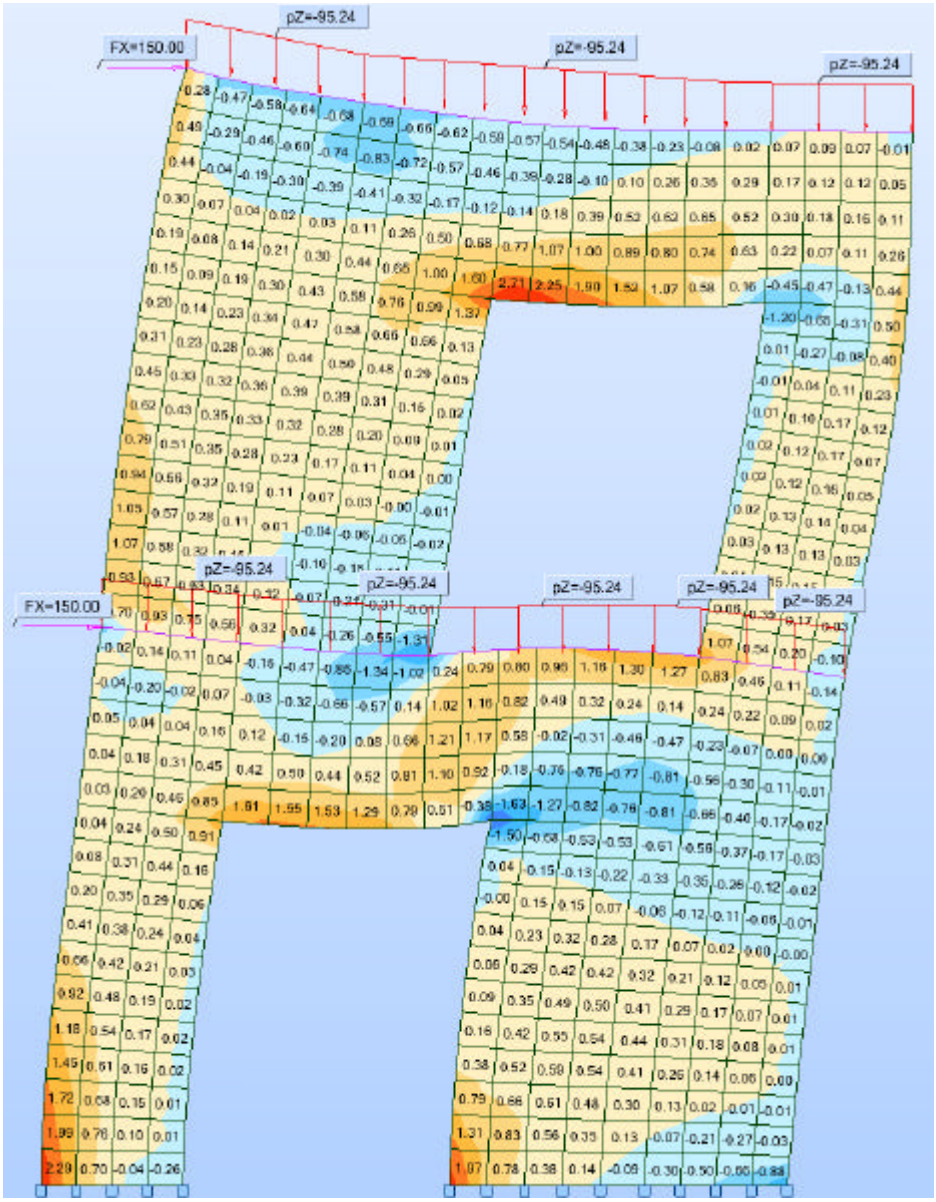

Fig. 5. Load case with seismic forces acting from left. Wall deformation and tensile principal stress fields. Units: KN (point loads); KN/m (distributed loads); N/mm2 (stresses)

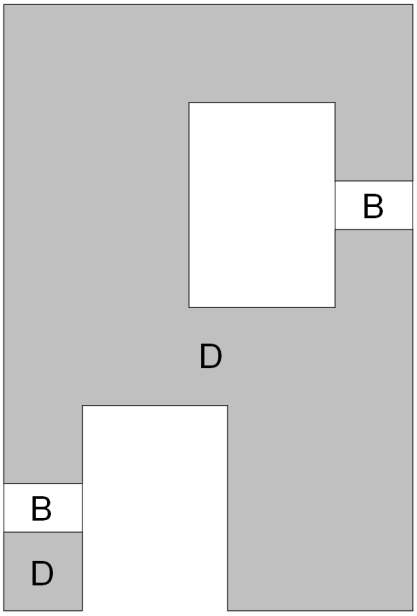

Fig. 6. B and D regions of the wall

Model was developed based on the elastic principal stress fields, using an iterative process.

For design was considered the possibility that seismic forces have bigger values that the ones estimated. Thus, truss bars with small tensile forces were assumed to be reinforced ties (T7, T10 in fig. 8), while others were assumed to be concrete tensile ties (T1 in fig. 8).

Also, in the reinforcement design process, it was assumed that orthogonal minimum reinforcement disposed acording to the codes (especially seismic codes) needs to be present. Then, for the ties that have different directions, additional reinforcement was disposed (fig. 10).

The same approach was used for orthogonal ties that needed greater amount of reinforcement. In this case, the designed reinforcement replaced the orthogonal minimum reinforcement (across the tie sections). All reinforcement bars need to have proper anchorage (not figured).

The shear wall was also designed based on classic design for concrete walls according to ACI 318. The reinforcement resulted from for this design is presented in fig. 9.

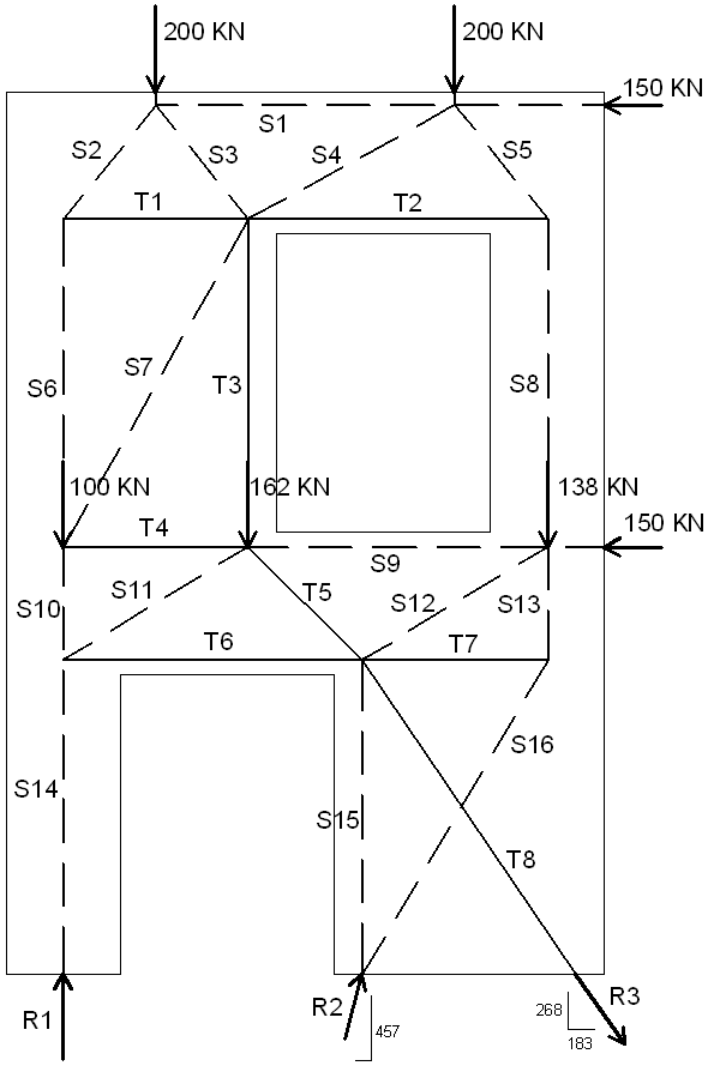

STRUT	S1	S2	S3	S4	S5	S6	S7	S8
[KN]	-2.8	-126.6	-131.1	-248.7	-102.9	-98.3	-304.8	-79.9
STRUT	S9	S10	S11	S12	S13	S14	S15	S16
[KN]	-118.3	-463.6	-281.1	-37.2	-198.4	-611.0	-258.8	-230.4
TIE	T1	T2	T3	T4	T5	T6	T7	T8
[KN]	79.8	64.9	43.5	150.0	40.8	239.4	117.2	324.5

Figura 7. Strut-and-tie model developed for the load case with seismic forces acting from right. Force values in truss elements.

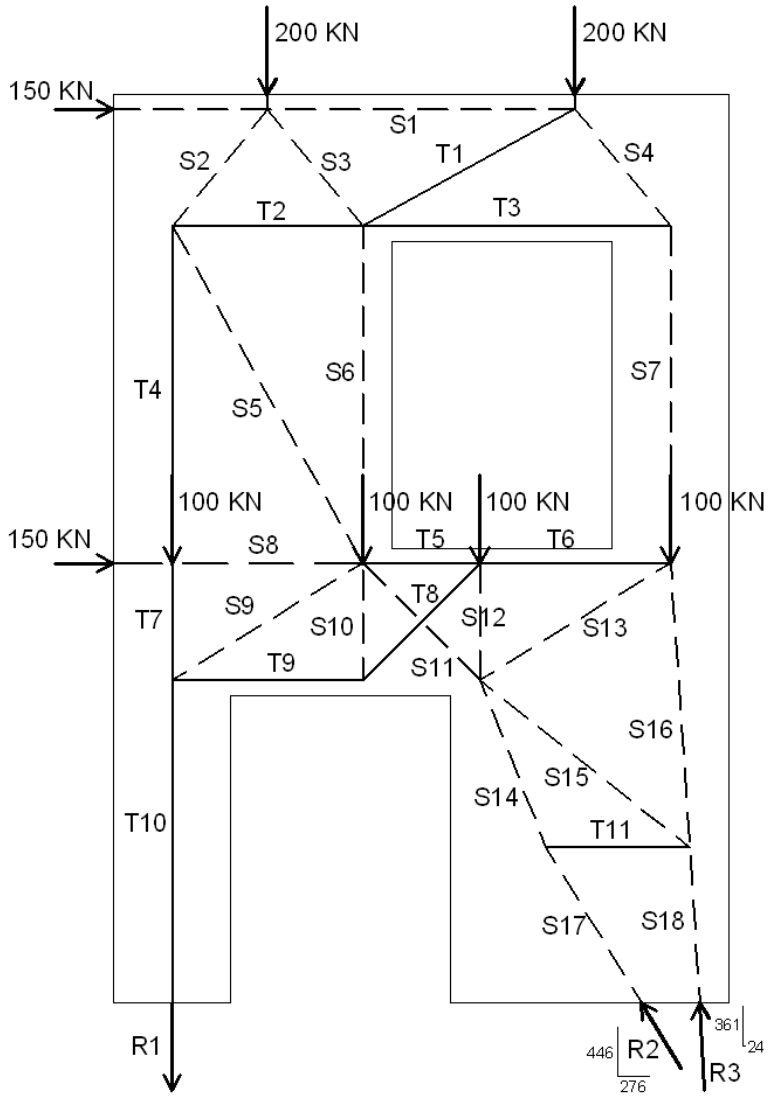

STRUT	S1	S2	S3	S4	S5	S6	S7	S8	S9	S10	S11
[KN]	-209.7	-176.2	-81.5	-280.9	-304.8	-45.2	-218.0	-150.0	-42.3	-36.0	-498.5
STRUT	S12	S13	S14	S15	S16	S17	S18				
[KN]	-136.0	-83.1	-478.7	-137.7	-275.1	-524.3	-361.5				
TIE	T1	T2	T3	T4	T5	T6	T7	T8	T9	T10	T11
[KN]	37.3	261.1	177.1	128.6	16.5	51.0	28.6	117.2	36.0	6.5	101.5

Figura 8. Strut-and-tie model developed for the load case with seismic forces acting from left. Force values in truss elements.

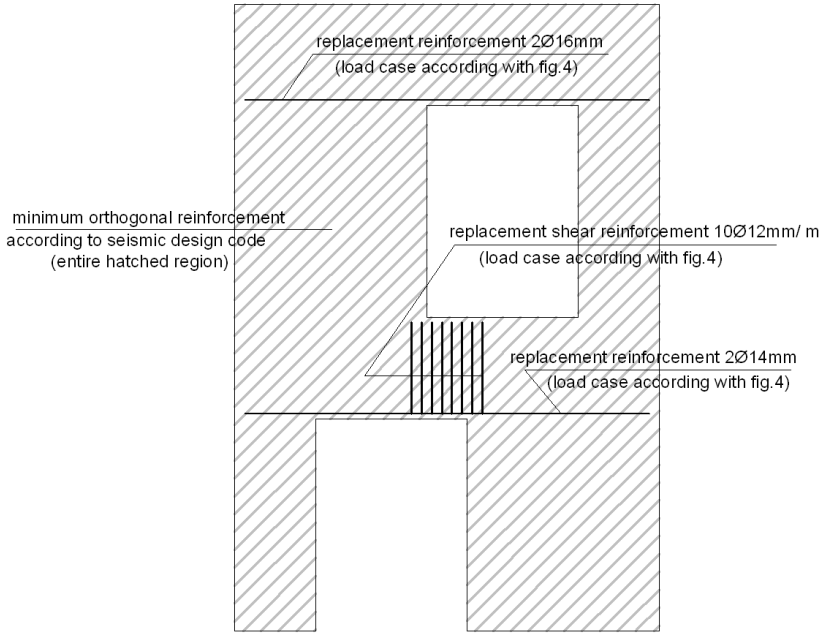

Fig. 9. Wall reinforcement from classic shear wall design

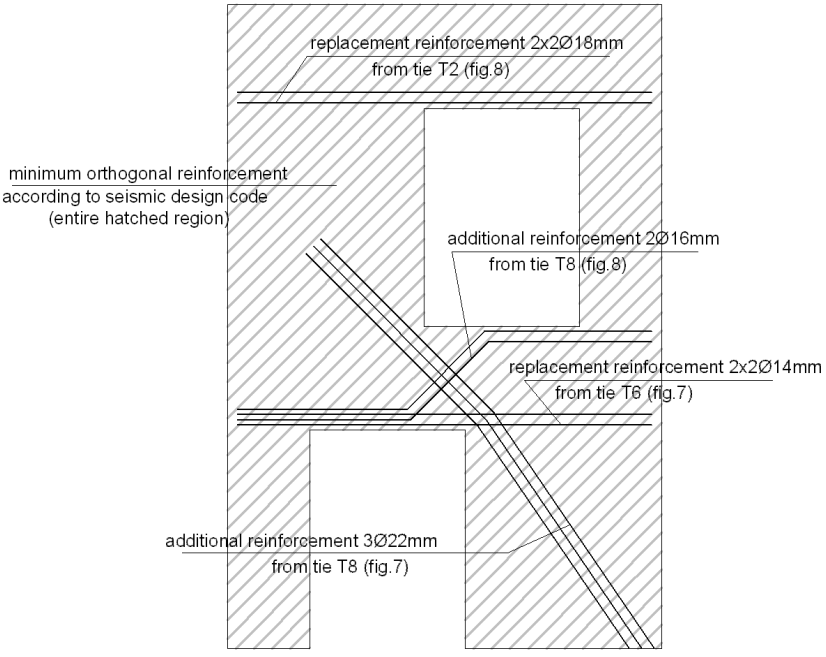

Fig. 10. Wall reinforcement from strut-and-tie design

CONCLUSIONS

Presence of irregular random openings in a shear wall leads to unusual stress states and questionable ductility. This type of wall should be used with caution in earthquake regions, conditioned by adequate computational analysis of its behavior.

Strut-and-tie models could be the right choise for seismic modeling of concrete shear walls with irregular openings. The concrete wall with reinforcement resulted from strut-and-tie models (fig.10) seem to have better ductility and follows the elastic stress state in a better way than the classic approach (fig. 9).

1. Schlaich, J., Schäfer, K., Jennewain, M., *Toward a consistent design of structural concrete*, PCI Journal, 1987
2. Schlaich, J., Schäfer, K., *Design and detailing of structural concrete using strut-and-tie models*, vol.69, The Structural Engineer, 1991
3. Reineck, Karl-Heinz, *Examples for the design of structural concrete with strut-and-tie models*, American Concrete Institute, 2002
4. ACI 318: *Building code requirements for structural concrete*, 2008
5. Eurocode 2: *Design of concrete structures*, 2004
6. Eurocode 8: *Design of structures for earthquake resistance*, 2003
7. Robot Structural Analysis (2010), *Technical Papers, Design Manuals*, Autodesk Inc., San Rafael, California
8. Etabs (2010), *Technical Papers, Design Manuals*, Computers and Structures Inc., University Avenue Berkeley, California